



Fedra Hajizadeh

Abstract

This chapter covers cases that could not be categorized into certain groups but are important to mention and illustrate. This chapter divided into: (1) posttraumatic pathologies, which covers choroidal rupture and growth of a neovascular membrane as its complication, and a traumatic macular hole and its evolution on serial OCT images; (2) solar retinopathy in the acute and chronic phases; (3) OCT in retinal detachment with changes in the detached retina and after attachment with scleral buckling and retinal surgery; (4) cystoid macular edema (CME) diagnosis, treatment, and follow-up for resolution and examples showing that early CME changes may be in the form of a small increase in the foveal volume or thickness; (5) hypotony maculopathy that often follows glaucoma surgery; (6) decompressive maculopathy with a case presentation and multimodal imaging; (7) postsurgical endophthalmitis and its eventual effects on the fovea; (8) Valsalva maculopathy; (9) subretinal deposits, which show changes in the retina at the DK-line remnant under the retina after vitrectomy surgery and light silicone injection; and (10) OCT in chloroquine toxicity, which illustrates the OCT changes in this drug toxicity in the early and advanced stages.

Keywords

Choroidal rupture • Solar retinopathy • Hypotony maculopathy • Retinal detachment surgery • Post-surgical endophthalmitis • Subretinal deposit • Valsalva maculopathy

12.1 Post-trauma Optical Coherence Tomography

After trauma, ocular tissues undergo different changes that are better evaluated by optical coherence tomography (OCT) in some instances. Traumatic choroidal rupture is a consequence of blunt ocular trauma with a tear in the choroidal vasculature. The healing process involves fibrovascular proliferation from the choroid that progresses to a dense fibrotic scar with variable stages of hyperplasia of the retinal pigment epithelium (RPE) (Figs. 12.1 and 12.2). This process usually evolves over a period of 3 weeks [1]. Optical coherence tomography can allow clinicians to predict visual recovery and the severity of damage produced by the trauma.

Most choroidal ruptures are concentric with the optic nerve and vertically oriented, which is consistent with a break in Bruch's membrane. This finding could be because of the tethering effect of the optic nerve. The rupture may be singular or multiple [2]. Figures 12.3 and 12.4 shows another example of a choroidal rupture that was complicated by neovascular tuft growth.

Significant backscattering of the underlying tissues in the choroidal ruptured area may be because of the healing process of the wound with fibrin and granulation tissue formation (Figs. 12.5, 12.6 and 12.7) and the initiation of scar tissue in the area.

Traumatic choroidal rupture sometimes may be accompanied by a sub-RPE hemorrhage. The development of choroidal neovascularization is a chronic complication [3]. The choroidal neovascular membrane that originates from the rupture site grows under the retina. The existence of subretinal fluid, which is usually minimal, indicates neovascular activity (Figs. 12.8, 12.9 and 12.10).

F. Hajizadeh (✉)
Noor Ophthalmology Research Center, Noor Eye Hospital,
No. 96, Esfandiar Blvd., Vali'asr Ave, Tehran, Iran
e-mail: fhajizadeh@noorvision.com

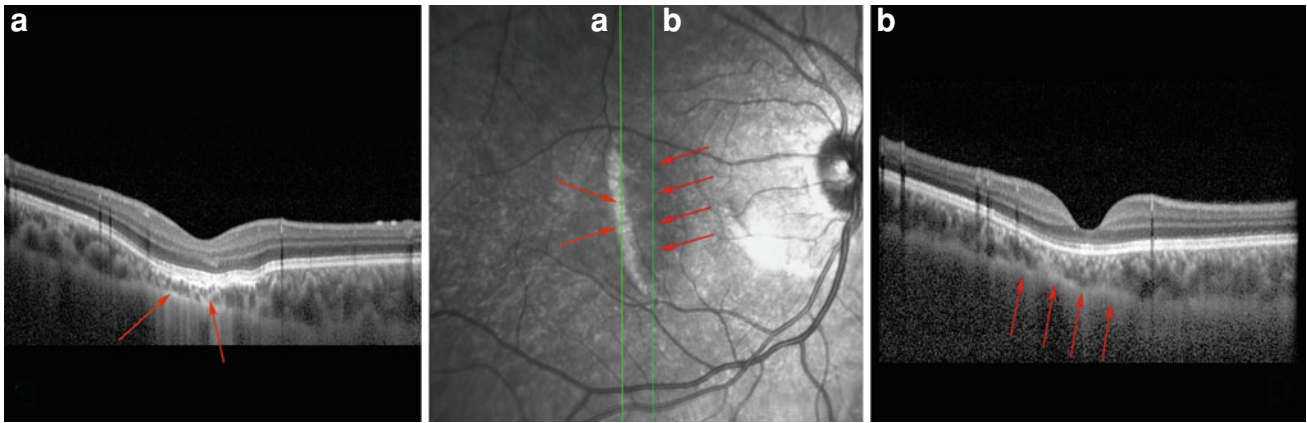


Fig. 12.1 These figures illustrate the posterior pole of the eye of a 21-year-old man who had experienced eye trauma 10 years earlier, and whose vision decreased to 20/120. These scans were produced using

the enhanced-depth imaging optical coherence tomography (EDI-OCT) method. The images reveal secondary choroidal atrophy and focal choroidal thinning (*red arrows*) in the parafoveal and foveal areas



Fig. 12.2 These images are from the same patient in Fig. 12.1. They were created by using conventional longitudinal OCT, which was passed through the central fovea. Retinal deviation through the atrophied choroid is evident (*red arrow*). *OCT* optical coherence tomography

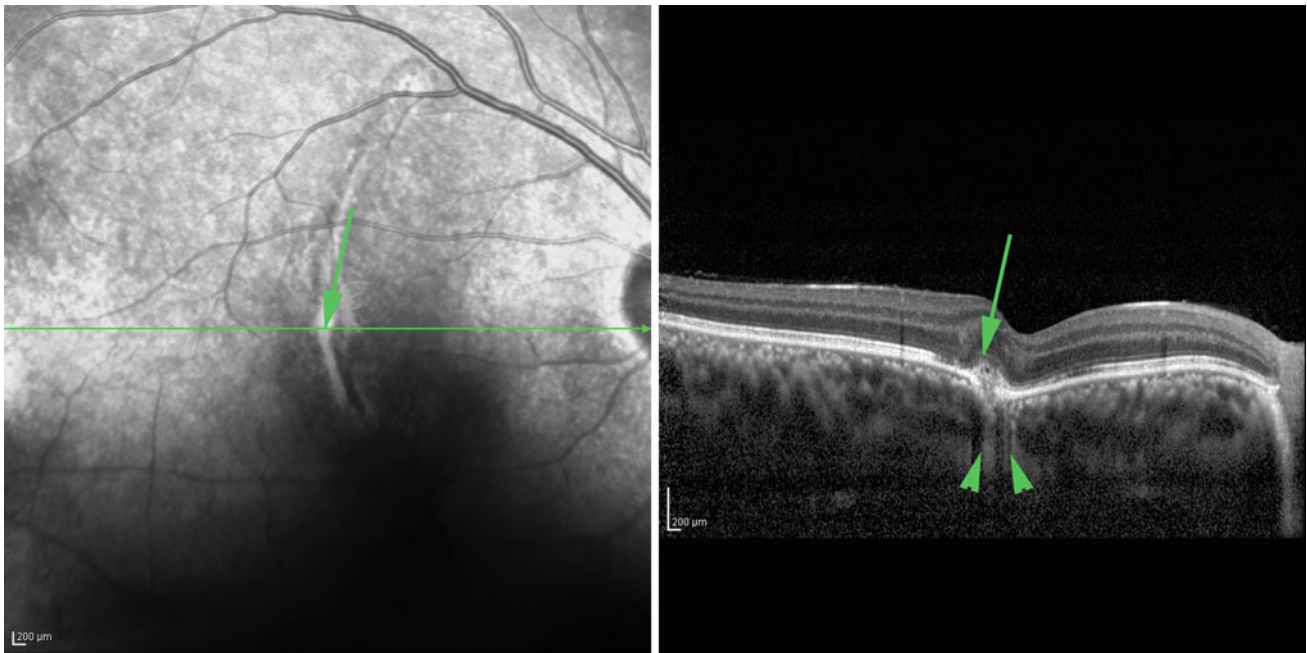


Fig. 12.3 This patient had experienced a blunt trauma few years earlier, and was referred to us. The patient complained of a recent vision loss. The arrowheads indicate the locations of the previous

choroidal rupture with localized choroidal thinning and fibrosis. A small medium reflective tissue has penetrated the retinal pigment epithelium (RPE) and retina, and has invaded the outer retinal layer

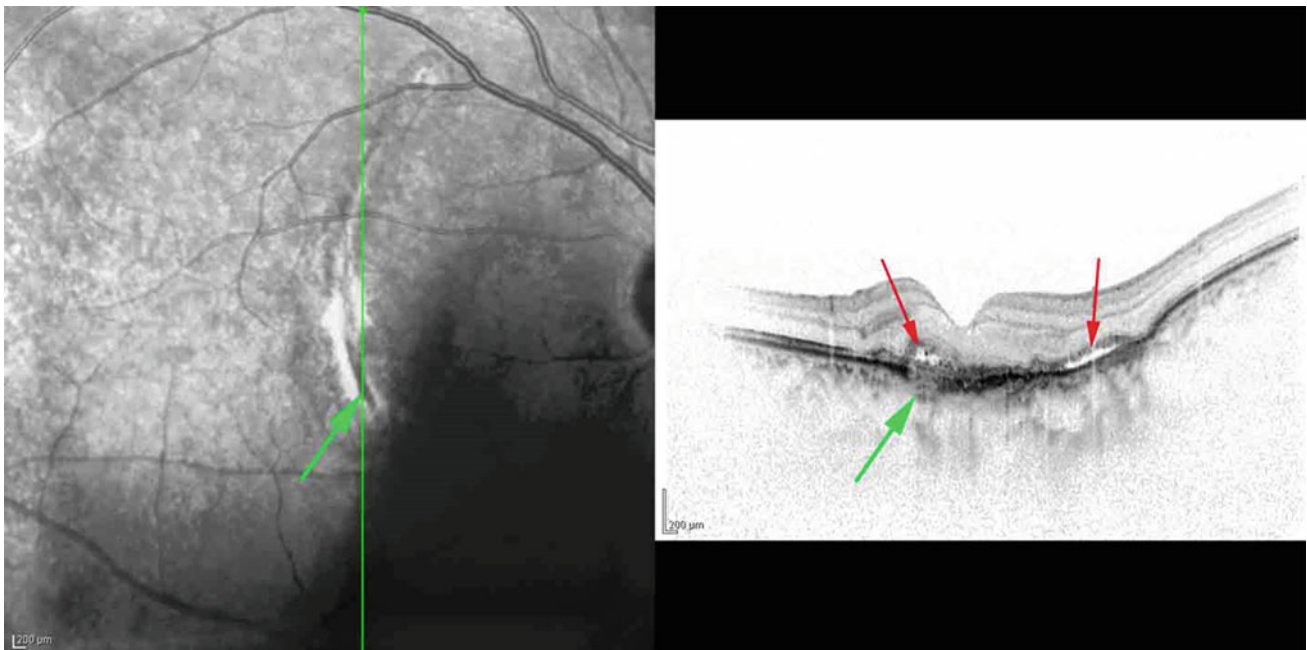


Fig. 12.4 The cross-sectional view of the macula depicts two foci of subretinal fluid collection (*red arrows*), which indicates neovascular activity. The green arrow indicates the location of the previous choroidal rupture

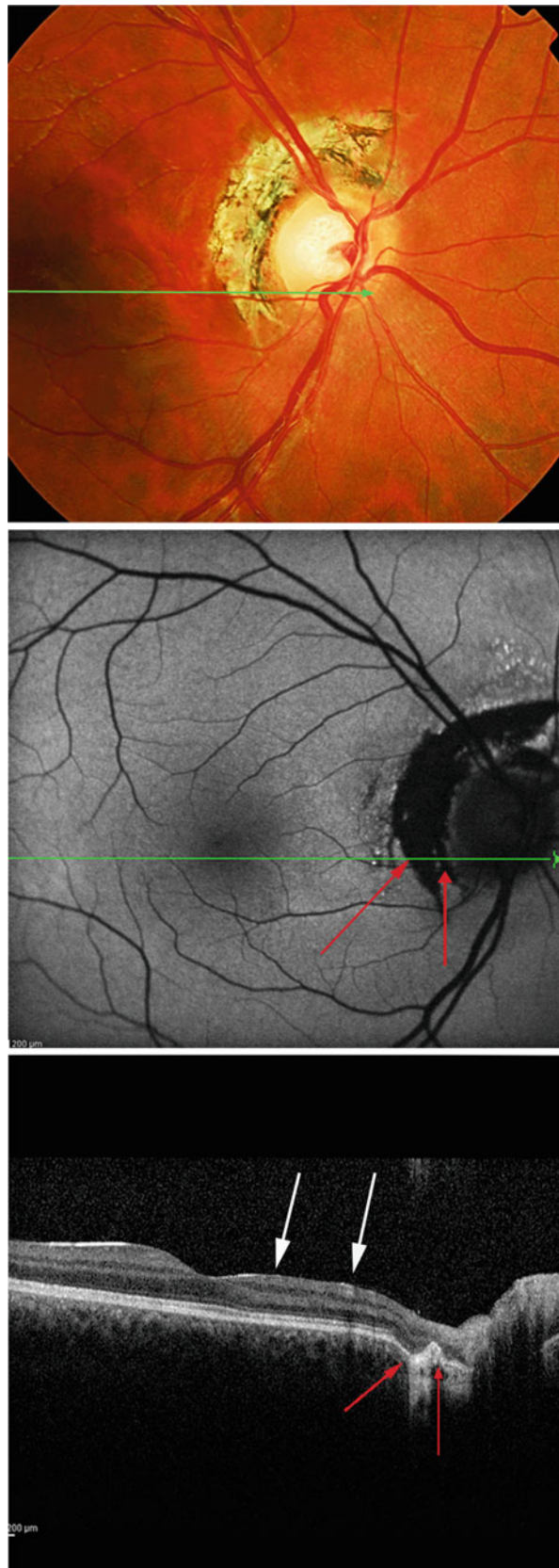


Fig. 12.5 The color fundus photograph and fundus autofluorescence image of an 18-year-old man with a 1-month history of eye trauma. The discontinuity of the retinal pigment epithelium (RPE) layer with increased

backscattering of the underlying tissues (*red arrows*) are apparent. The inner layers of the papillomacular bundle show atrophy (*white arrows*) and occurs because of localized damage to the nerve fiber layers

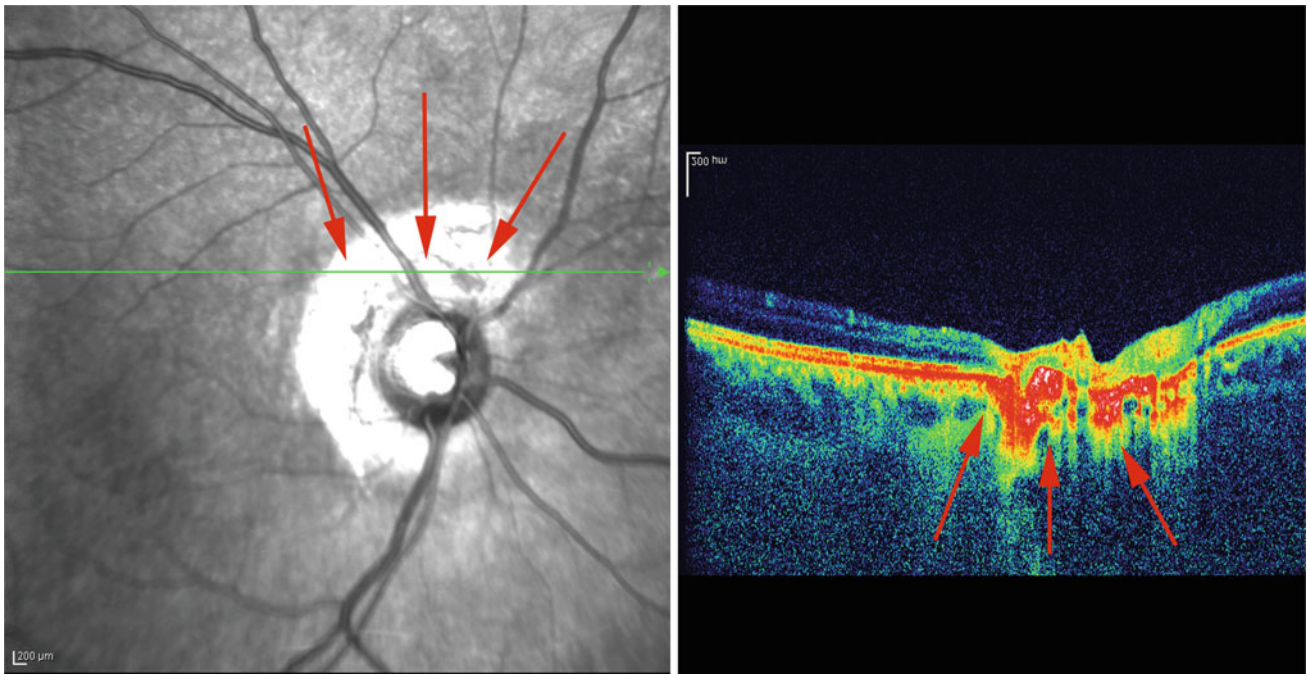


Fig. 12.6 The EDI-SLO-OCT image is from the same patient in Fig. 12.5. It illustrates the high reflectivity of the underlying tissue around the optic disc. *EDI* enhanced depth imaging, *SLO* scanning laser ophthalmoscopy, *OCT* optical coherence tomography

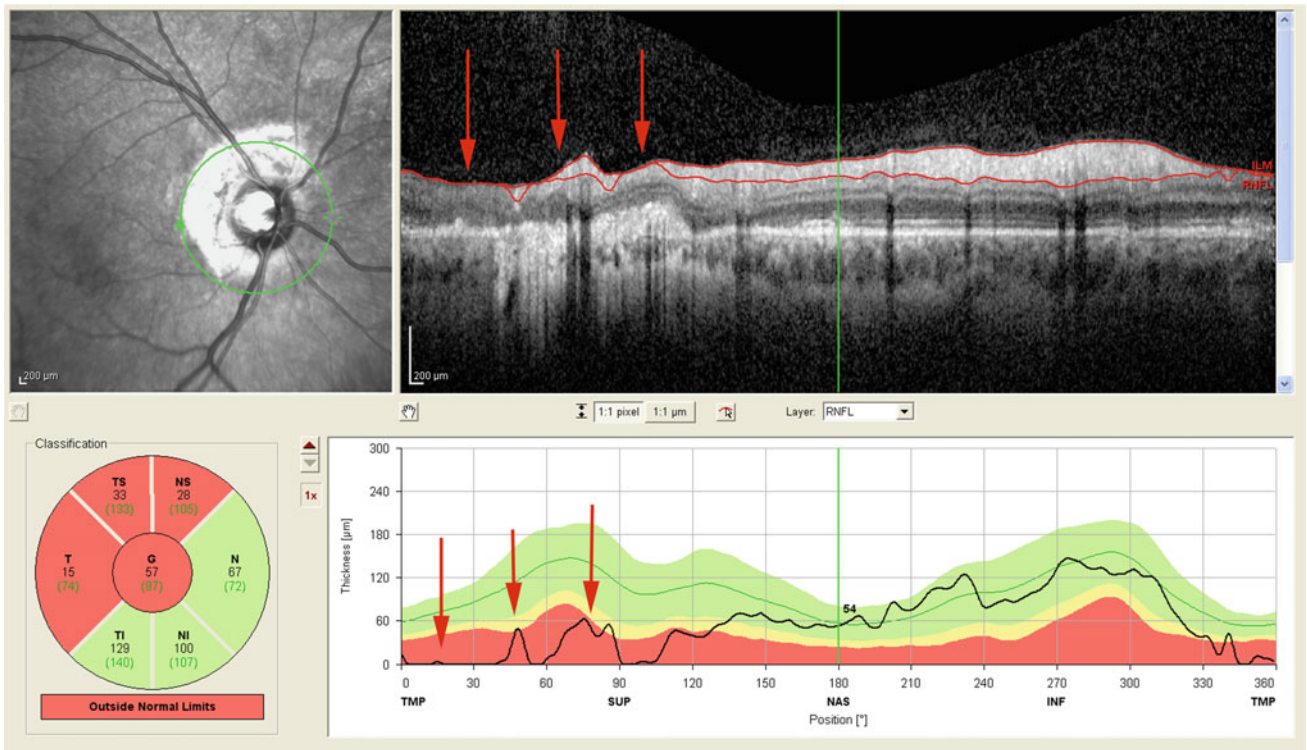


Fig. 12.7 Inner retinal layer atrophy in the nasal fovea (*red arrows*) is visible, which may occur because of retinal nerve fiber layer damage in the temporal and superior parts of the optic disc

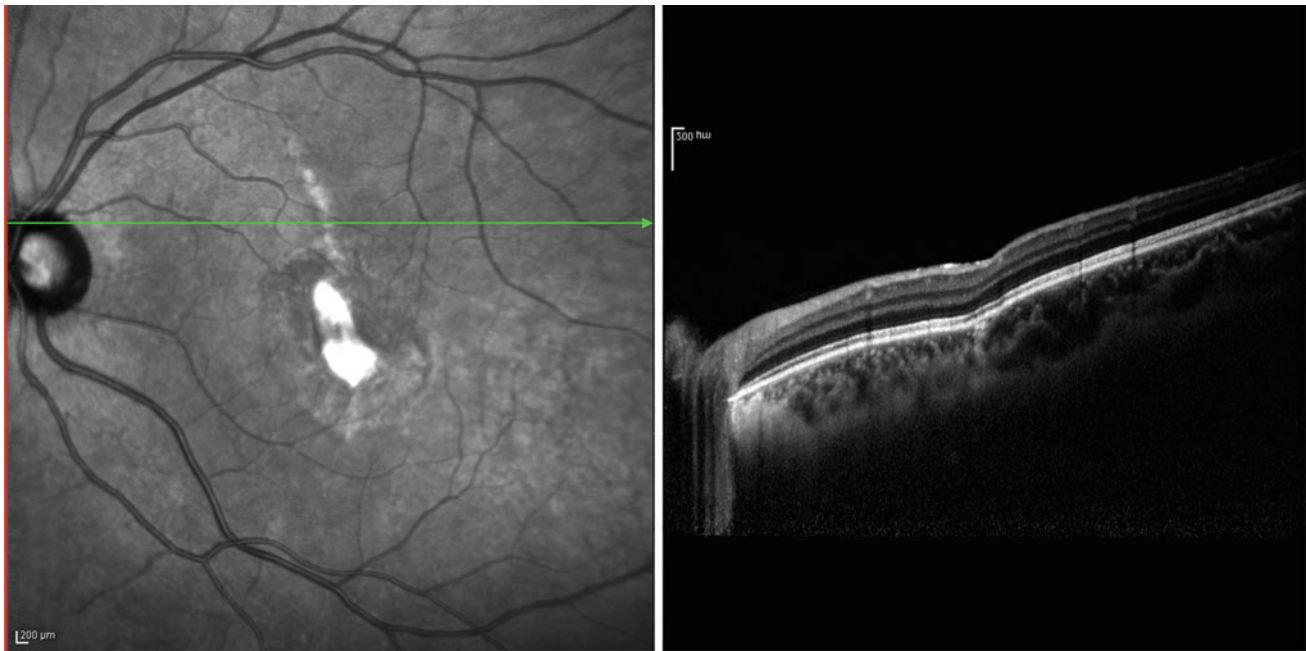


Fig. 12.8 Another example of an old choroidal rupture, which crosses the central fovea. The superior cross-sectional EDI-OCT scan shows inferior retinal deviation and choroidal atrophy with a fibrous scar. *EDI-OCT* enhanced depth imaging optical coherence tomography

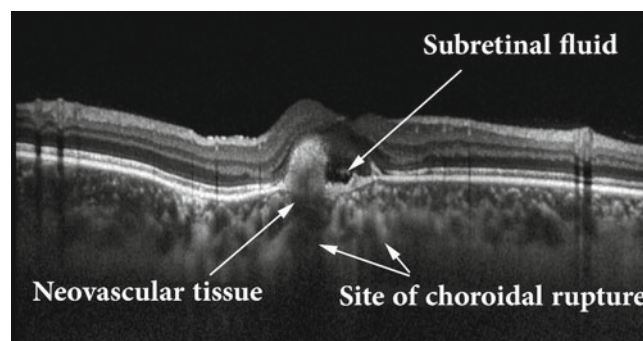


Fig. 12.9 This EDI-OCT image are from the same patient and was taken from the lower part of the rupture. It shows the growth of a neovascular membrane, subretinal fluid collection, and the site of the

previous rupture, which is revealed by thinning and fibrosis of the choroid. *EDI-OCT* enhanced depth imaging optical coherence tomography

Treatments such as argon lasers [3], which were used in the past, and photodynamic therapy [4] can help manage this complication. Antivascular endothelial growth factor therapy is a more recent therapeutic approach and more effective in the treatment of such traumatic complications [5, 6].

12.2 Acute Trauma

After a severe blunt trauma to the globe, commotio retinae (i.e., Berlin's edema), acute traumatic maculopathy, severe edema, and a small subfoveal neurosensory retinal detachment may occur (Figs. 12.11 and 12.12). The OCT image shows high reflectivity of intraretinal tissues. Such findings

were also reported by Pham et al. [7] in patients with trauma caused by a motor vehicle accident.

Severe commotio retinae can also result in a full-thickness macular hole [8]. In a case report by Ismail et al. [8], commotio retinae associated with full-thickness macular hole closed spontaneously after 1 year. The mechanism of this phenomenon may be because of traumatic damage to the outer retinal layer, including the photoreceptor layer [8]. The retina has the least support from Müller cells in the fovea and the photoreceptor outer segment, and is therefore likely to undergo the greatest deformation.

A traumatic macular hole is another consequence of ocular trauma—especially blunt trauma—and was first reported by Knapp in 1869 [9] (Figs. 12.13, 12.14, 12.15,

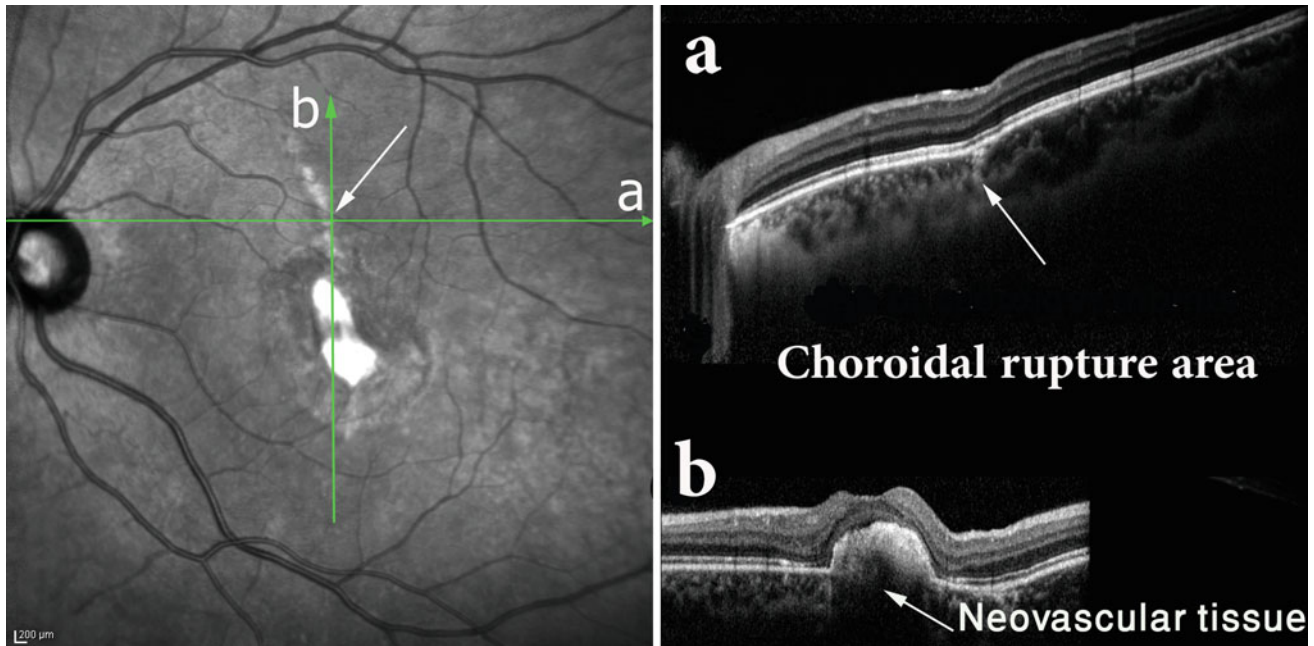
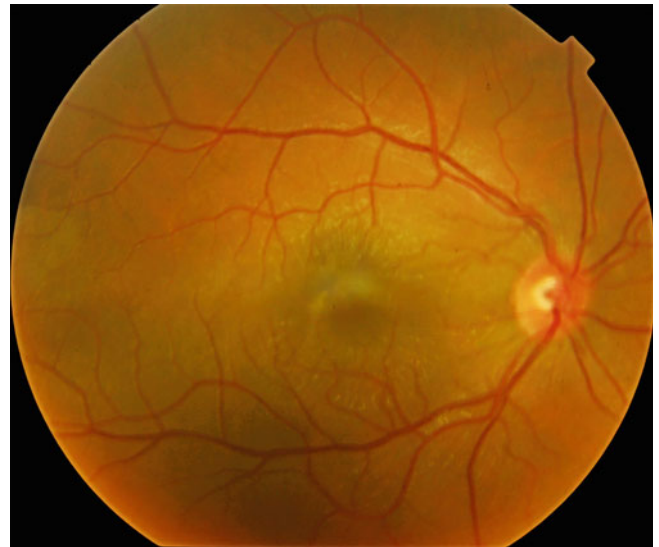


Fig. 12.10 These compound images of SLO-OCT and EDI-OCT reveal more details about this patient. In part **a**, which characterizes the EDI pattern, the exact site of the choroidal rupture is demonstrated by choroidal thinning and fibrosis. In part **b**, a large neovascular tuft with

high-reflective surface is apparent. *EDI-OCT* enhanced depth imaging optical coherence tomography, *SLO-OCT* scanning laser ophthalmoscopy optical coherence tomography

Fig. 12.11 The fundus photograph of a patient who experienced trauma caused by a gun bullet in the lower lid of the right eye and concomitant vitreous hemorrhage, vitreous base avulsion, and large inferior retinal dialysis. Not all of the aforementioned findings are presented in the color fundus photographs. The patient's vision decreased to 20/160



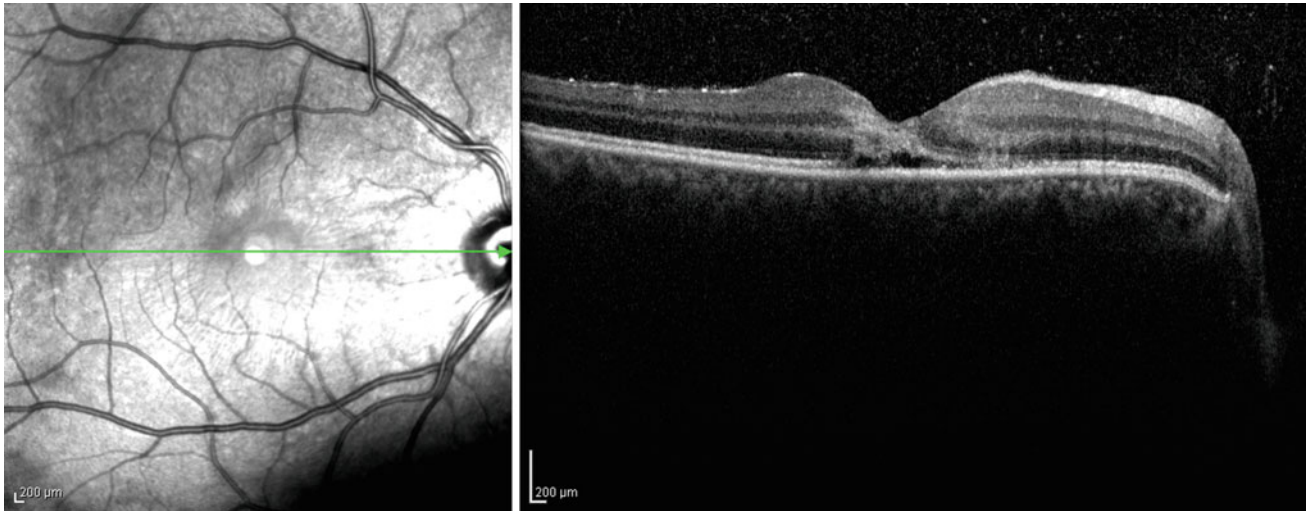


Fig. 12.12 The longitudinal optical coherence tomography image shows a small collection of subfoveal fluid with high reflectivity of the retinal layer at the central fovea. Furthermore, “foveal avulsion” occurs,

which is accompanied by decreased vision. Commotio retinae may even result in a full-thickness macular hole [8] or may resolve completely

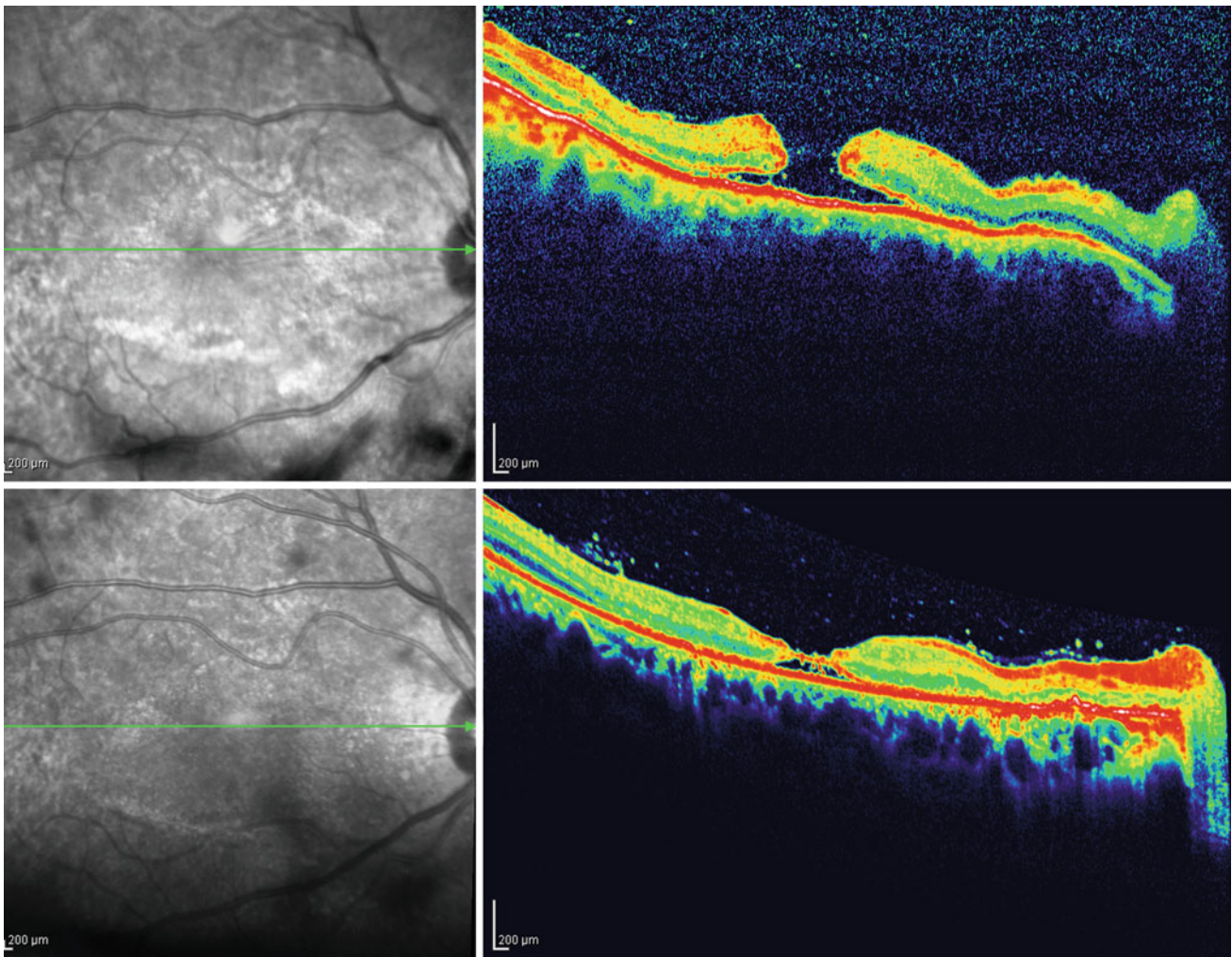


Fig. 12.13 These two OCT images were taken 12 days apart. The upper OCT image was taken a few hours after the trauma. The lower OCT image was taken 12 days later and was associated with vision

improvement. However, retinal atrophy (primarily because of the loss of photoreceptor/outer nuclear layer) predicts a poor visual outcome for this patient. *OCT* optical coherence tomography

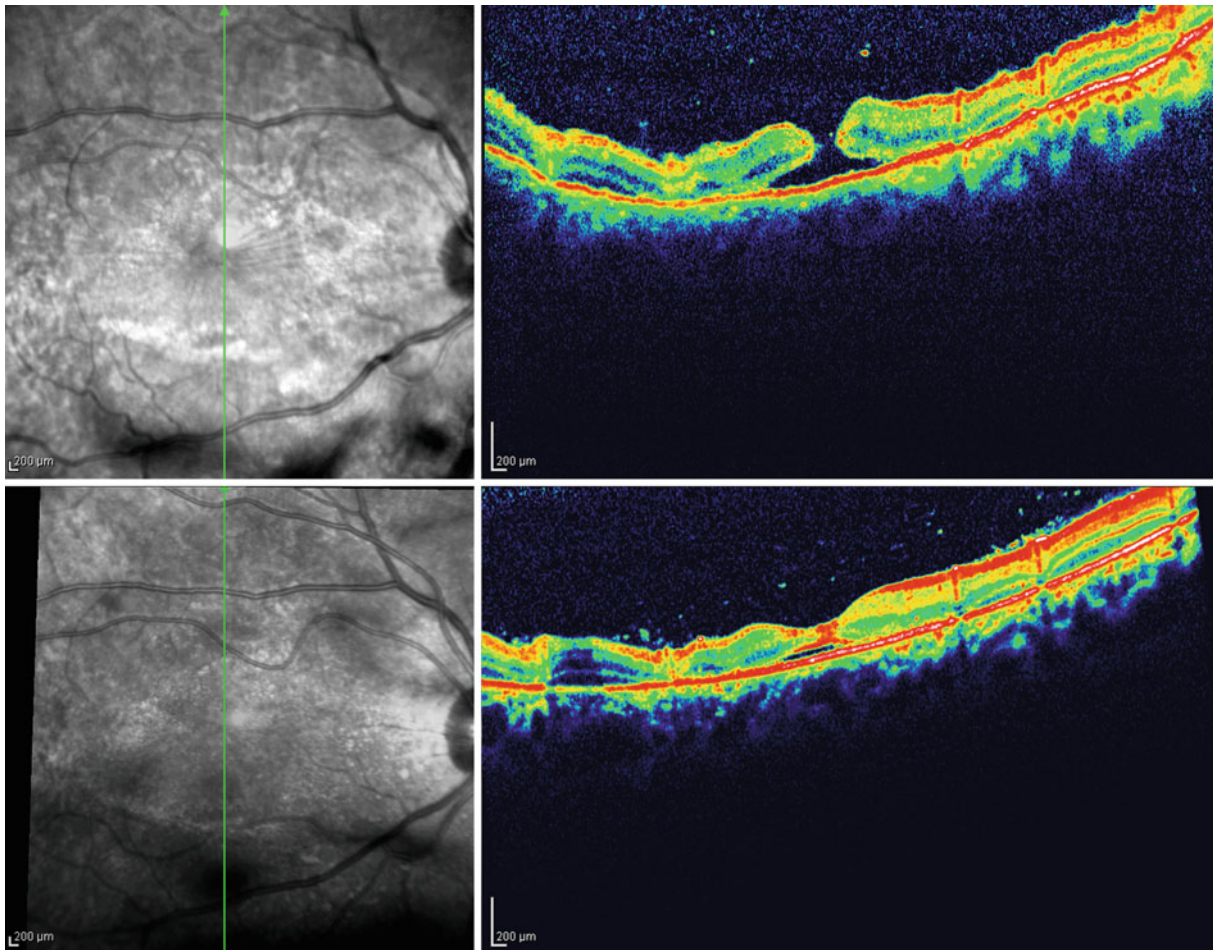


Fig. 12.14 These two OCT images show different sections from the same patient in Fig. 12.13. Central foveal layer continuity is established. OCT optical coherence tomography

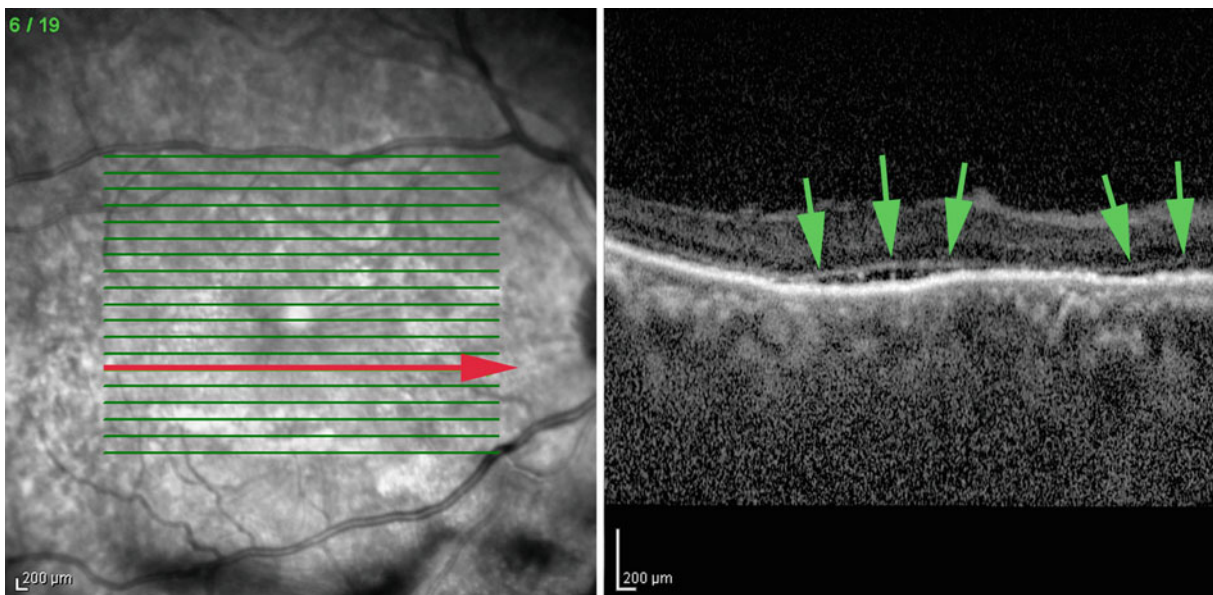


Fig. 12.15 This is the same patient (in Fig. 12.13) with different cross-sectional longitudinal OCT scans apart from the fovea. The green arrows indicate two small submacular retinal detachments. OCT optical coherence tomography

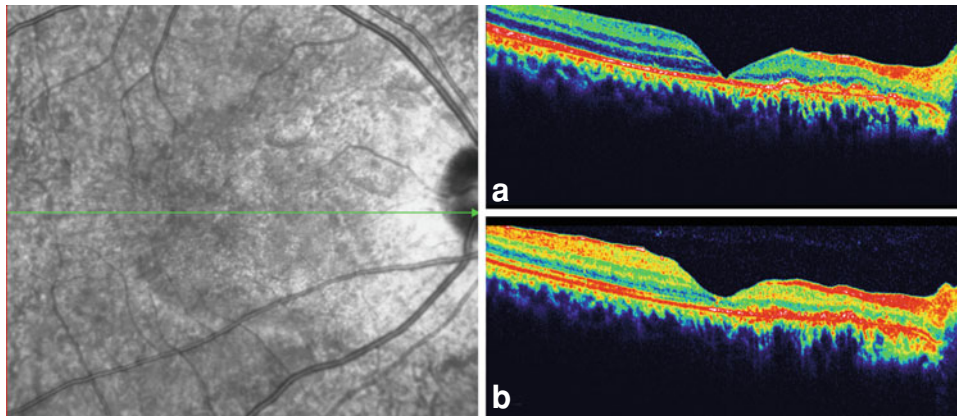


Fig. 12.16 **a** A young male patient with recent blunt trauma to the right eye, which has full-thickness macular hole with atrophic edges. His visual acuity was reduced to less than 20/200. **b** After 6 months, it

was surprising to find that the hole spontaneously closed with the regeneration of the photoreceptor layer. These findings were accompanied by increased vision to more than 20/80

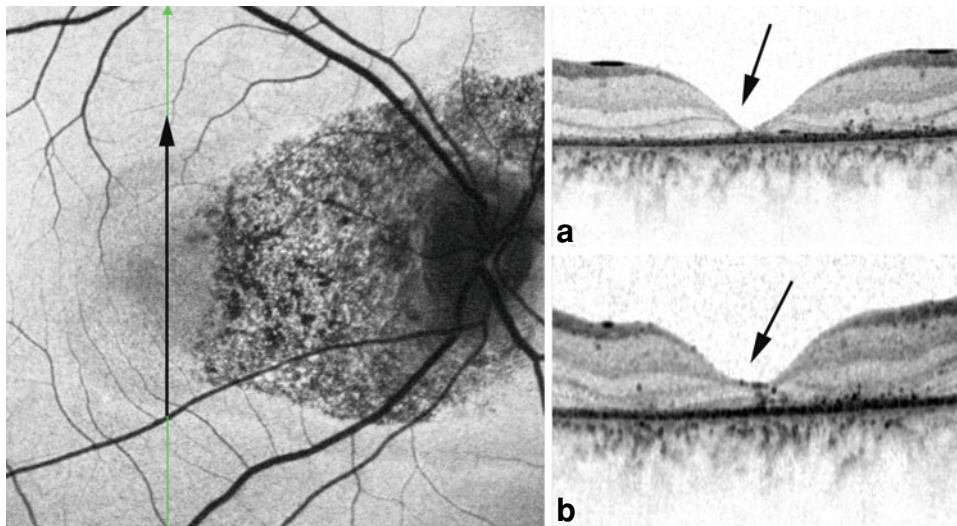


Fig. 12.17 The fundus autofluorescence image was taken after resolving the macular trauma. There is considerable and extensive retinal pigment epithelium (RPE) damage and hypertrophy around the optic disc. The regeneration of the photoreceptor layer is clearly demonstrated in the large images of the fovea. The mechanism of hole

formation in this patient may be ocular impaction and severe macular edema, which evolves to a full-thickness macular hole. The proliferation of the RPE, the glial cells, and the proliferation of the photoreceptor layer may explain the hole closure and the visual acuity improvement

12.16 and 12.17). The mechanisms for macular hole formation after ocular trauma has been evaluated by many ophthalmologists [10–12]. The presence of asymmetrical edema due to hyperpermeability of the retinal vessels after trauma; the mechanical avulsion of adherent vitreous at the time of concussion; or the extraordinary impact of the macula, which evolves to delayed macular hole after trauma, are presumptive causes for a traumatic macular hole. Traumatic macular hole usually develops shortly and simultaneously with a trauma or may have a delayed development

(approximately 1 month after the trauma [13]). Several case reports on spontaneous macular hole closure have previously been described [8, 13–15]. There are multiple mechanisms for traumatic macular hole closure: (1) the proliferation of the glial cells or the RPE, which exist around the hole, may close the defect [16]; (2) contracture of the epiretinal membrane, which may have existed around the hole, may help in bringing about apposition of the hole edge [17]; and (3) reattachment of the vitreous operculum [18].

The OCT image of a traumatic macular hole may demonstrate full-thickness retinal layer dehiscence in the fovea with irregular edges [13] or depict a thin and narrow border, or reveal typical findings that are similar to idiopathic macular holes [13] (i.e., round and elevated edges with cysts and retinal thickening at its borders). Figure 12.13 is a case of traumatic macular hole in a young female patient with severe shuttering blunt ocular trauma to her right eye who underwent OCT examination a few hours after the incident.

After a severe blunt trauma, multiple serous retinal detachments appear in the posterior pole (Fig. 12.15).

Hemorrhagic detachment of the RPE can occur after blunt trauma (Figs. 12.18, 12.19 and 12.20). The OCT image shows a dome-shaped elevation of the RPE at each hemorrhagic retinal lesion. Hemorrhagic detachment of the RPE may be associated with minimal and multiple choroidal rupture, which may be completely resolved, as depicted on OCT images. Furthermore, visual acuity may completely return to its normal value. Discontinuity in Bruch's

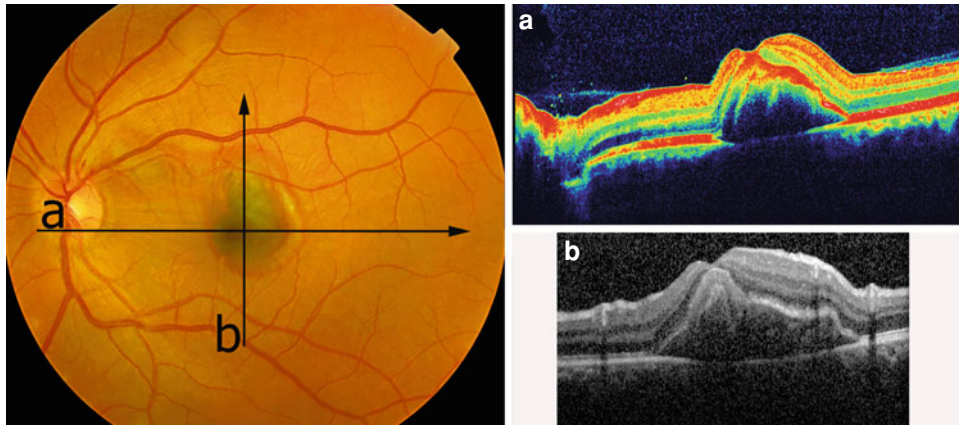


Fig. 12.18 The optical coherence tomography (OCT) image from a young man who experienced severe blunt trauma to his left eye a few hours before image acquisition. In the vertical and horizontal

cross-sectional longitudinal OCT scan, macular elevation with the accumulation of high-reflective material, which is blood, is visible

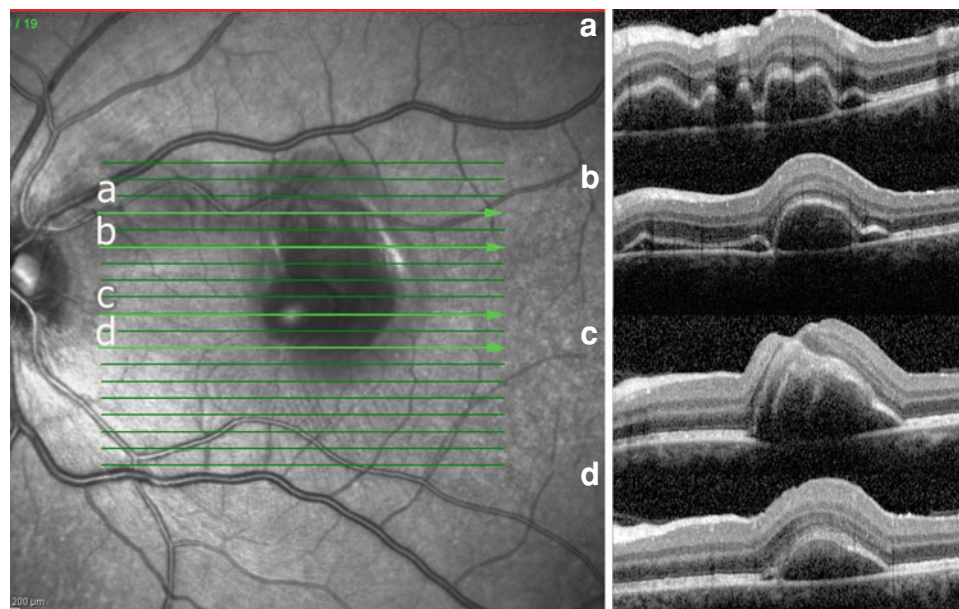


Fig. 12.19 This image includes multiple cross-sectional scans along the macular lesion and reveals clear and hyporeflective fluid accumulation around the blood

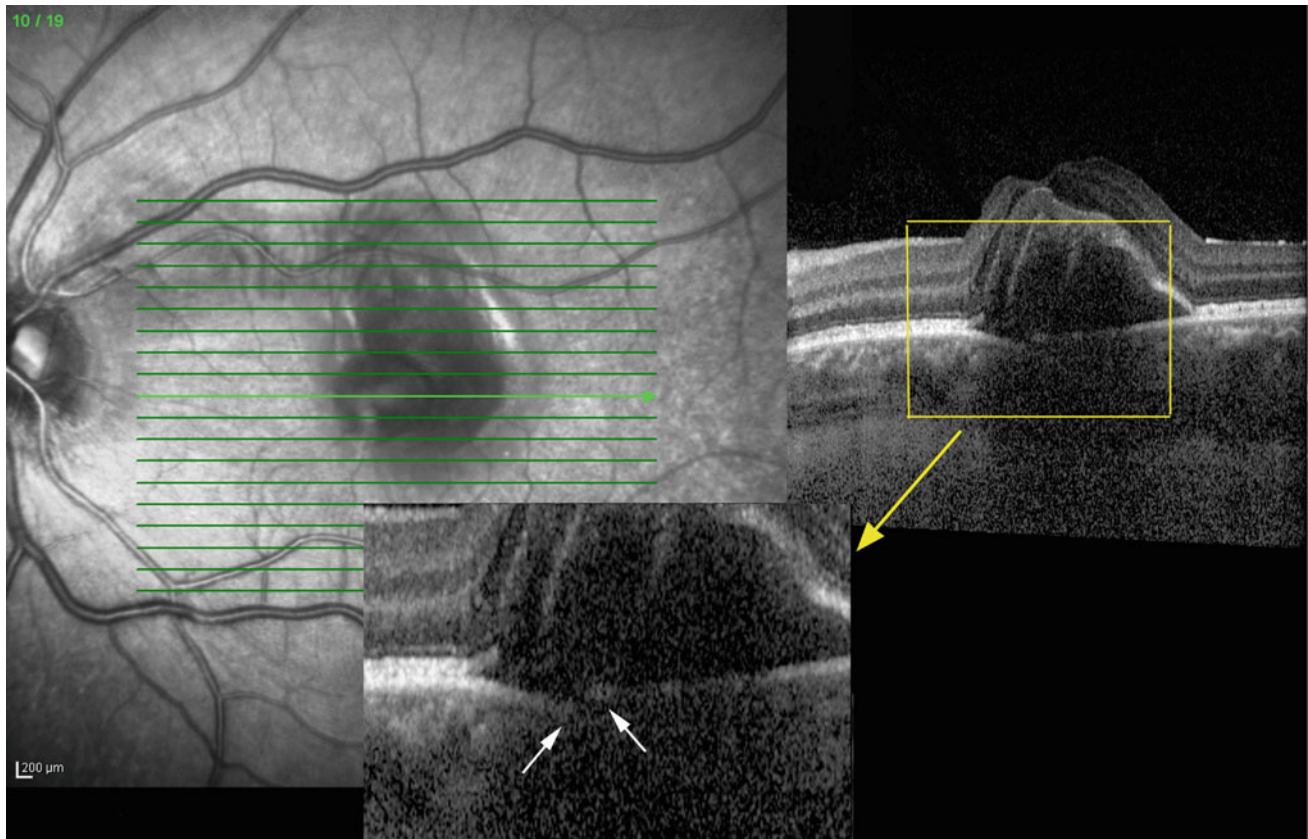


Fig. 12.20 This image is from the same patient in Fig. 12.19 and shows the site of Bruch's membrane rupture and the origin of the subretinal pigment epithelium hemorrhage, which is presumed to be choroidal vessels

membrane can lead to bleeding from choriocapillaris into the subretinal pigment epithelium or subretinal space. The sub-RPE blood is usually darker than the subretinal blood; however, the overlying commotio retina makes differentiation difficult [19]. A more severe trauma may result in Bruch's membrane rupture and subsequent sub-RPE hemorrhage and fluid collection.

12.3 Solar Retinopathy

Foveal burning can result from activities such as direct sun-gazing or working with arch-welding instruments and/or laser-pointing toys. In the early phase of solar burning, the hyporeflectivity of the outer foveal layer can be noted (Figs. 12.21, 12.22, 12.23, 12.24 and 12.25). After a few weeks, the only finding is a small outer retinal defect, which is primarily in the photoreceptor layers (Fig. 12.26).

12.4 Optical Coherence Tomography in Retinal Detachment and After Intraocular Surgery

Retinal detachment can be a complication of posterior vitreous detachment or intraocular surgery. In the first stages of detachment, OCT demonstrates a clear and hyporeflective fluid that accumulates below retina. It is sometimes difficult to differentiate between extensive central serous retinopathy with considerable subretinal clear fluid accumulation and retinal detachment with macular involvement. In retinal detachment, the outer boundary of fluid and the amount of fluid increase in the periphery cannot be clearly defined; this finding may help in differentiation (Figs. 12.27 and 12.28).

In more chronic cases, the fluid may enter intraretinal tissue, especially the outer nuclear layer, and cause considerable retinal thickening and edema.

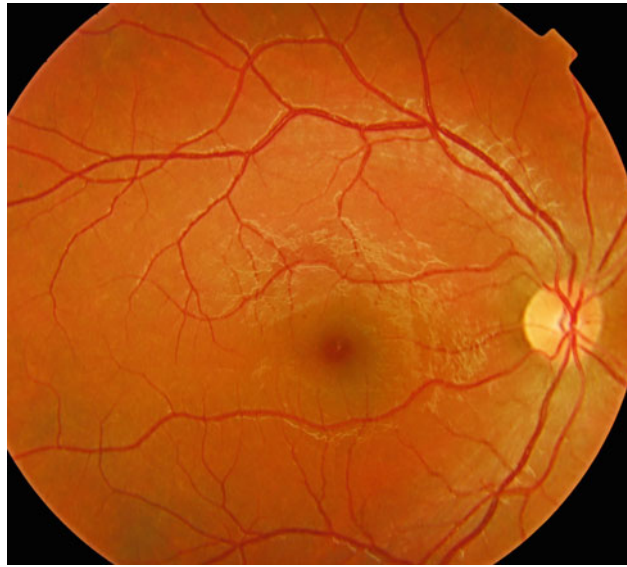


Fig. 12.21 The color fundus photograph of the right eye of a 23-year-old man 3 hours after sun-gazing. Fovea seems to have larger diameter of red color

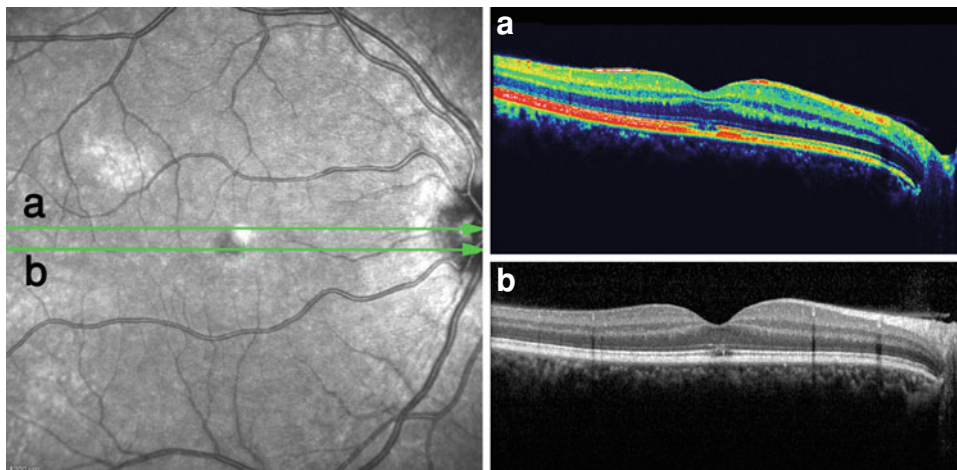


Fig. 12.22 The SLO-OCT longitudinal B-scans are of the right eye of the same patient in Fig.12.21. In the perifoveal area, the hyporeflectivity is more noticeable, and the lesion is in the perifoveal area rather

than underneath it. *SLO-OCT* scanning laser ophthalmoscopy optical coherence tomography

After ocular surgery, especially scleral buckling surgery, failure to improve vision is a challenging dilemma for ophthalmic surgeons. Despite a successful retinal detachment surgery, which involves macular and complete retinal reattachment on fundus examination, visual improvement may remain incomplete. Several pre- and postoperative factors may contribute to incomplete improvement such as the duration of the detachment, cystoid macular edema in post-surgical period [20], the consequence of development

of or persistence of an epiretinal membrane [21], pigment migration, macular hole, retinal folds, myopic shift, and cataract. Even in the absence of such complications, poor final postoperative visual acuity can occur [22].

The distortion of the inner segment/outer segment (IS/OS) junction occurs in 82% of patients, cystoid macular edema in 12% of patients, subretinal fluid in 18% of patients, and formation of an epiretinal membrane in 59% of patients [23]. After the invention of OCT, studies have shown that



Fig. 12.23 These color fundus photographs are from another young man, who worked with arch-welding equipment without using protective goggles. He experienced bilateral paracentral scotoma a few hours before his visit

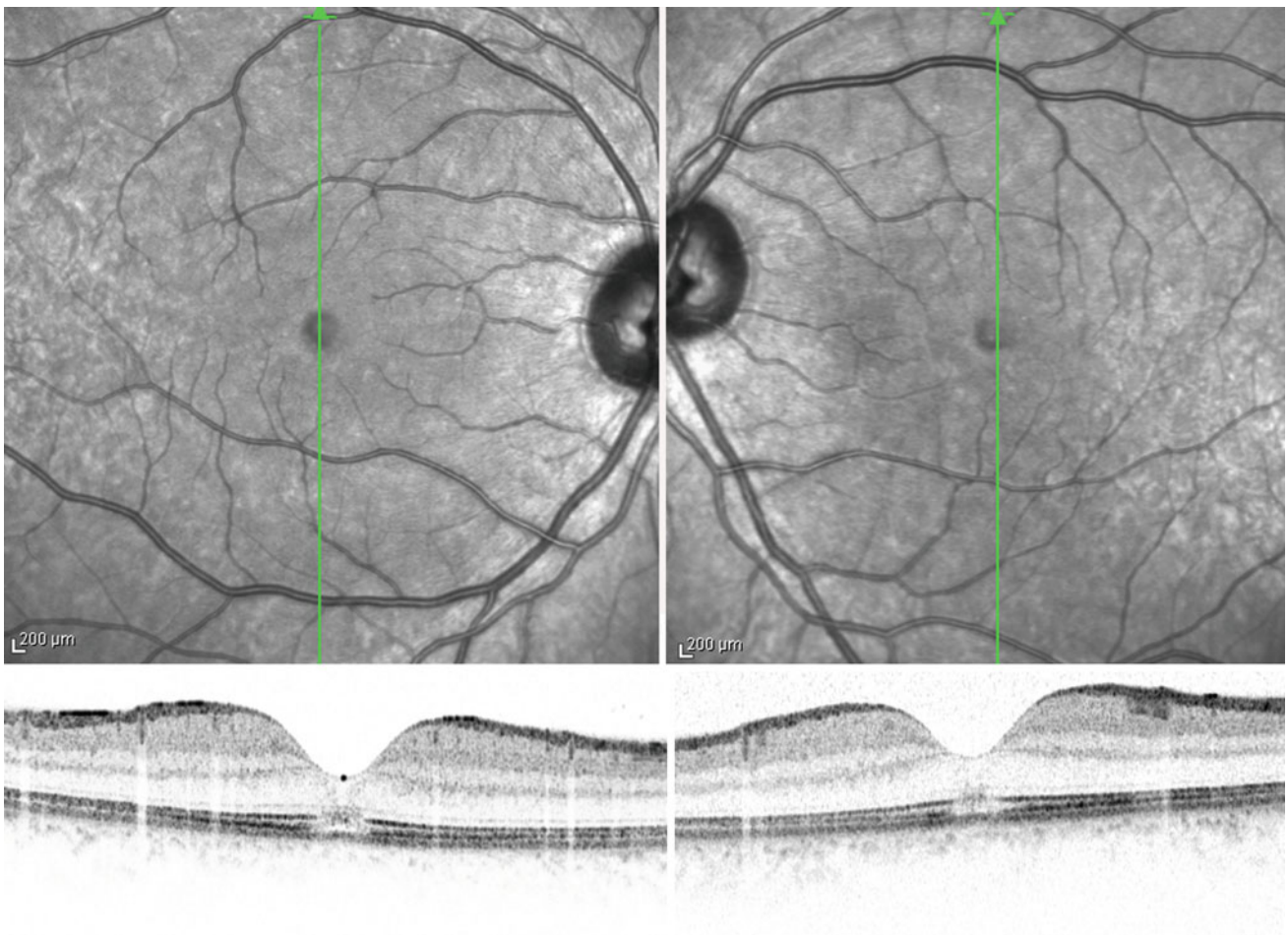


Fig. 12.24 These SLO-OCT images are from the same patient in Fig.12.23. Loss of outer retinal contour at foveal center is remarkable. *SLO-OCT* scanning laser ophthalmoscopy optical coherence tomography

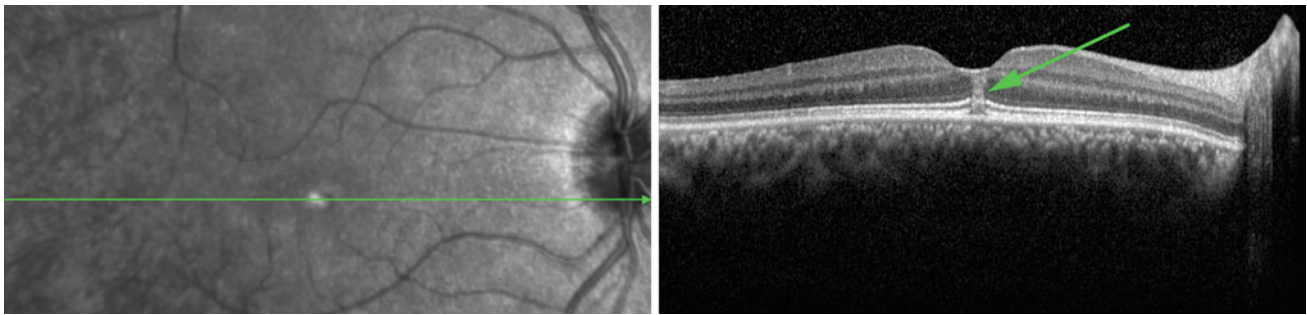


Fig. 12.25 The SLO-OCT image is of the eye of a 12-year-old boy who experienced scotoma due to prolonged gazing at laser pointers. The individual's vision had subsequently decreased to 20/80. In this

patient, the burning and foveal full-thickness damage are evident. *SLO-OCT* scanning laser ophthalmoscopy optical coherence tomography

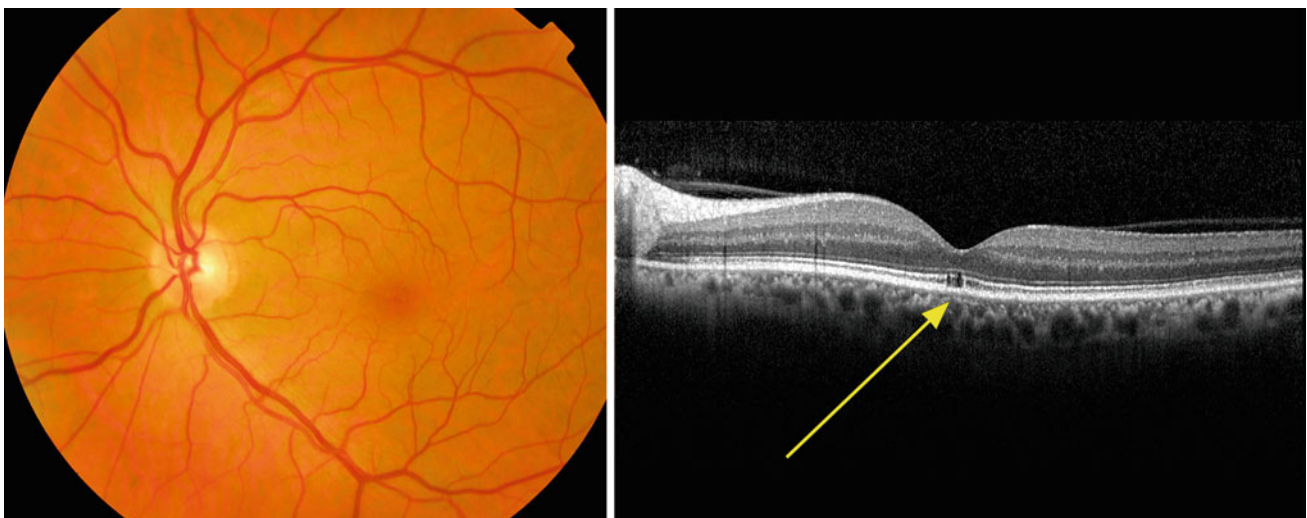


Fig. 12.26 Color fundus photo and OCT of a 64-year-old male with history of solar burn few years ago and vision of 20/30. Yellow arrow denote toward small outer retinal defect

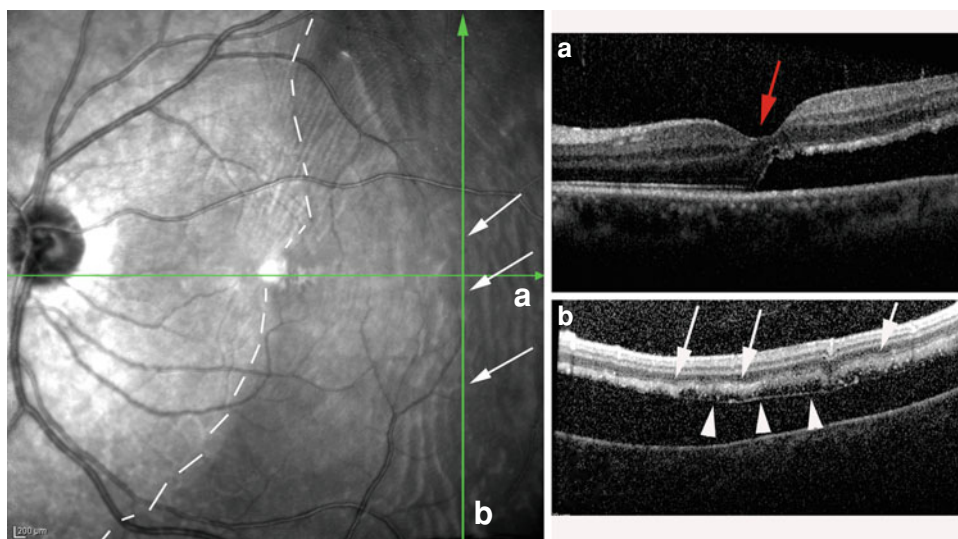


Fig. 12.27 Inner layer undulations (*white arrows*) help in differentiating retinal detachment. These undulations are consistent with retinal undulations, which are seen in fundus examinations in rhegmatogenous retinal detachment. The dashed white line represents the outer boundary

of the detachment, which partially involves the fovea. Early stage of a subretinal fibrous band (*arrowheads*) is visible at the outer layer of the detached retina. These findings are usually noted in longstanding detachments

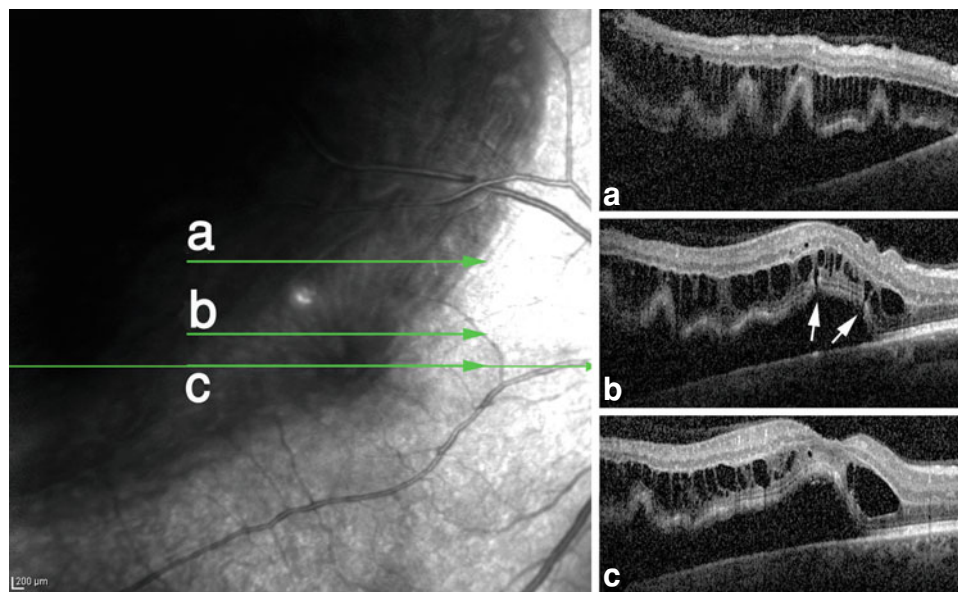


Fig. 12.28 The patient has longstanding localized retinal detachment that involves central fovea. Parts a-c represent multiple horizontal longitudinal OCT scans and were taken in multiple sections. Part “a” shows severe undulations at the outer layers of the detached retina. This image shows longstanding retinal detachment associated with

retinoschisis. In part “b”, the white arrows show the pathways through which the fluid enters the intraretinal space. Part “c” crosses the fovea. Multiple cystic spaces in the fovea and considerable outer nuclear edema are visible

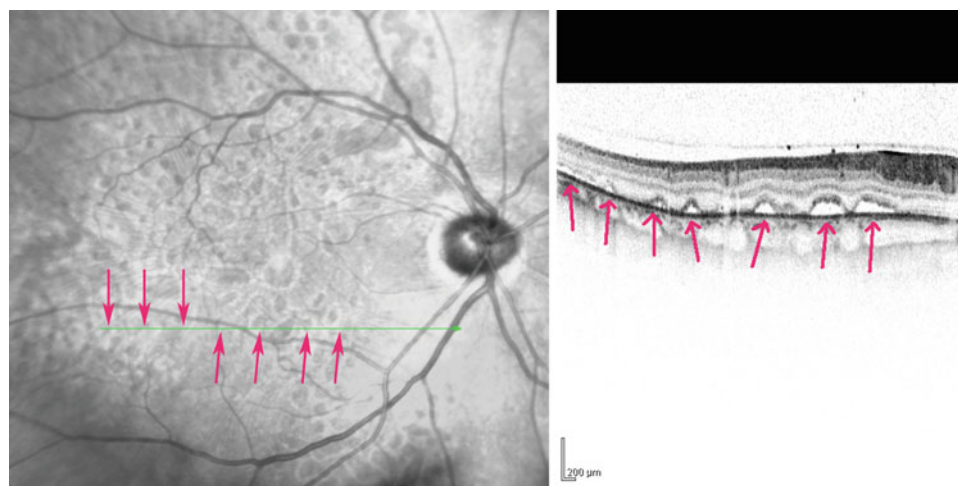


Fig. 12.29 The SLO-OCT images from a patient who underwent scleral buckling surgery with residual blurring of vision 2 months after the operation. Multiple pockets of subretinal fluid (red arrows) are often detected after retinal detachment surgery, and extend to areas that

were previously detached. Subfoveal fluid retention in this patient explains the mild residual blurring of vision. *SLO-OCT* scanning laser ophthalmoscopy optical coherence tomography

long-term persistence of subfoveal fluid, especially after sclera buckling surgery, may be associated with limited visual recovery [22, 24–26].

After a retinal detachment surgery, residual subretinal fluid, especially in the subfoveal area, is a factor that precludes complete vision improvement (Figs. 12.29, 12.30,

12.31, 12.32, 12.33, 12.34 and 12.35). However, Baba et al. [27] found that, at least 6 months after surgery, residual subretinal fluid did not influence the recovery of vision in their study.

In 55–68% of patients with retinal detachment associated with foveal detachment with sclera buckling, residual

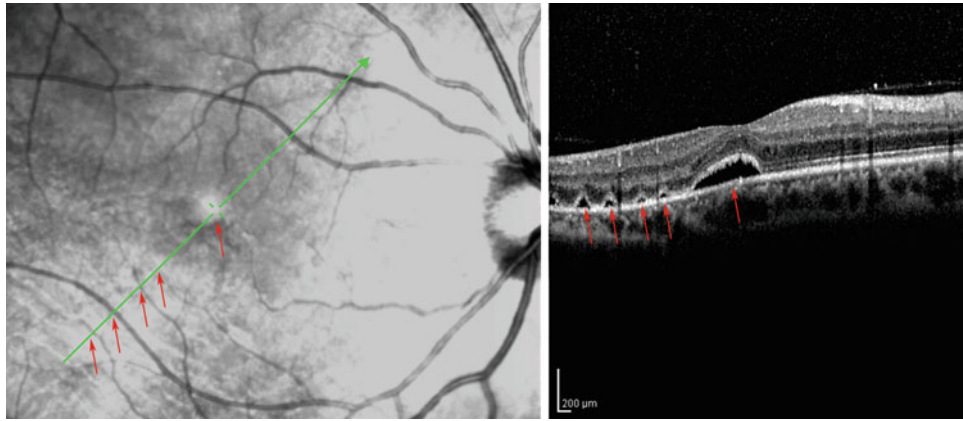


Fig. 12.30 The SLO-OCT images from a patient who underwent scleral buckling surgery with residual blurring of vision 2 months after the operation. Multiple pockets of subretinal fluid (*red arrows*) are often detected after retinal detachment surgery, and extend to areas that

were previously detached. Subfoveal fluid retention in this patient explains the mild residual blurring of vision. *SLO-OCT* scanning laser ophthalmoscopy optical coherence tomography

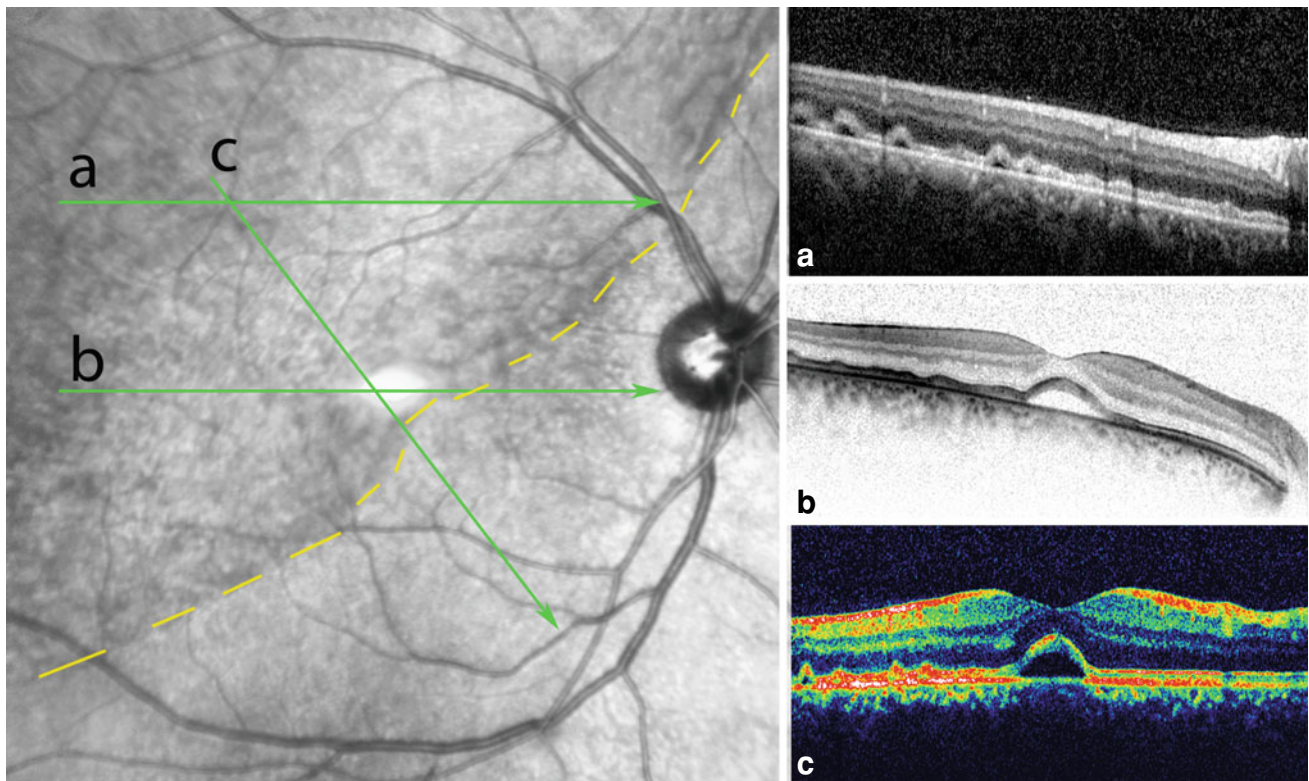


Fig. 12.31 The SLO-OCT image of the eye of a 29-year-old man with rhegmatogenous retinal detachment who had scleral buckling surgery with cryopexy and subretinal fluid drainage. He complained of dysmorphopsia and blurred vision 1 month after surgery. The previously detached area, which is in the superotemporal area, is demarcated and localized by the yellow line. The left panel shows the different cuts

across the retina. The SLO image displays multiple round and dark areas, which represent residual subretinal fluid pockets. In the OCT image, the undulations of the photoreceptor layer in the previously detached retina are visible with neurosensory retinal detachment in the subfoveal area. *SLO* scanning laser ophthalmoscopy, *OCT* optical coherence tomography

Fig. 12.32 The OCT image of the eye of a 44-year-old man who did not experience complete vision recovery after undergoing scleral buckling surgery. His visual acuity was 20/80 and 20/60 at 2 months and 6 months, respectively, after surgery. At 6 months, pockets of subretinal fluid in the extrafoveal area are considerably absorbed (*red arrows*); however, the subfoveal fluid accumulation remains unchanged. The elongation in the photoreceptors' outer segment (*yellow arrow*) indicates chronic subretinal fluid accumulation

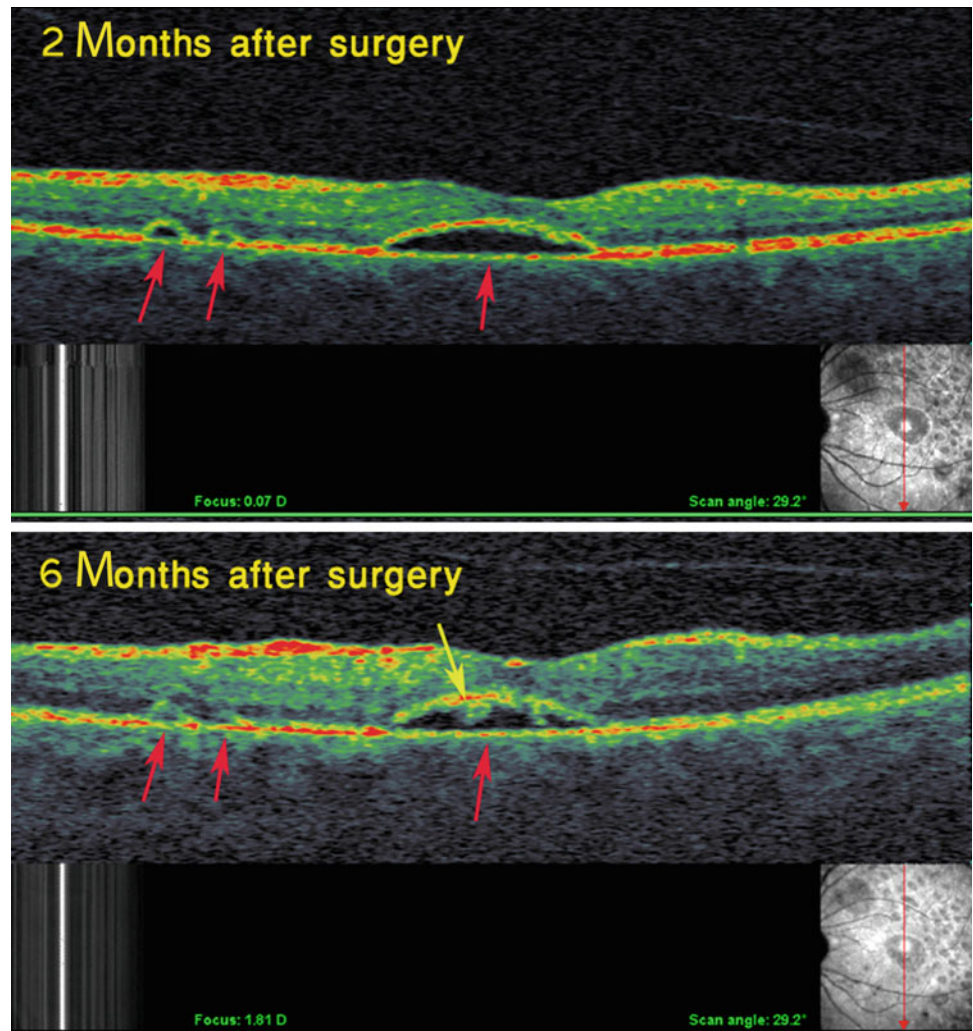


Fig. 12.33 The C-scan (coronal scan) and SLO images from the same patient in Fig. 12.32. Pockets of subretinal fluids appear as small or large circular lesions. *SLO* scanning laser ophthalmoscopy

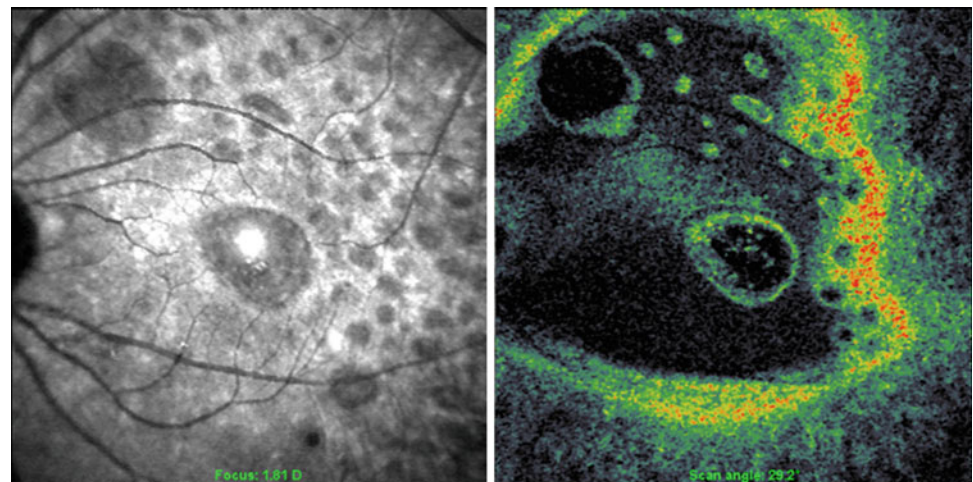


Fig. 12.34 The overlay of the SLO C-scan of a patient who had undergone scleral buckling surgery two weeks before the image was created. In the C-scan, the areas of subretinal fluid collection (*red arrows*) represent the residual fluid in previously detached retina. SLO scanning laser ophthalmoscopy

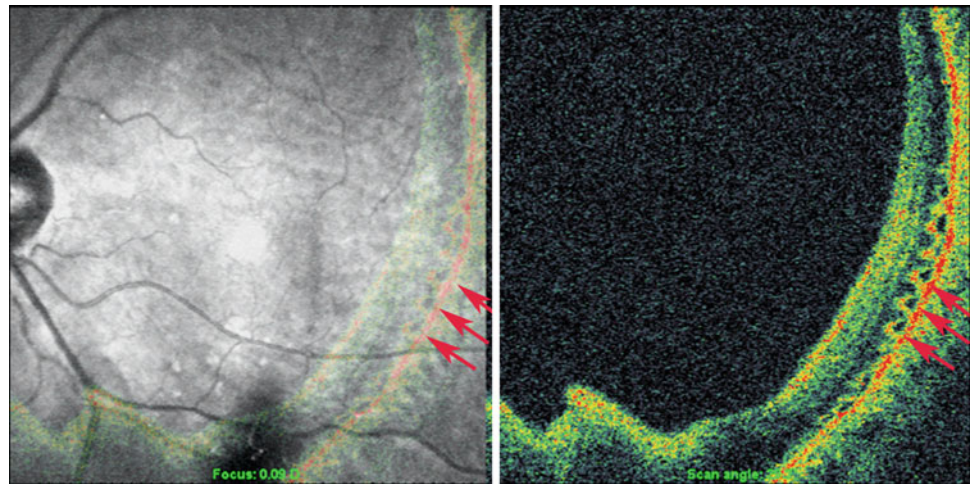
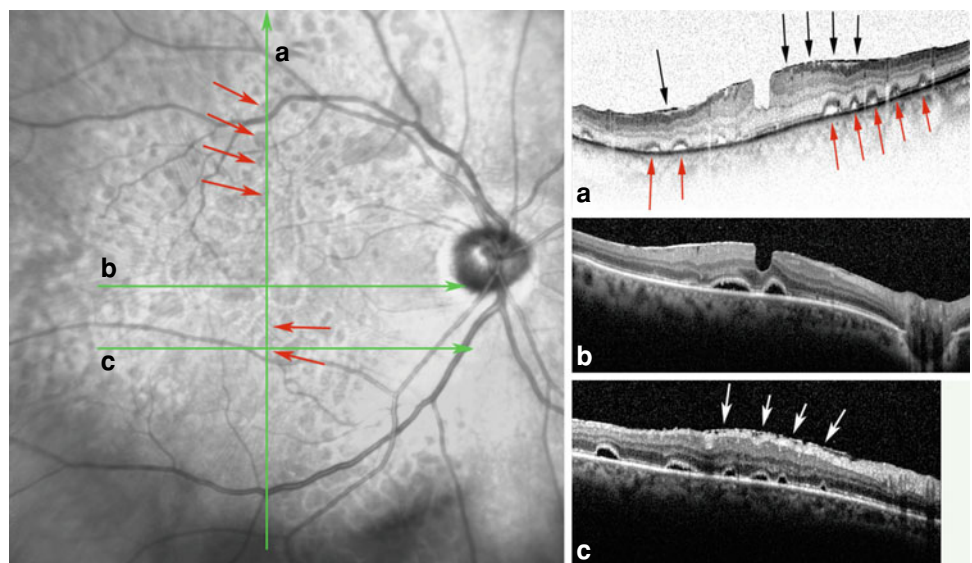


Fig. 12.35 The SLO-OCT image of an eye with high myopia in a 54-year-old woman who had undergone scleral buckling surgery 5 months before image acquisition. Multiple pockets of residual subretinal fluid are visible (*red arrows*). The epiretinal membrane, which results in retinal surface wrinkling, and lamellar macular hole formation are indicated by the white and black arrows



subretinal fluid was visible in OCT images [22, 27, 28]. The mechanism remain incompletely understood. Contributing factors may be retinal redundancy [22]; RPE dysfunction after surgery [28]; decreased choroidal blood flow by the encircling buckle [29, 30] and residual viscous fluid, which is difficult to take up by the RPE [22, 28].

Young patients with inferior retinal detachments associated with foveal detachment and an incomplete liquefied vitreous may show persistent postoperative fluid under the macula for longer periods of time than described previously, and it is unrelated to external fluid derangements during surgery [21]. This usually does not happen in patients who

undergo pars plana vitrectomy [22]. A characteristic of residual subretinal fluid is multiple subretinal pockets of residual fluid in the previously detached area of the retina.

Another etiology for inhibited visual improvement after retinal detachment surgery is damage to the photoreceptor layer due to longstanding subretinal fluid accumulation, (Fig. 12.36) which results in retinal layer malnutrition and disturbance in oxygenation. In a study by Sheth et al. [31], 100% of individuals who did not have optimal postoperative visual acuity recovery (i.e., visual acuity of lower than 20/40) experienced the disruption of the photoreceptor IS/OS junction; however, 28% of individuals had an optimal

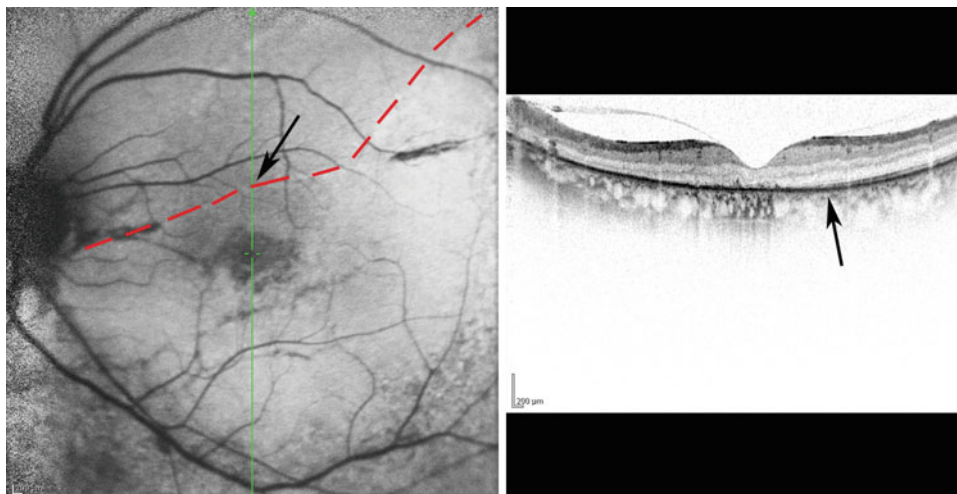


Fig. 12.36 The OCT image of the eye of a patient who had undergone retinal detachment surgery in the past. The upper limit of the subretinal fluid is indicated by the red dashed line. The photoreceptor layer damage began at the upper limit of the red line (*black arrows*). Atrophy and segmentation of the photoreceptor layer in the fovea with

subsequent outer nuclear layer atrophy explain the patient's poor visual recovery after the operation. The damage to the RPE in the foveal area, which results in the visibility of the underlying choroidal plexus, is also depicted. *OCT* optical coherence tomography, *RPE* retinal pigment epithelium

postoperative visual acuity of greater than 20/40. The anatomic result of retinal detachment surgery was excellent, although the visual result was undesirable because these factors contributed to atrophy and destruction of the photoreceptor layer. Optical coherence tomography can detect these changes accurately, and especially in cases that are not apparent by ophthalmoscopy.

12.5 Cystoid Macular Edema

Cystoid macular edema (CME), especially after a complicated cataract surgery, is one of the most common reasons for decreased vision (Fig. 12.37). Macular thickness increases during the postoperative early period after uncomplicated cataract surgery [32, 33] (Fig. 12.38). The OCT is a powerful

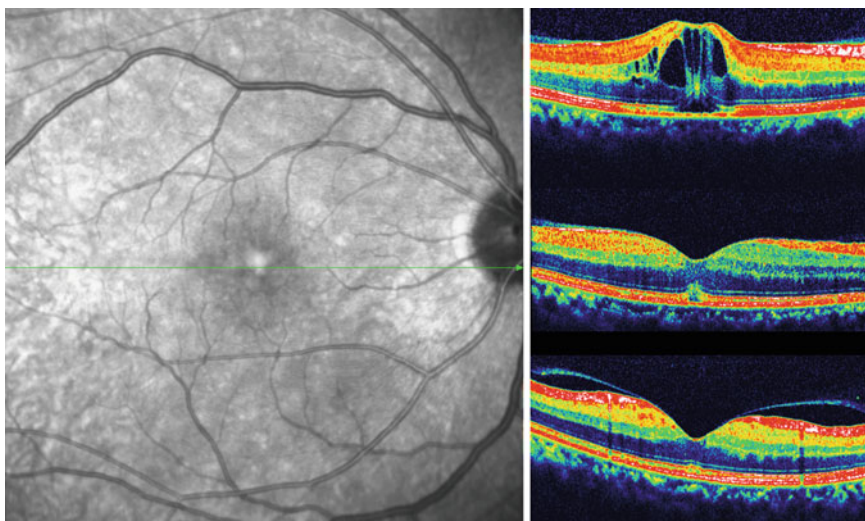


Fig. 12.37 The SLO-OCT image of the eye of a 55-year-old woman who had undergone cataract surgery and IOL implantation. Two days after the surgery, her VA was 20/25; 1 month later, her vision had decreased and her VA was 20/60. The OCT images obtained 1 month, 2.5 months, and 4.5 months postsurgery reveal large cystic changes in the fovea and foveal elevation, and small subfoveal fluid collection. After 2.5 months, the cystic changes resolved, and only a small residual

subfoveal detachment remained. Greene et al. [37] report that small subfoveal detachment implies mild CME. At this patient's final visit, there was complete resolution of the cystoid edema; however, macular thickness remained higher than the normal range. *CME* cystoid macular edema, *IOL* intraocular lens, *SLO-OCT* scanning laser ophthalmoscopy optical coherence tomography, *VA* visual acuity

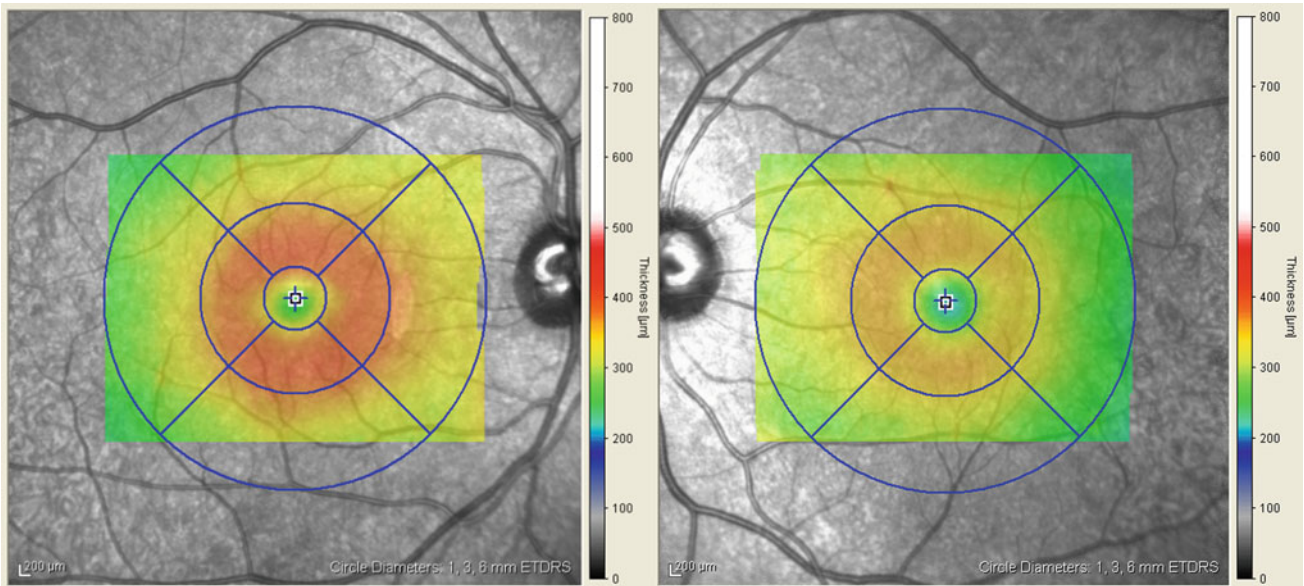


Fig. 12.38 Two topographic maps from a patient who had undergone cataract surgery 2 months before the date of image acquisition. The patient had experienced decreased vision a few weeks after the surgery.

The total macular volume in the right eye and the left eye is 8.08 mm^3 and 7.45 mm^3 , respectively

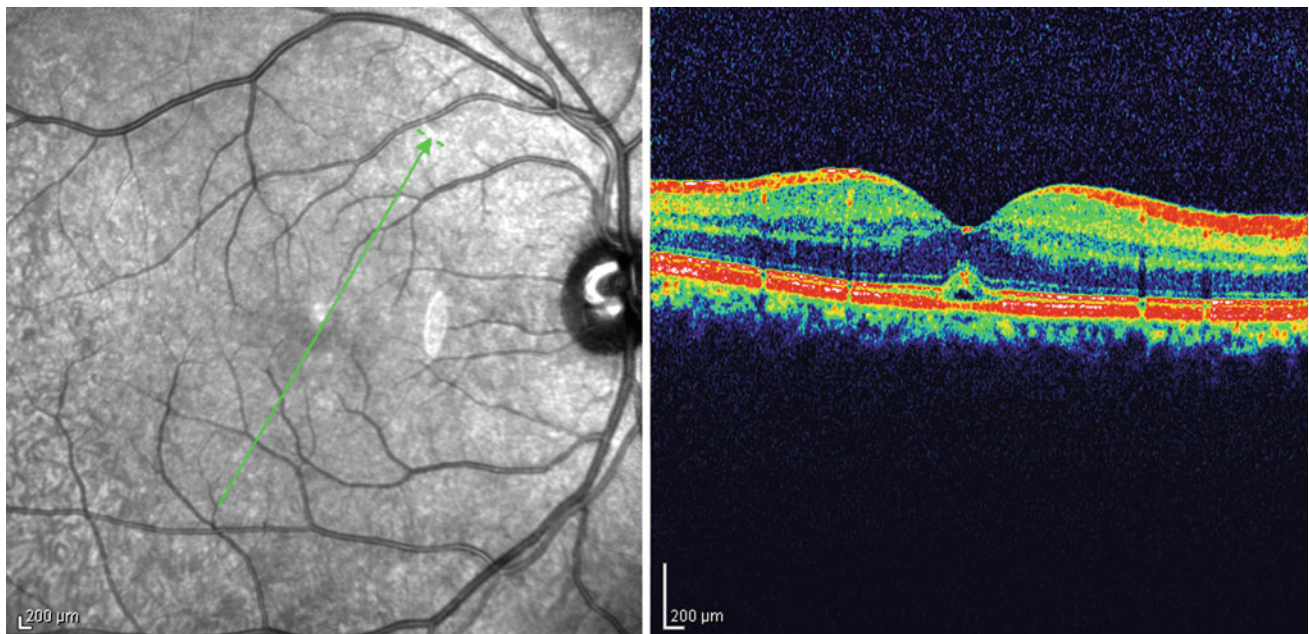


Fig. 12.39 The increased macular volume suggests CME. However, the OCT examination shows only small subfoveal retinal detachment with mild foveal thickening. There is no discrete cystic space in the

fovea. This condition suggests early or mild CME. *CME* cystoid macular edema, *OCT* optical coherence tomography

and noninvasive test for the diagnosis and follow up of these patients [34]. Some research indicates that three-dimensional OCT (3D-OCT) is more sensitive and has better intergrader agreement for detecting CME, compared to fluorescein angiography (FA) [35]. The sensitivity for the detection of definite CME is higher for 3D-OCT (95%) than for FA (44%). In a comparison of the two methods for detecting macular edema in diabetic patients, Ozdek et al. [36] found

that OCT was more sensitive than FA, especially for the cystoid pattern of macular edema.

A small subfoveal detachment that is accompanied by foveal thickening but without a discrete cystic space may represent mild resolving CME (Fig. 12.39). In very mild cases, retinal thickening in the macular area may be the only sign of CME (Figs. 12.40 and 12.41).

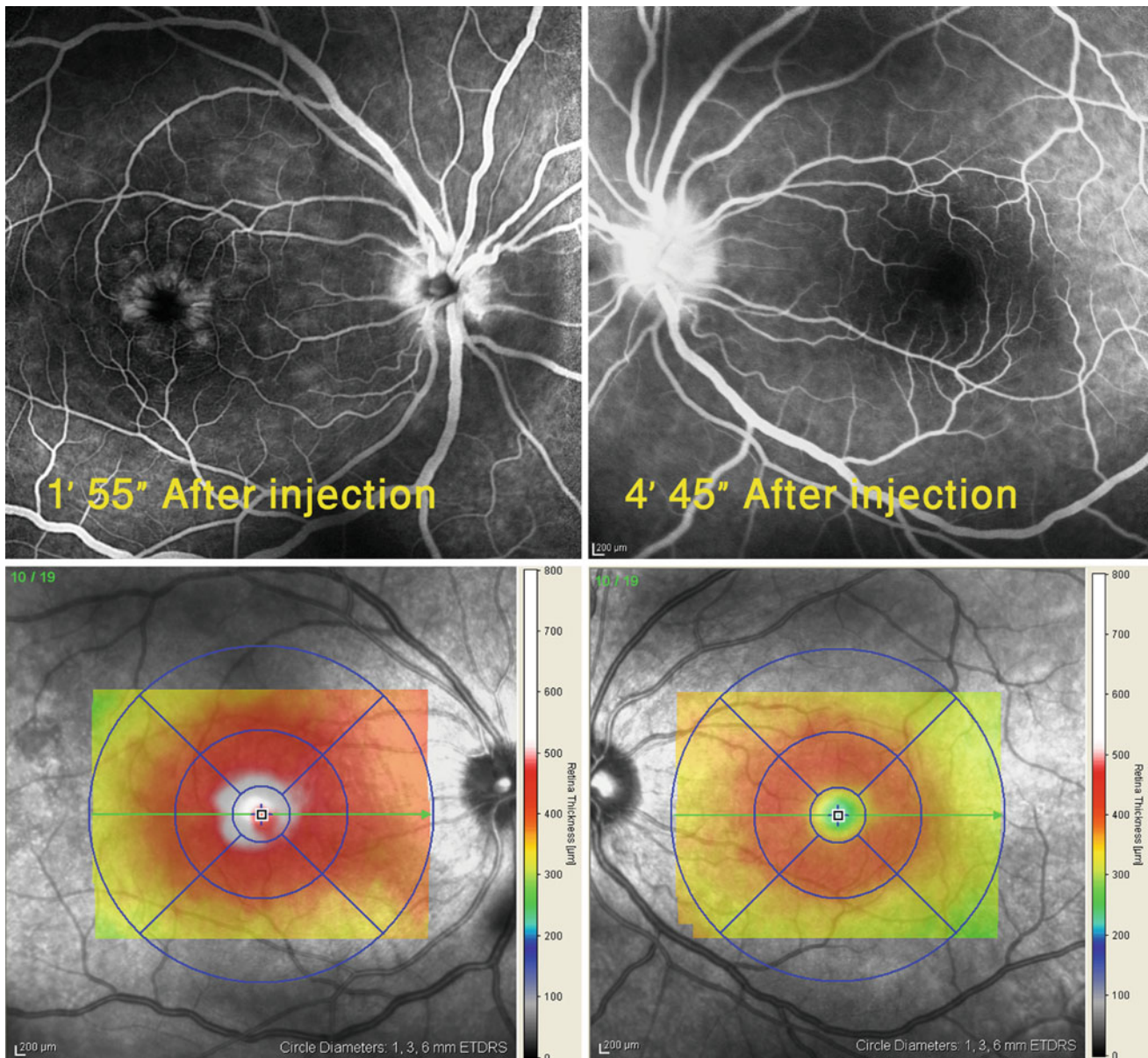


Fig. 12.40 These topographic maps and fluorescein angiography images are from a young man with bilateral uveitis and severe cystoid macular edema and vitritis in the right eye and normal macular examination by indirect ophthalmoscopy in the left eye. On fluorescein angiography, the disruption of the blood ocular barrier is more precise in the right eye. The pooling of the dye in multiple cystic spaces and the

honeycomb pattern in the macula of the right eye with optic disc hyperfluorescence in both eyes represent disruption of the blood ocular barrier. The topographic map of the right eye is consistent with central foveal edema and elevation. However, in the left eye, only total macular volume and the retinal thickness increases are visible

Early CME changes may be in the form of a small increase in the foveal volume or thickness. With increased severity of CME, a small subfoveal detachment may appear. However, cystic changes appear only in more advanced forms of CME.

In most new OCT system, the software application is used to draw the line of thickness. In the follow-up OCT examination, the computer software compares the exact points to one another and thus can compare similar points in the macula from the previous examination. This comparison

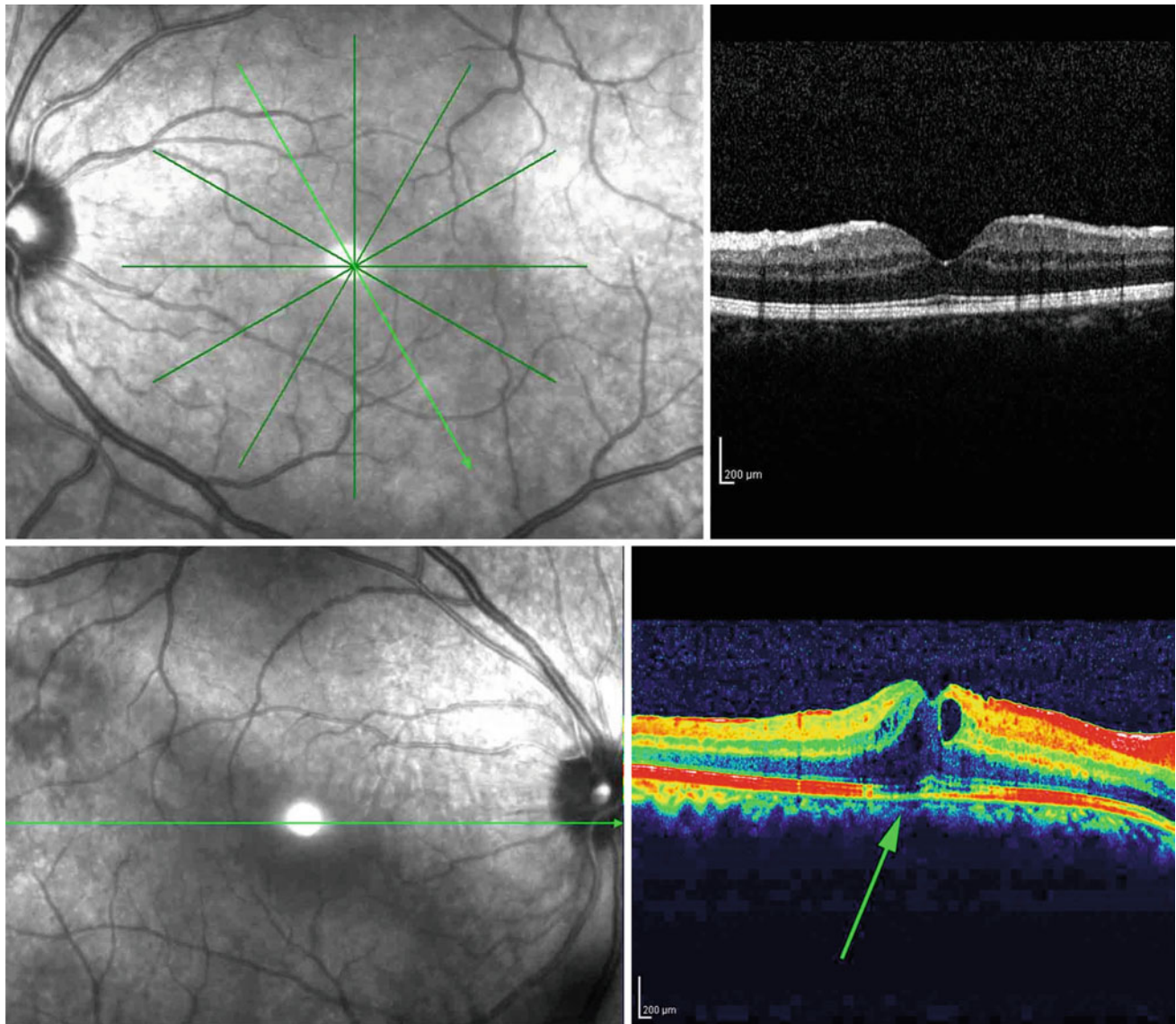


Fig. 12.41 The longitudinal cross-section OCT image of the right eye shows foveal elevation and large cystic spaces. Hyporeflectivity in the base of the fovea (*arrow*) results from the barrier effect of the vitreous

opacity for the laser wave penetration and shadowing on the retina. In the left eye, homogeneous retinal thickening exists but cystic spaces are not visible. *OCT* optical coherence tomography

is very helpful for the follow up of patients with CME, (Fig. 12.42) and allows appropriate decisions for their future treatment plans.

12.6 Hypotony Maculopathy

Hypotony maculopathy is retinopathy associated with hypotonicity of the globe, and was first described by Delaporta [38]. Surgery, especially for the treatment of glaucoma (20%) [39–41], may be complicated by hypotony and

subsequent retinal changes. This condition may also occur after perforating eye injuries. The predisposing factors for this type of retinopathy include the following: the use of antimetabolites [39–45], young age [38, 46], myopia [47–50], primary filtering surgery, systemic illnesses, and the elevated preoperative intraocular pressure (IOP). The signs of hypotony maculopathy in the fundus view include papilledema, retinal vascular tortuosity, full-thickness retinal and choroidal folds, and choroidal vessel dilation and engorgement. Collapse of the inward scleral wall may lead to chorioretinal wrinkling. Associated signs could be cystoid

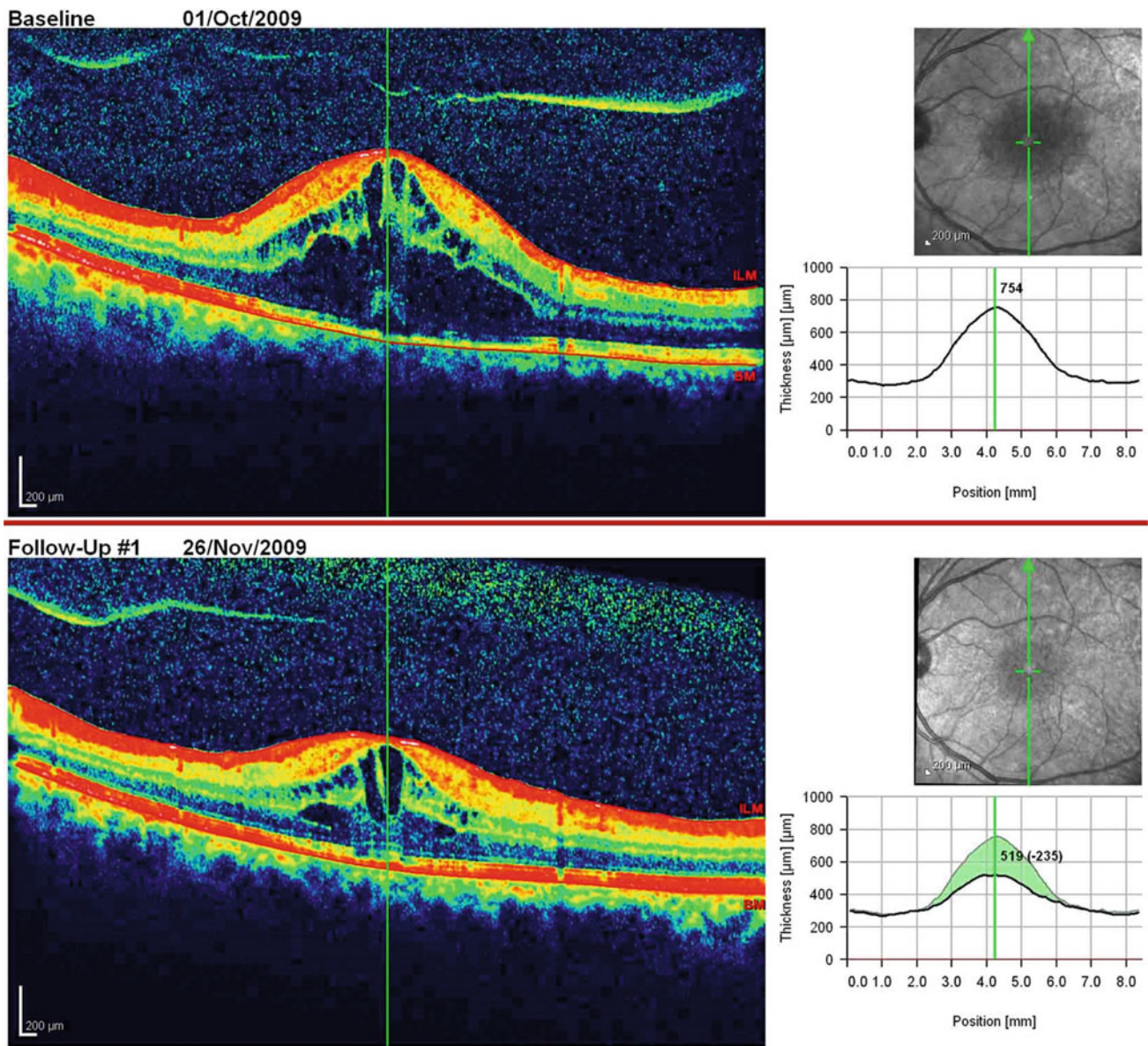


Fig. 12.42 Illustrates the results of two OCT examinations of a patient. The images were created 56 days apart. They exhibit the improvement and partial resolution of CME. CME cystoid macular edema, OCT optical coherence tomography

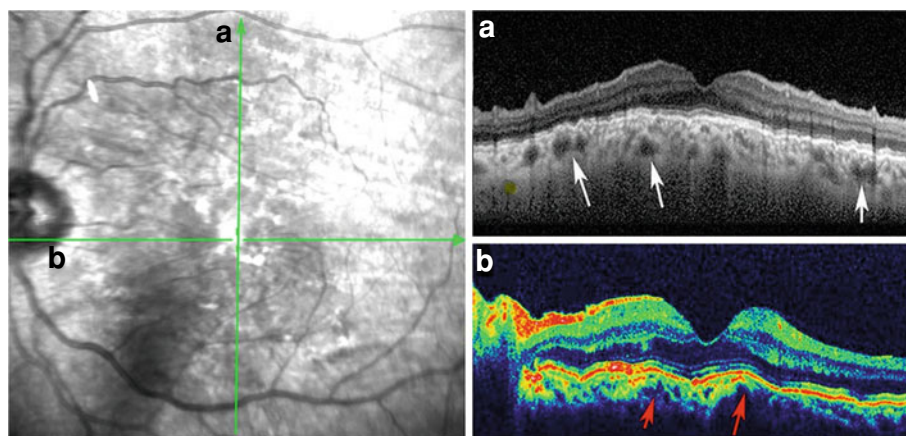


Fig. 12.43 The two vertical and horizontal macular cross-sections show engorgement of choroidal vessels (white and red arrows)

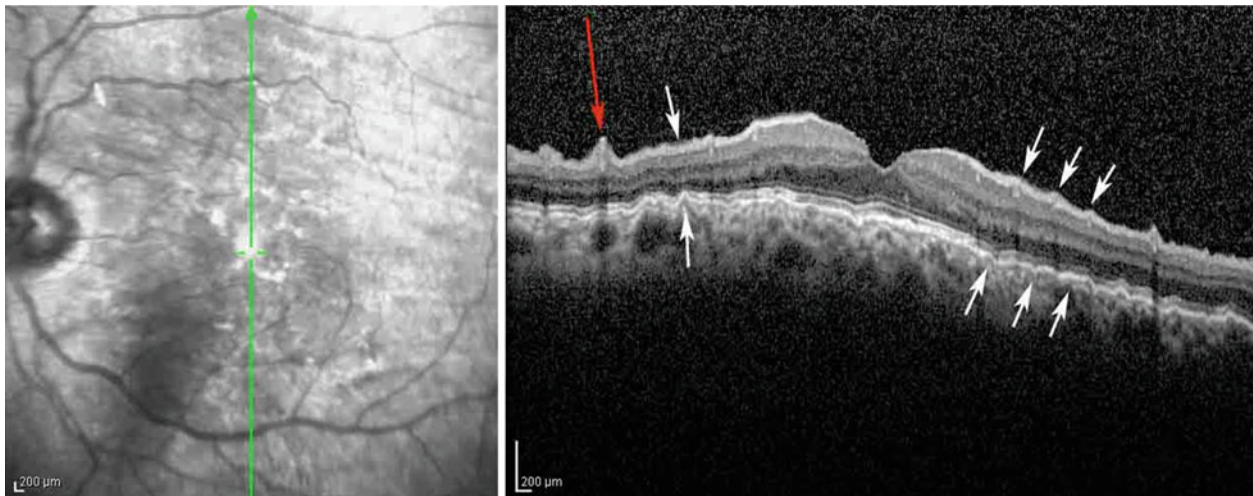


Fig. 12.44 Chorioretinal folds (*white arrows*) and a retinal vascular fold (*red arrows*) in the left eye of a patient with longstanding ocular hypotony. Choroidal vessel engorgement is best demonstrated by

EDI-OCT, as in part “a” of Fig. 12.43. EDI-OCT enhanced depth imaging optical coherence tomography

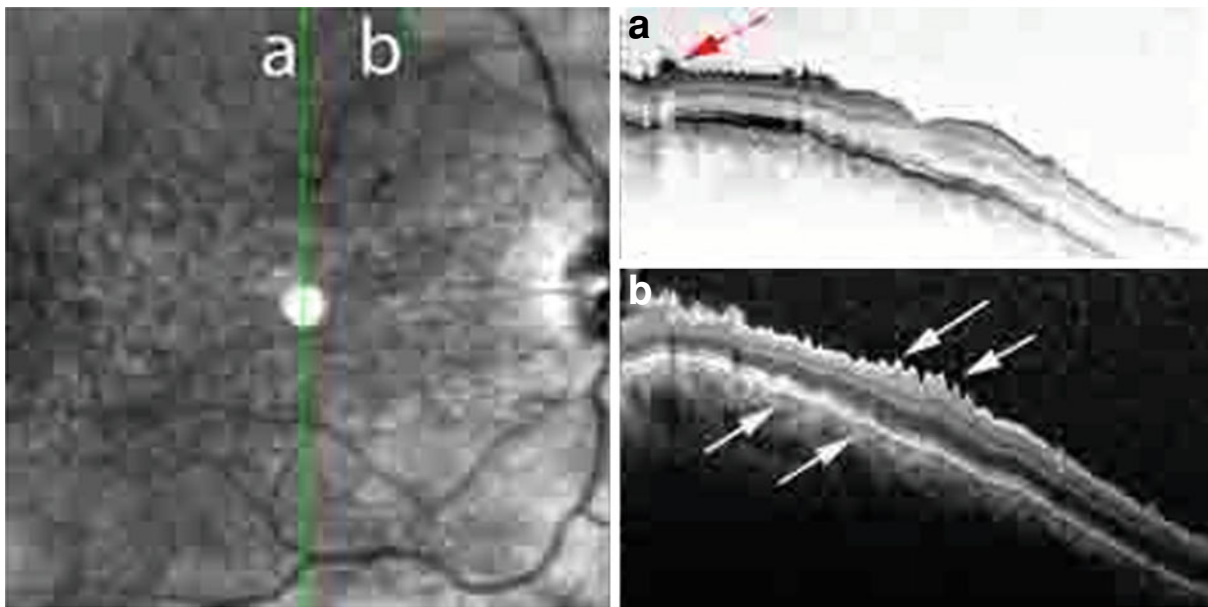


Fig. 12.45 The longitudinal OCT B-scan of the macula of a 27-year-old man who underwent Lasik surgery 6 years before the scan. He experienced the complications of flap haze and glaucoma secondary to corticosteroid use and filtering surgery. Over the past few months, the patient’s vision decreased from 20/20 to 20/40, and he

experienced severe hypotony with an intraocular pressure near zero. The white arrows indicate full thickness choroidal and retinal wrinkles. Vascular microfolds also exist (*red arrow*) and occur because of the collapse of the globe. OCT optical coherence tomography

macular edema, which may be caused by abnormal retinal capillary permeability, and reduced interstitial pressure [51, 52]. The importance of OCT imaging is it allows clinicians the ability to diagnose these cases without fundus findings and visual acuity loss [53]. After the normalization of the

IOP, the folds disappear. However, longstanding hypotony may result in irreversible fibrosis within the retina, choroid, or sclera, and thereby maintain the choroid in a folded position [47] (Figs. 12.43, 12.44, 12.45, 12.46, 12.47, 12.48, 12.49, 12.50, 12.51, 12.52, 12.53, 12.54 and 12.55).

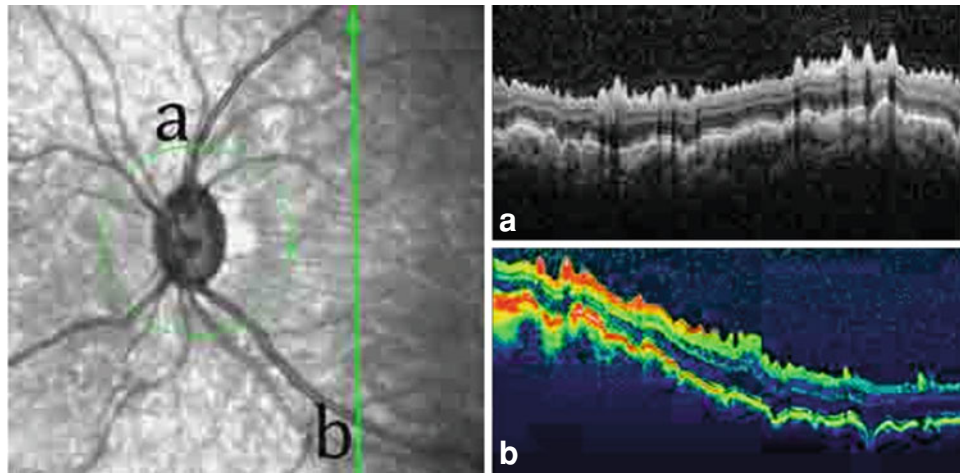


Fig. 12.46 Long-standing ocular hypotony in a patient. The retinal nerve fiber layer cut around the optic disc shows full thickness globe wrinkling

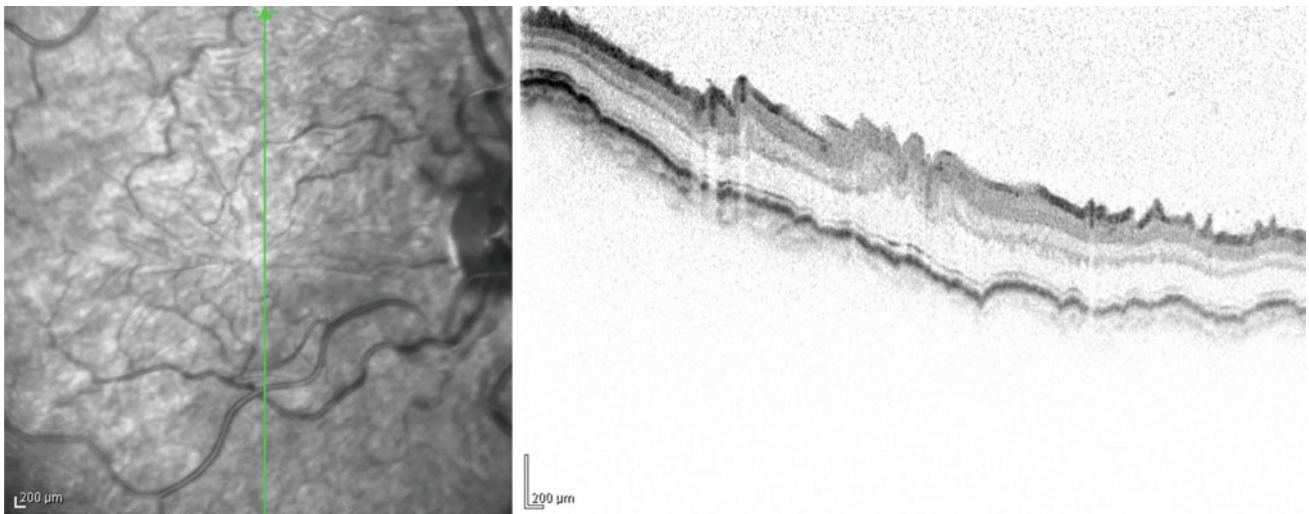


Fig. 12.47 Another patient with long-standing hypotony. The diagnosis will be more feasible by focusing on full thickness folds, which involve the retina and the choroid. Foveal shape disruption decreased the vision in this patient

Fig. 12.48 The SLO-OCT image is from a 64-year-old man who underwent trabeculectomy a few days before the scan. He experienced decreased vision thereafter. Severe global collapse is accompanied by severe ocular hypotony and severe optic disc edema. The foveal fold results in severe visual loss. *SLO-OCT* spectral domain optical coherence tomography

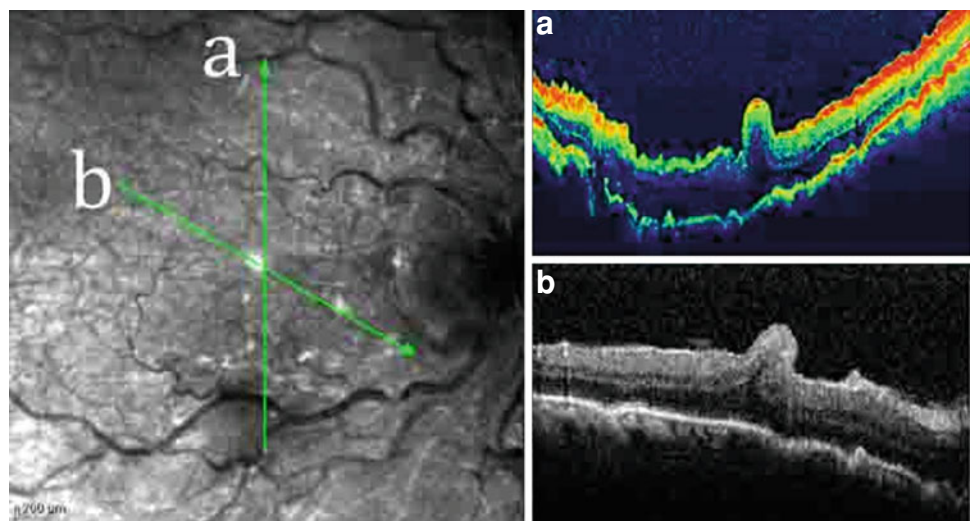




Fig. 12.49 The color fundus photography of the same patient in Fig. 12.48 reveals severe papilledema and macular folds

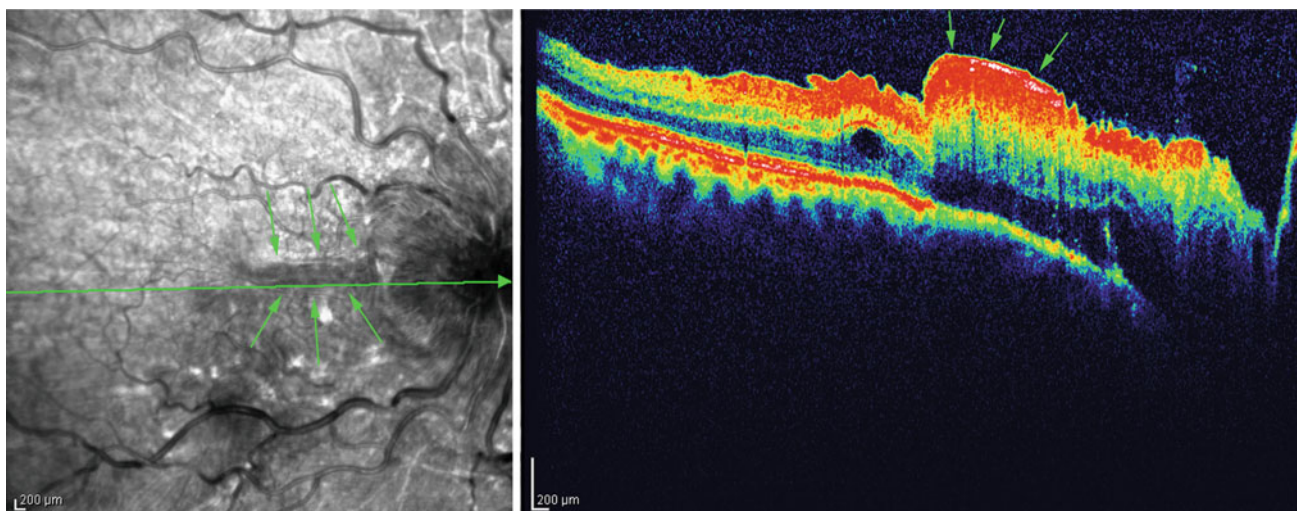


Fig. 12.50 Another longitudinal OCT image from the same patient in Fig. 12.48 shows a large and high maculopapillary fold (*green arrows*), which is hyper-reflective, and may result from severe impairment of ocular circulation

Anatomic normalization corresponds well with the clinical findings of IOP restoration and improved visual acuity [54]. Macular folds may sometimes persist, despite the resolution of hypotony. Removal of the internal limiting membrane at the time of vitrectomy may restore the normal retinal contour and improve visual acuity [55].

Serous retinal detachments and foveal cystic changes are other findings in hypotony maculopathy, especially in the chronic stages [51]. The foveal pit disruption, which is detectable by spectral domain OCT (SD-OCT), may contribute to decreased vision [56].

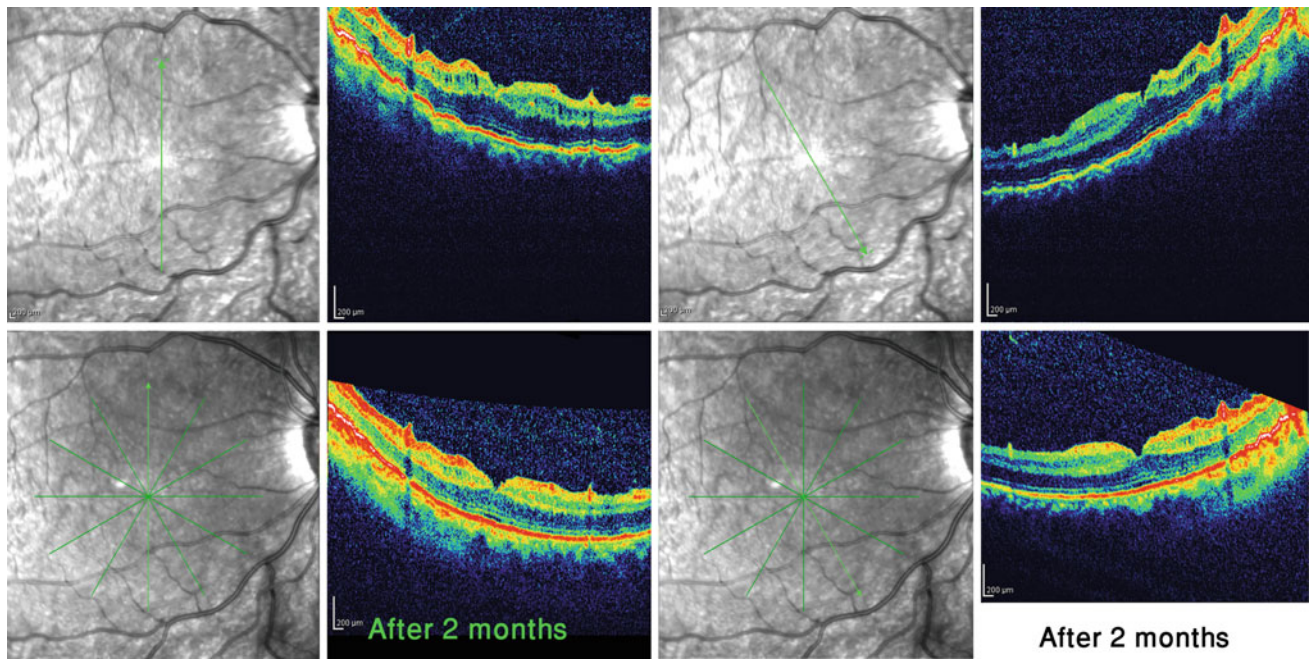


Fig. 12.51 The OCT scan of a patient with hypotony maculopathy. Two months after bleb revision and increased intraocular pressure, the macular configuration improved and the choroidal folds disappeared. *OCT* optical coherence tomography

12.7 Decompression Retinopathy

In 2005, Gupta et al. [57] described decompression retinopathy in a patient with macular central retinal artery occlusion who had undergone anterior chamber parasyntesis. Decompression retinopathy can occur after peripheral laser iridoplasty [58]. It can also occur with ocular surgical procedures such as cataract extraction, filtering surgery, cyclodialysis, cyclodestruction, vitreoretinal surgery, orbital decompression [59], anterior chamber parasyntesis [57], and after orbital decompression surgery [59].

The fundus examination reveals multiple preretinal hemorrhages. The OCT examination reveals multiple foci of high-reflective blood accumulation at the superficial retina

under the internal limiting membrane. Egg-shaped pockets of hemorrhages may be accompanied by serous retinal detachment [60].

In a severe hypotensive condition after eye surgery, extensive blot hemorrhage and intraretinal hemorrhages are accompanied by subretinal fluid collection and superficial high-reflective material accumulation in the retina. This finding is consistent with preretinal hemorrhage, and is visible on an OCT examination of the retina (Figs. 12.56, 12.57 and 12.58). A characteristic of a hemorrhagic retina with preretinal hemorrhages is high-reflective oval-shaped material accumulated under the internal limiting membrane. Subretinal fluid accumulation is also noted in such cases.

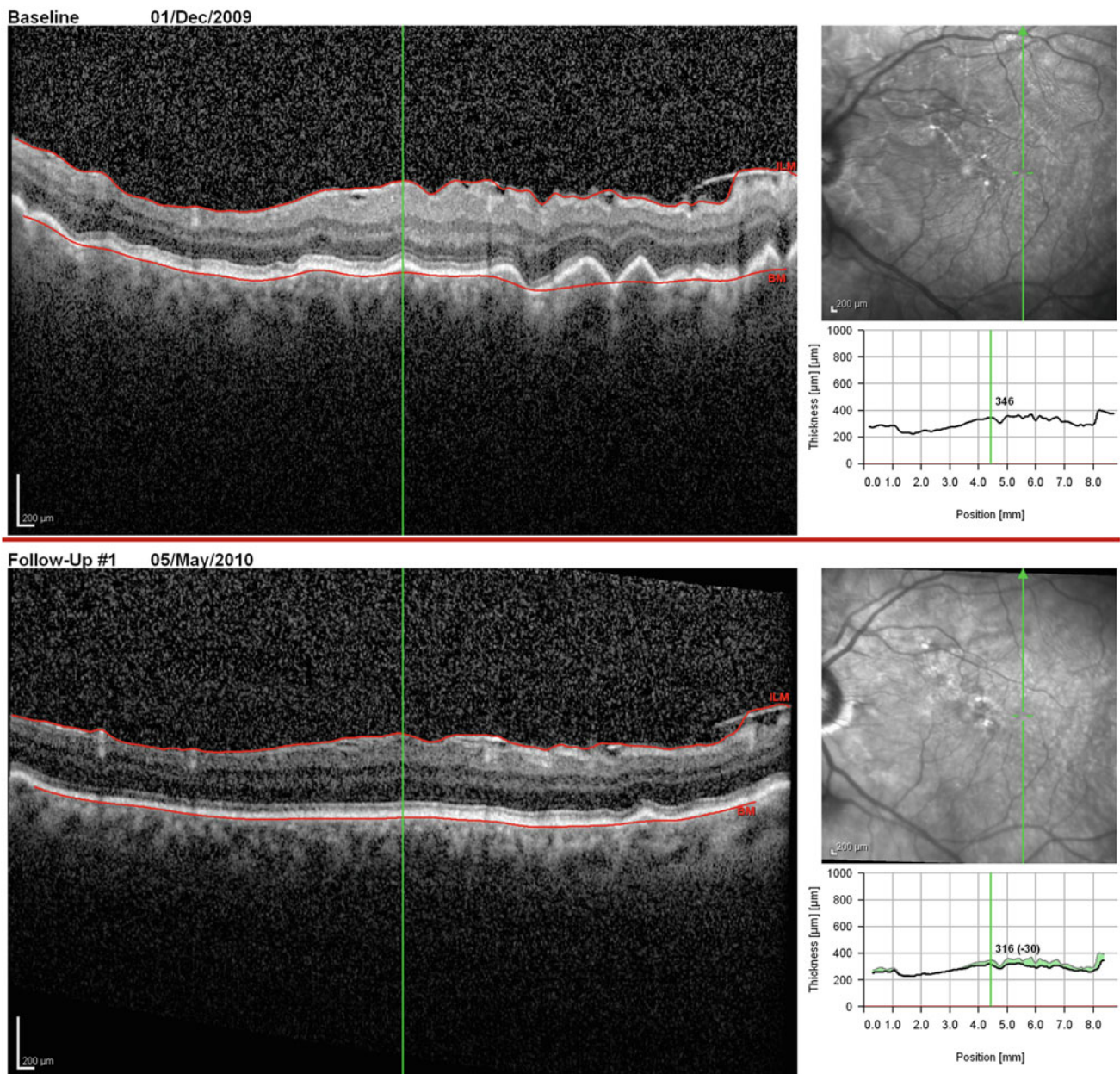


Fig. 12.52 These two comparative images are from a 70-year-old man with ocular hypotony and who subsequently underwent bleb revision. The choroidal folds have disappeared, but some residual retinal wrinkling persists

12.8 Post-surgical Endophthalmitis

Postsurgical endophthalmitis is a frightening complication, which presents as vitritis, retinal vasculitis, and preretinal exudates. The causes of poor visual gain after endophthalmitis in the Endophthalmitis Vitrectomy Study included

pigmentary degeneration of the macula (33%), macular edema (32%), preretinal membrane (15%), presumed optic nerve damage (13%), retinal detachment (RD) (8%), macular ischemia (6%), and vitreous opacification (3%). Investigators in the Endophthalmitis Vitrectomy Study [61] reported that, in 26% of cases, the cause of decreased visual acuity in postsurgical endophthalmitis is not apparent. In a study by

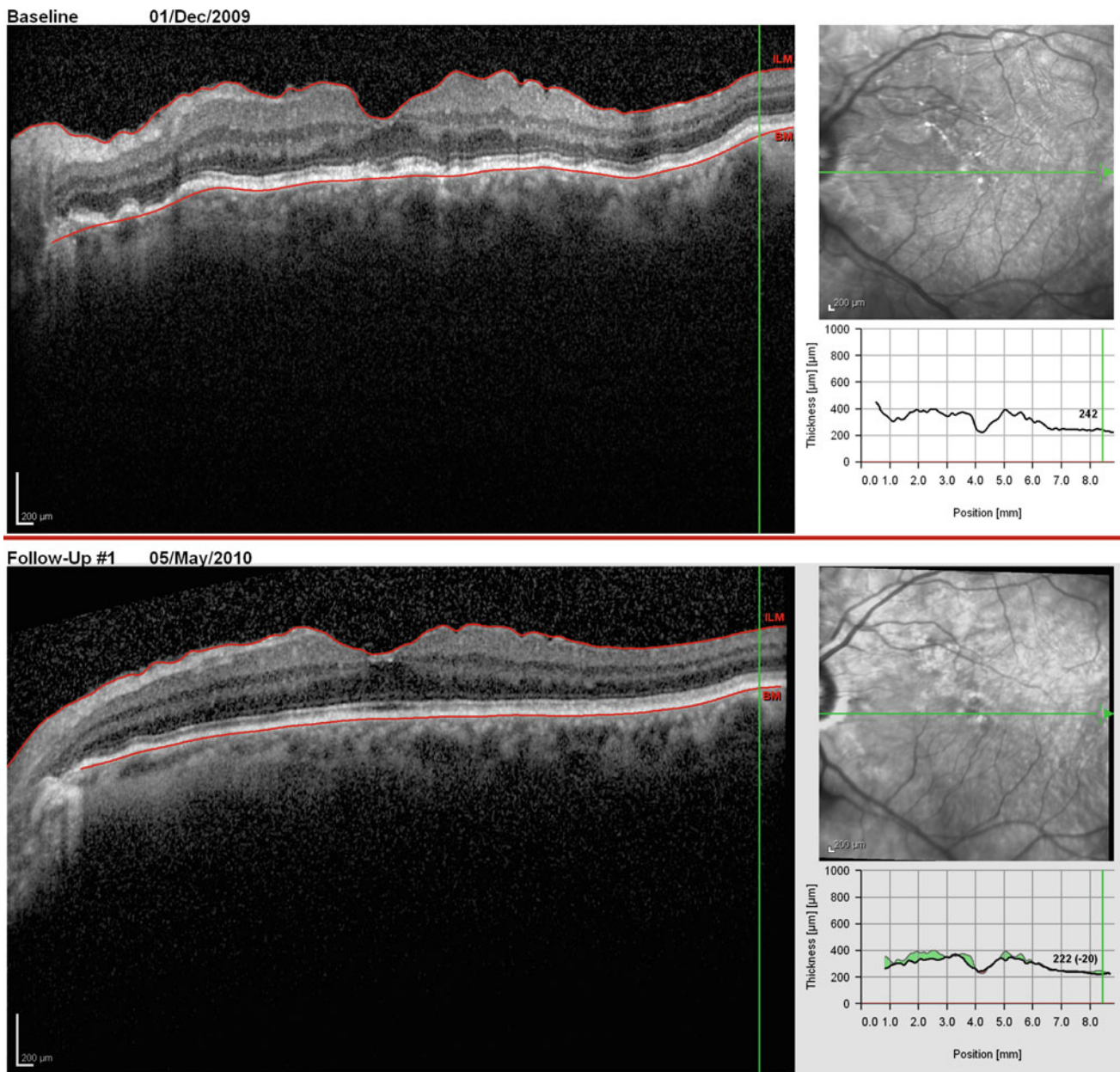


Fig. 12.53 These another two comparative images are from the same patient in Fig. 12.52. The choroidal folds have disappeared after improving ocular hypotony, but some residual retinal wrinkling persists

Singh et al. [62], 45% of patients with successful management of the endophthalmitis had no apparent cause for poor vision. In these patients, the OCT of the fovea revealed that foveal atrophy was accompanied by an epiretinal membrane, subfoveal neurosensory retinal detachment, and loss of the

neurosensory retina. Therefore, the inflammatory destruction of the neurosensory layer at the fovea results in poor visual outcome after maximal treatment, (Figs. 12.59 and 12.60) which may not be detected by other examination methods.

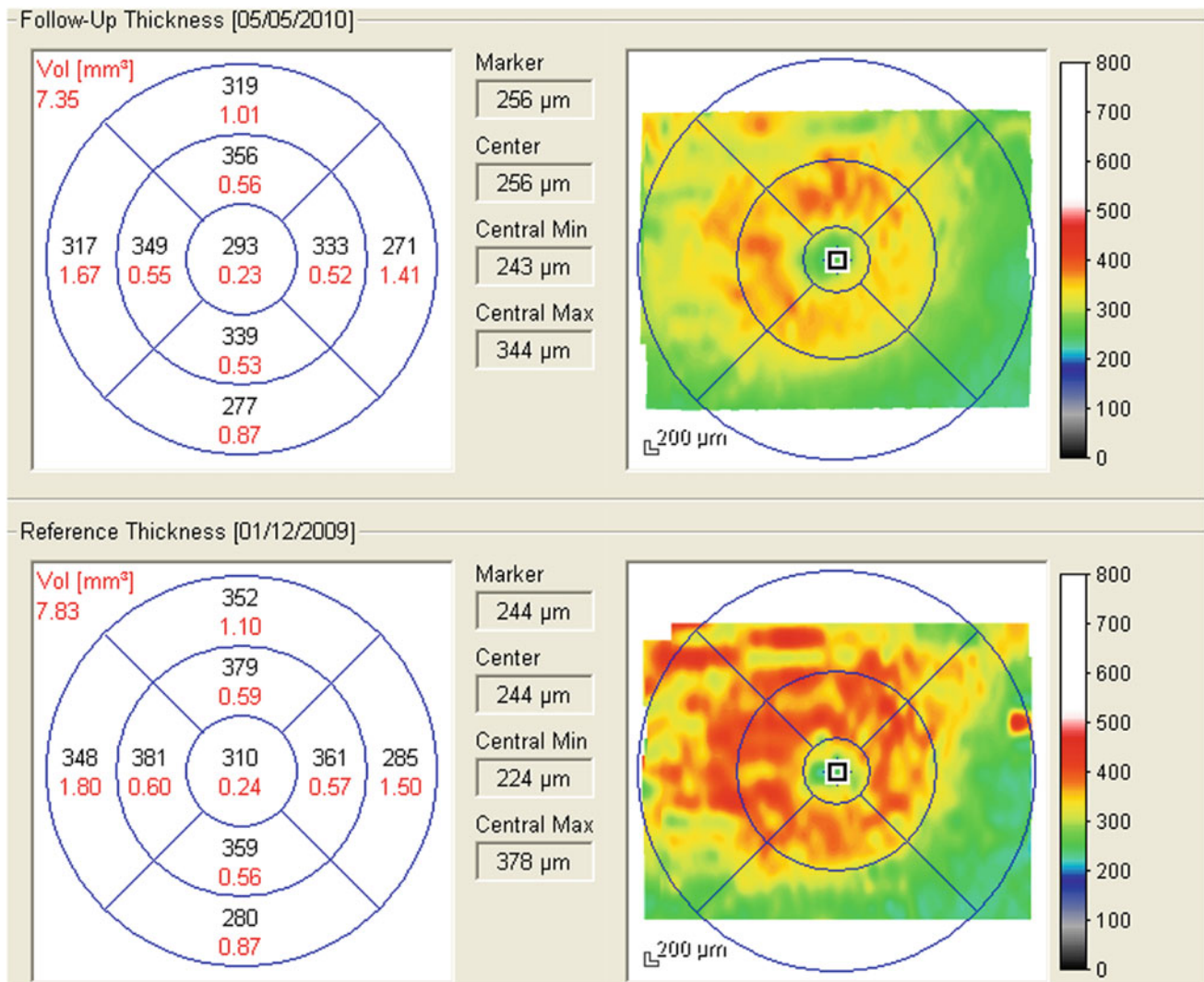


Fig. 12.54 The comparative topographic maps allow better understanding of retinal thickness changes

12.9 Valsalva Maculopathy

A rapid rise in intraocular venous pressure can lead to the spontaneous rupture of the perifoveal capillaries, and result in the characteristic clinical picture of a preretinal hemorrhage in an otherwise healthy eye. The hemorrhage typically occurs at the central part of macula, and in most cases, resolves without compromising visual acuity (Figs. 12.61, 12.62, 12.63, 12.64, 12.65 and 12.66). Valsalva maculopathy is a self-limited and isolated event. Head and neck strain

that increases intravenous and thoracic pressure (e.g., severe coughing [63], aerobic exercise [64] and body building [65], severe vomiting, choking [66], etc.) may be accompanied by Valsalva maculopathy. Valsalva maculopathy presents as a round or oval superficial high-to-moderate reflective material that accumulates near the fovea.

Sometimes, strain trauma is so severe that the pattern spreads over the macula and resembles Purtscher's retinopathy (Figs. 12.67, 12.68 and 12.69). However, the absence of cotton wool spots and optic engorgement may help in distinguishing it.

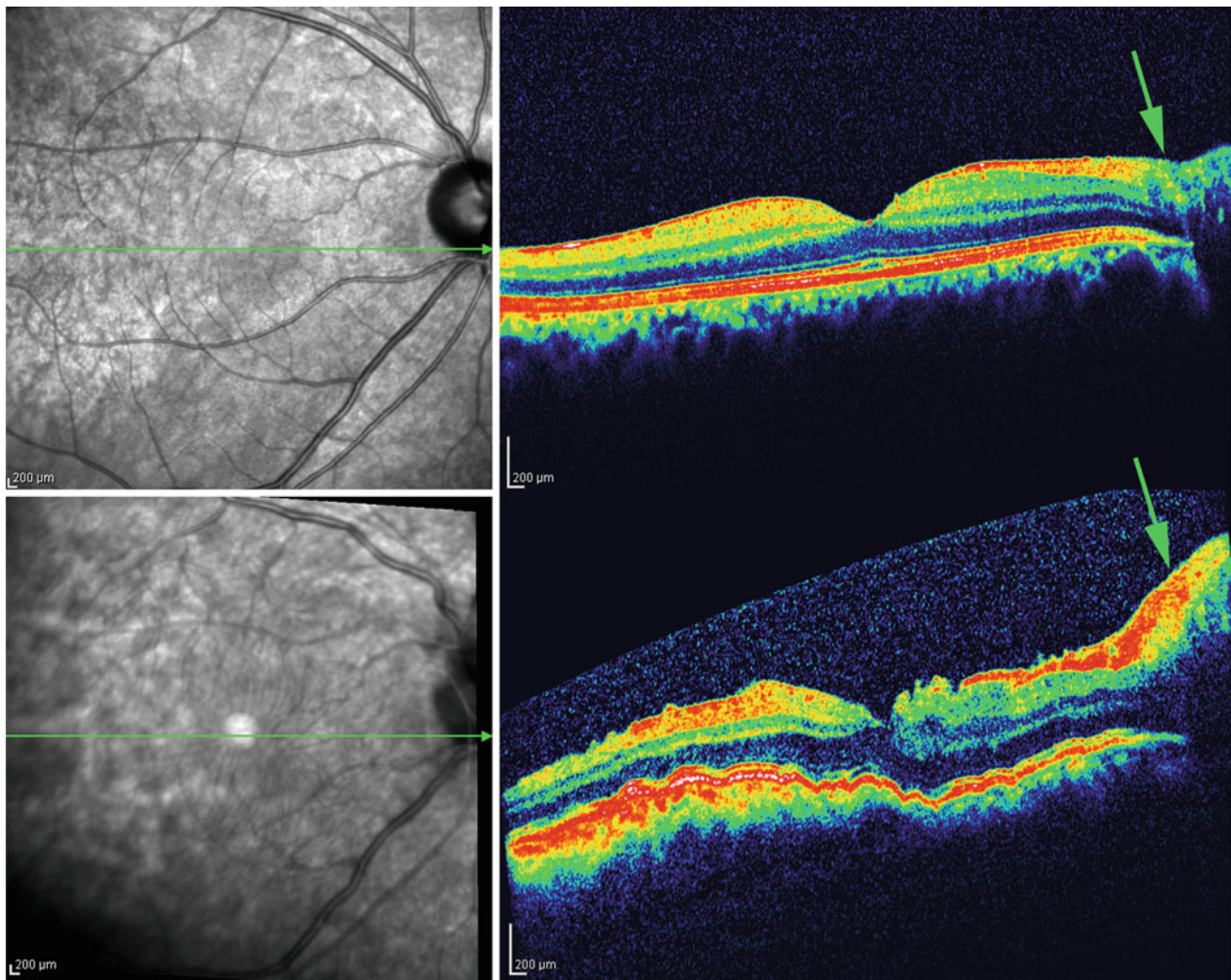


Fig. 12.55 The compound image is from a young man with a history of glaucoma and longstanding use of topical steroids. He underwent trabeculectomy surgery, which was complicated by hypotony. The upper image was taken before the surgery and the lower image was

taken 2 weeks after the surgery. Generalized retinal thickening and choroidal wrinkling and the optic disc edema are evident (*green arrows*)

12.10 Subretinal Deposits

After vitreoretinal surgery, the application of perfluorodecalin may result in the retention of residual material in subretinal spaces. The mechanical compressive changes include the distortion of the outer photoreceptor segment, retinal atrophy, and narrowing of the outer plexiform layer,

as previously reported [67–69]. After surgery, the retention of perfluorocarbon liquid (PFCL) in the subfoveal spaces can have drastic consequences on the visual outcome because of its potential direct toxic effects on the retinal pigment epithelium (RPE) and photoreceptor layers [70–72]. Most surgeons recommend that the PFCL that is on the subfoveal area, and persists after vitreoretinal surgery, should be removed when the central visual acuity is

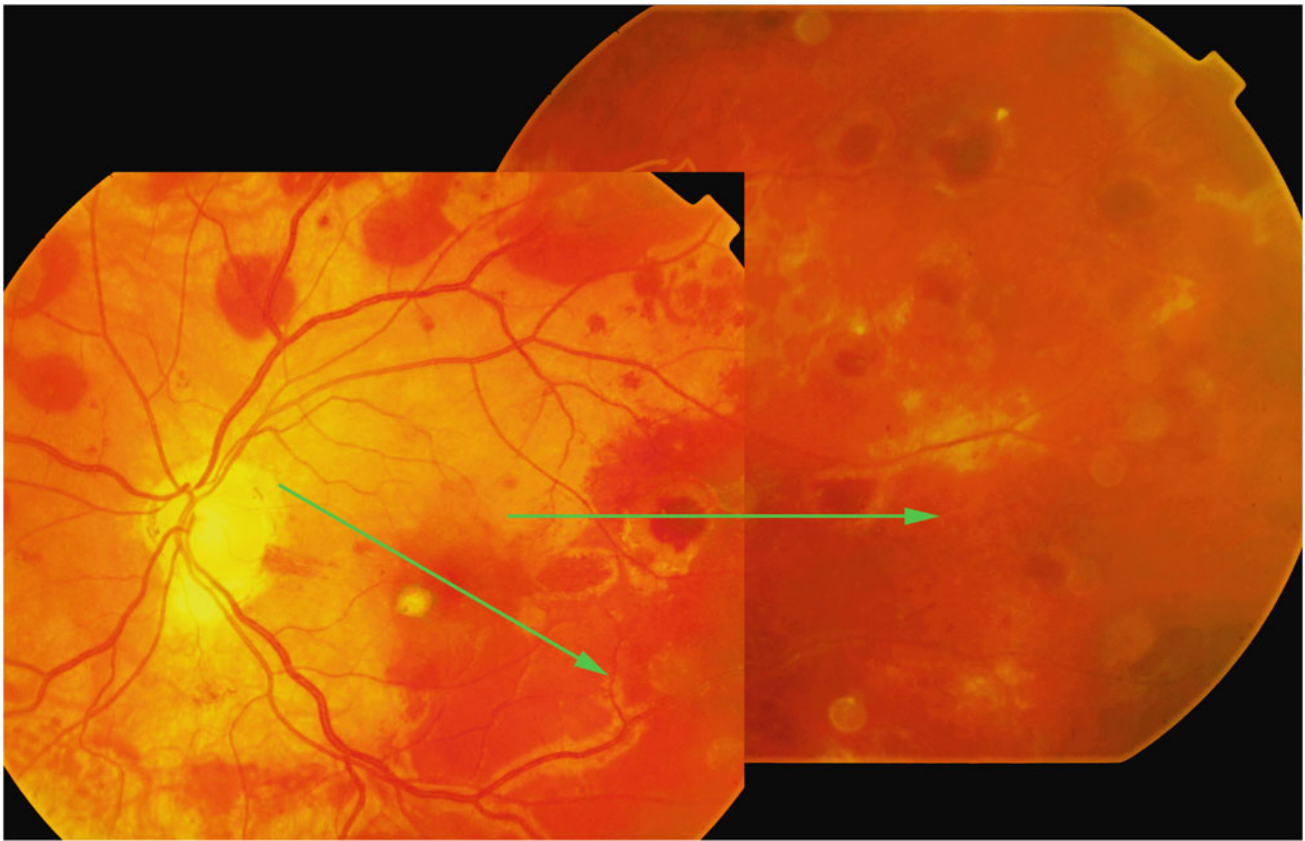


Fig. 12.56 Fundus photograph of multiple sections of the macula and the extramacular area from the eye of a female patient after cataract surgery. During the early postoperative period, the patient experienced

intraocular hypotonia. Multiple circular pre-retinal hemorrhage spots overlying an extensive deeper layer hemorrhages are remarkable

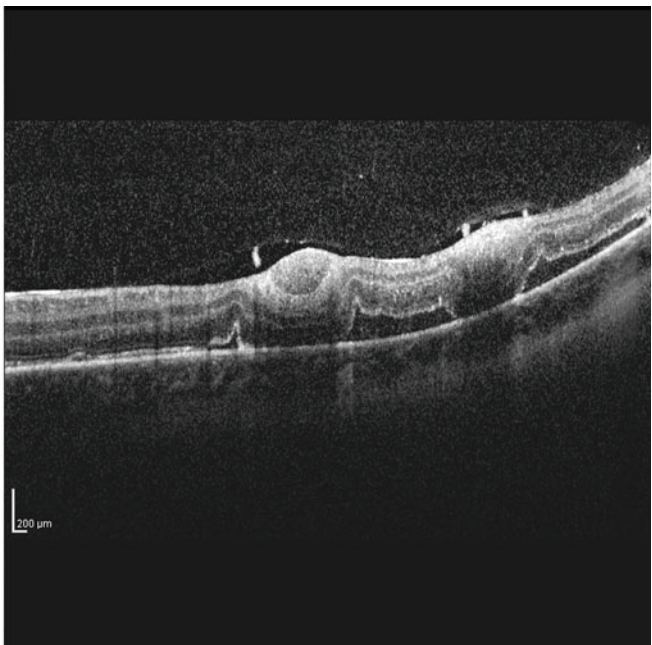
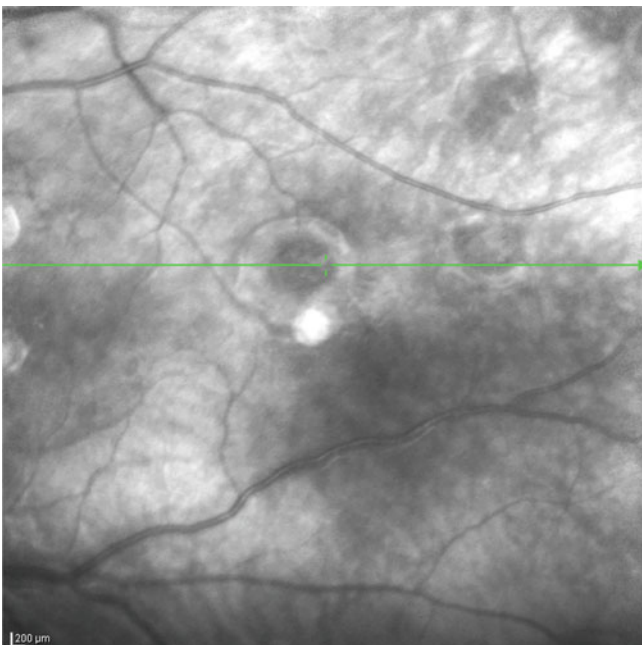


Fig. 12.57 SLO-OCT images of the same patient in Fig.12.56. Hyper-reflective, superficial lesions at the level of internal limiting membrane corresponding to circular lesions on color fundus image.

Sub-retinal fluid corresponding to serous-blood fluid accumulation that spread under retina. *SLO-OCT* scanning laser ophthalmoscopy, optical coherence tomography

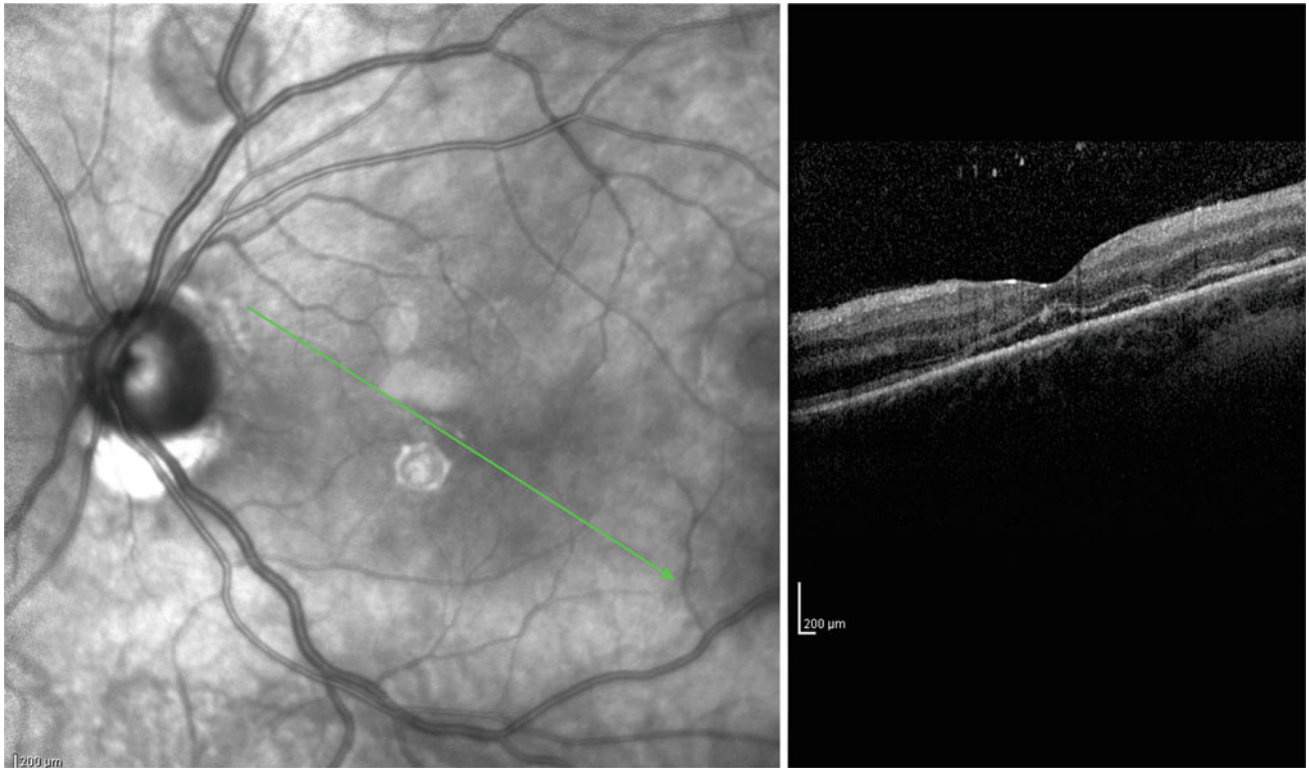


Fig. 12.58 Another SLO-OCT images of the same patient in Fig.12.56. Subfoveal serous-blood fluid accumulation is the reason for considerable visual disturbance. *SLO-OCT* scanning laser ophthalmoscopy, optical coherence tomography

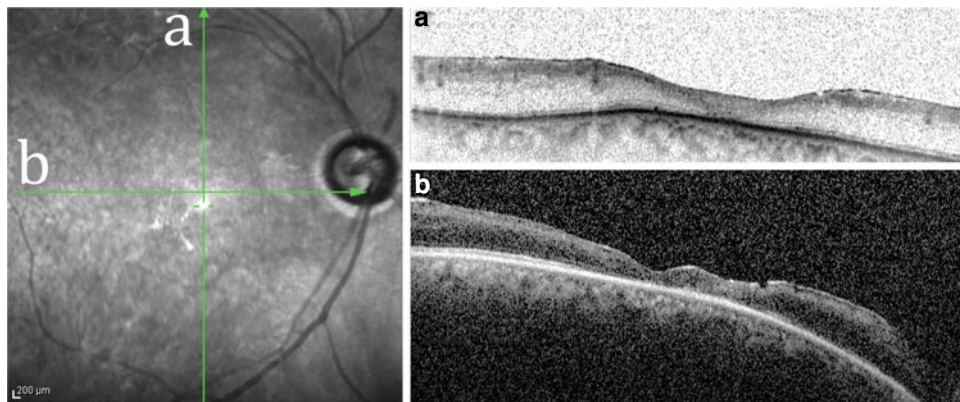


Fig. 12.59 The SLO-OCT images of a female patient with a history of endophthalmitis postcataract surgery. One month before this image, she had undergone vitrectomy and intraocular antibiotic injection. The destruction of the foveal structure is accompanied by severe foveal atrophy and the loss and atrophy of all retinal layers

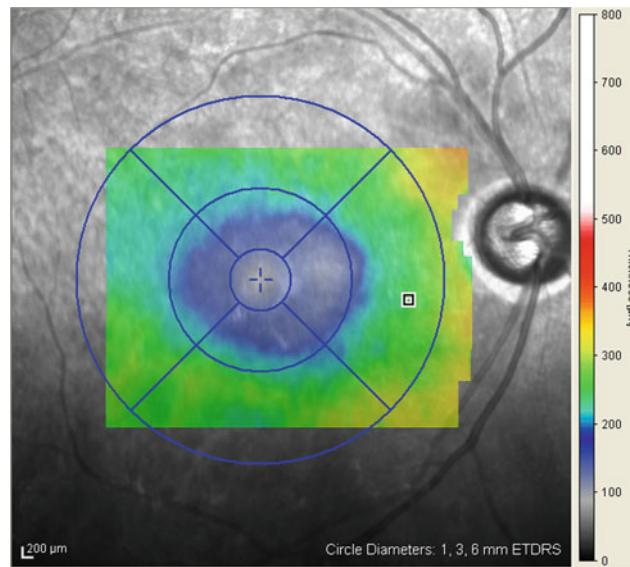


Fig. 12.60 The topographic map of the same patient in Fig. 12.59 demonstrates considerable foveal atrophy

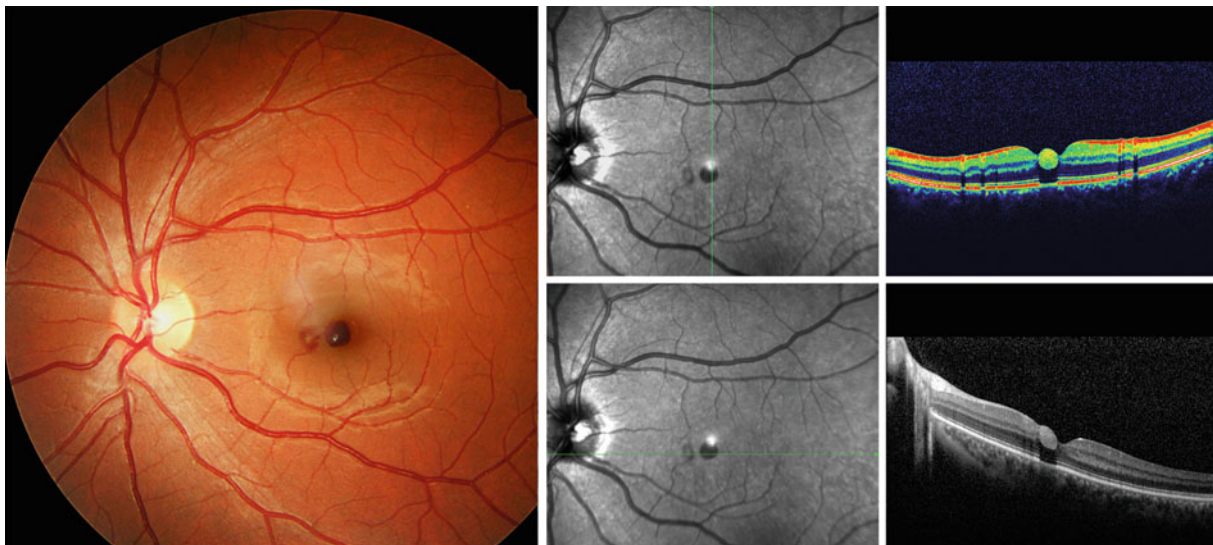


Fig. 12.61 The findings in the eye of a 32-year-old woman who experienced decreased vision a few days before the image was taken and after she had performed a Valsalva maneuver. Her vision was 20/40

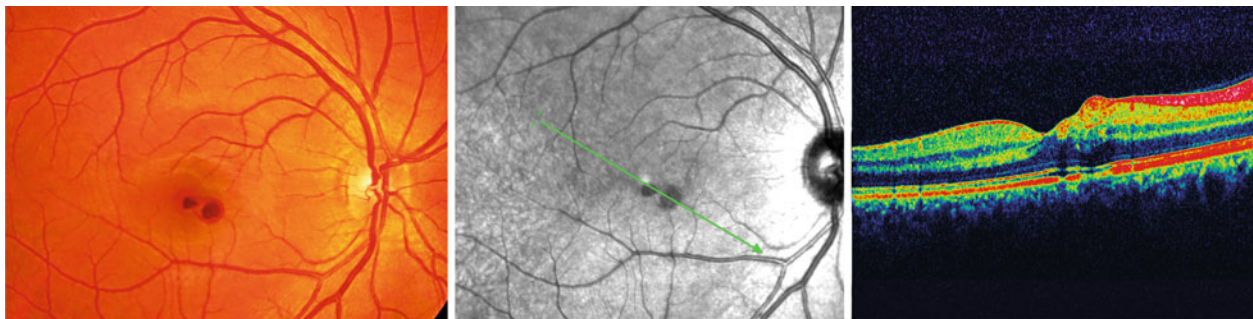


Fig. 12.62 These images provide a better view of Valsalva maculopathy in a patient, and show two small superficial hemorrhages. In all OCT images, the superficial retinal highly reflective oval or round material accumulation is visible. *OCT* optical coherence tomography



Fig. 12.63 SLO-OCT images of the same patient in Fig. 12.62. The superficial retinal highly reflective oval or round material accumulation is visible. *SLO-OCT* scanning laser ophthalmoscopy optical coherence tomography

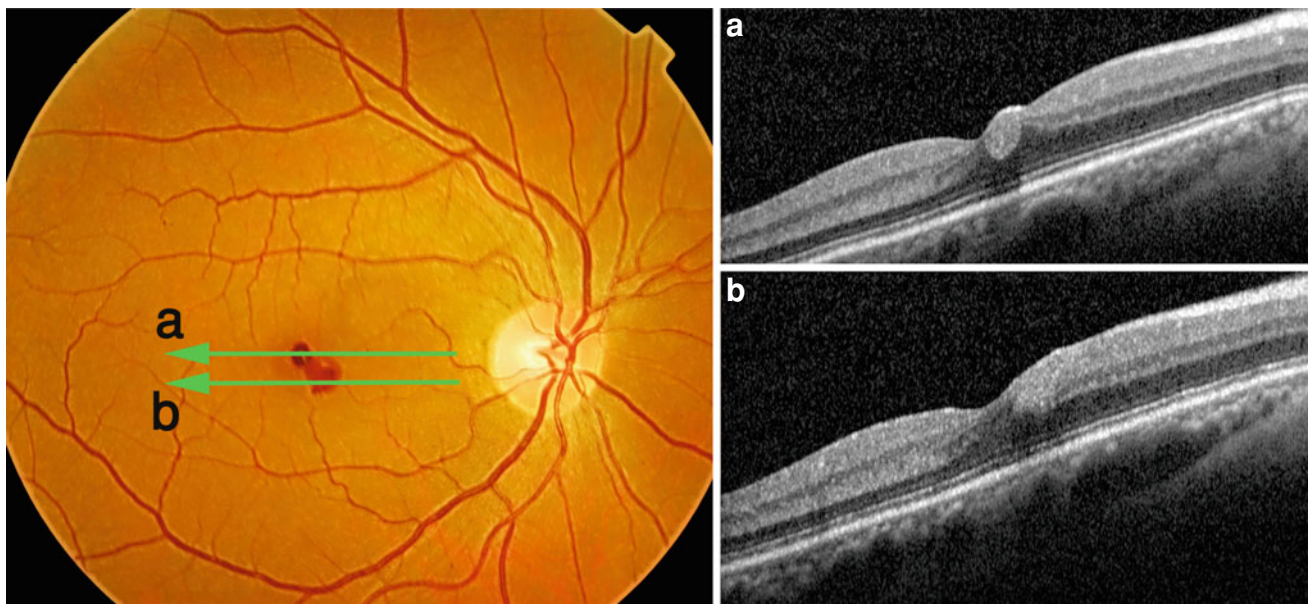


Fig. 12.64 The extent of a hemorrhage may vary, according to the severity of the pressure. In the “a” section, at the center of hemorrhage, the blood margins are clearly defined. In the “b” section, in the periphery, blurred margins are blended with the retinal layer



Fig. 12.65 In the chronic and resolution phases, fibrin replacement in the hemorrhagic area increases reflectivity. In the color fundus photograph, the white patch is at the core of the lesion

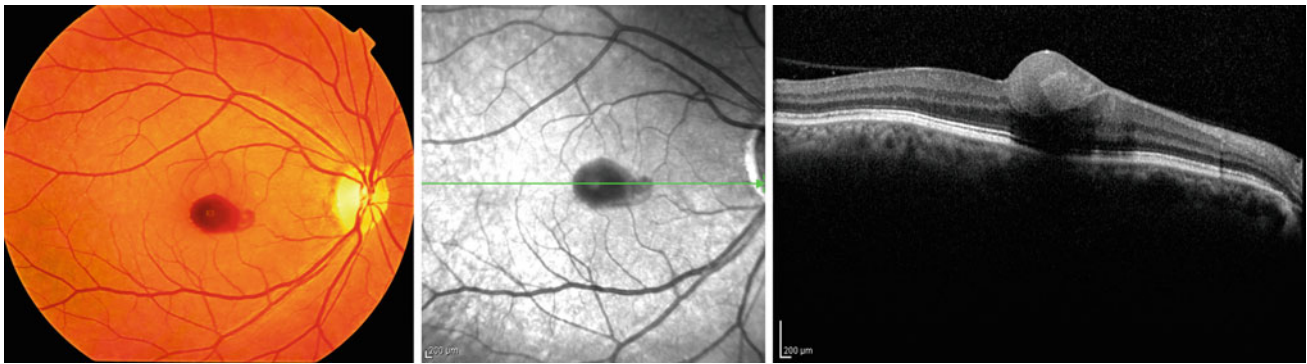


Fig. 12.66 The findings in the eye of a 55-year-old woman with a history of recent vomiting. Extensive preretinal hemorrhage with an adjacent round core is a characteristic finding



Fig. 12.67 The findings in the eye of a young man who had recently experienced a severe strain to his chest. The hemorrhages extend farther than the fovea and spread along the superior vascular arcade. The OCT images show multiple mediums to high reflective material, which lies in the superficial retinal layer

substantially impaired [70, 73–75]. Small amounts of residual perfluorodecalin in subretinal spaces do not seem to cause significant damage or unwanted effects [67, 76–78].

In OCT images, circular bubbles with low-reflectivity spaces under the retina are noted. The location of PFCL is very important because of its drastic effect on the visual

acuity if it lies under the foveal area. Differentiating it from subretinal fluid and the pigmented epithelial detachment (PED) is simple (Fig. 12.70). In subretinal fluid, the low-reflectivity areas have acute angles, and often, a concave configuration. In PED, the RPE has a dome-shaped semi-circle elevation. However, in subretinal perfluorodecalin



Fig. 12.68 The scanning laser ophthalmoscopy and fluorescein angiography images of the same patient in Fig. 12.67. *OCT* optical coherence tomography

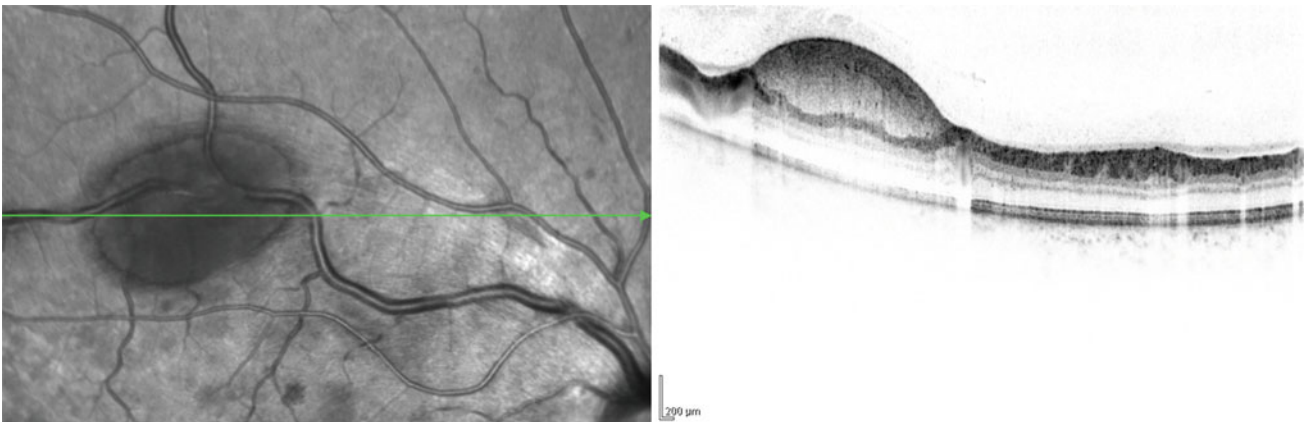


Fig. 12.69 This is an atypical and extensive form of the Valsalva maculopathy. This image represents the longitudinal cross-sectional OCT scan, which extends through the preretinal hemorrhage. The

hemorrhage shows a hyper-reflective pattern and is superficially located over the nerve fiber layer. *OCT* optical coherence tomography

retention, the circular area under the retina resembles a nearly complete circle (Figs. 12.71, 12.72 and 12.73) (i.e., larger than a semicircle). Yag laser can release small amount of perfluorodecalin into vitreous cavity and resolve retinal elevation specially if it would be near to fovea with visual disturbances (Fig. 12.74).

After injecting an intraocular drug such as corticosteroid or antivascular endothelial growth factor, the response to the treatment is best evaluated using OCT (Fig. 12.75)

In eyes filled with silicone, we can see the outer border of silicone oil on OCT (Fig. 12.76).

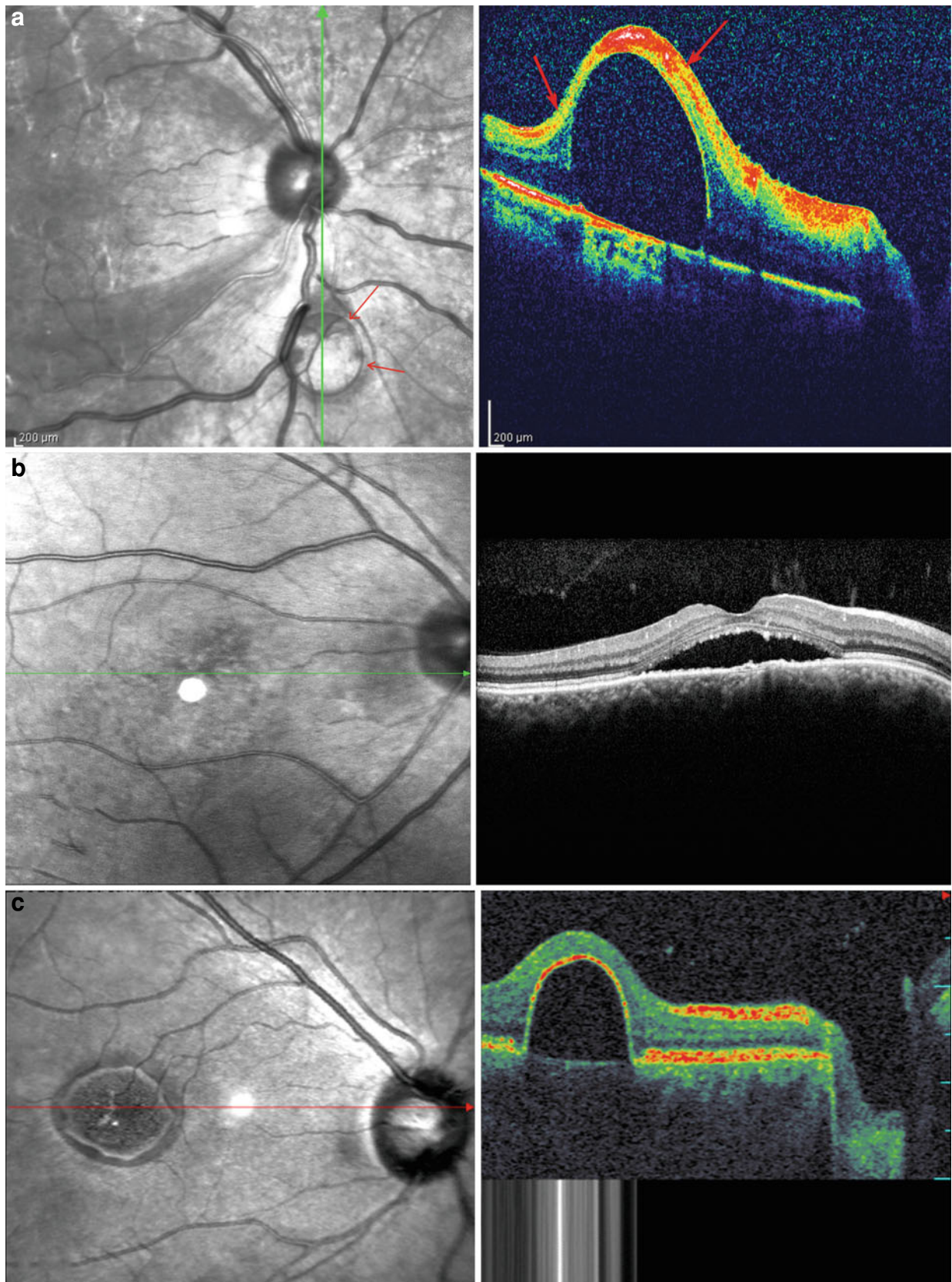


Fig. 12.70 Features that differentiate between “a” subretinal perfluorodecalin retention, “b” subretinal fluid, and “c” pigmented epithelial detachment (PED). Recognizing the PED may be difficult;

however, the shape of the low-reflectivity space, the patient’s history, and the bubble-shaped appearance of the subretinal perfluorodecalin can help differentiate it from the others

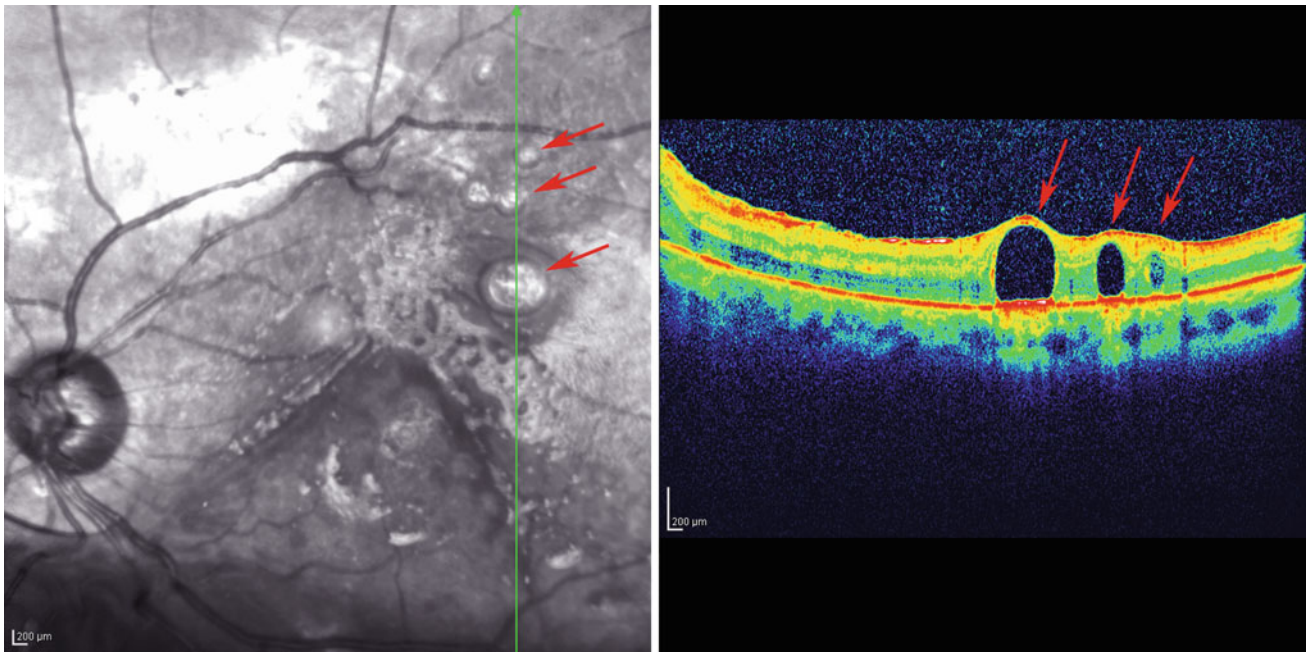


Fig. 12.71 The SLO image of retinal wrinkling and contracture with multiple round subretinal bubbles. The OCT image depicts multiple circular subretinal perfluorodecalin retention spaces (*red arrows*). *OCT* optical coherence tomography, *SLO* scanning laser ophthalmoscopy

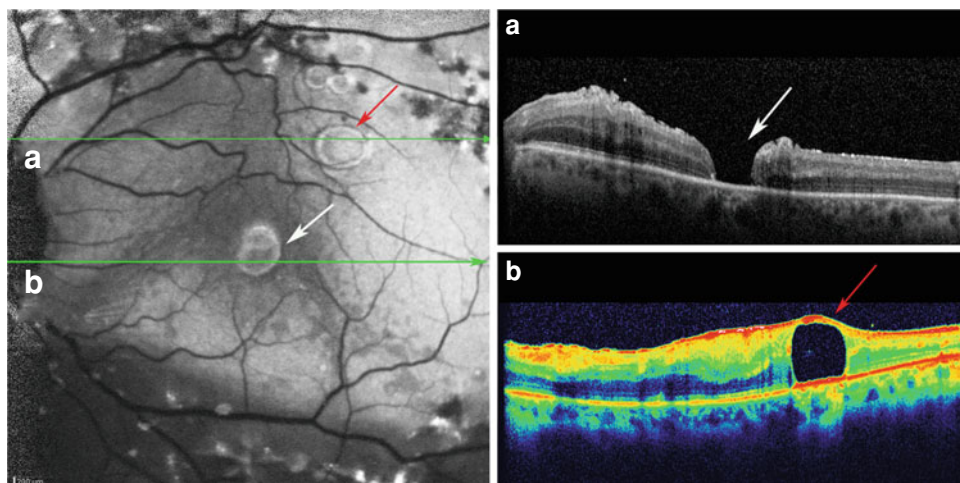


Fig. 12.72 The FAF view with longitudinal OCT B-scan of the same patient in Fig. 12.71 shows a full-thickness macular hole (*white arrows*) and perfluorodecalin retention (*red arrows*) in the subretinal

space. The view pattern of the macular hole and the subretinal perfluorodecalin retention in the FAF are similar. *FAF* fundus autofluorescence, *OCT* optical coherence tomography

12.11 OCT in Chloroquine Toxicity

The classic RPE changes due to chloroquine toxicity were first described by Cambiaggi in 1957 [79]. In 1959, Hobbs recognized a distinct association between the long-term use of chloroquine and the subsequent development of retinal

pathology [80]. Early chloroquine retinopathy is an acquired paracentral scotoma on visual field testing with no detectable retinal findings, whereas advanced retinopathy is associated with parafoveal RPE atrophy [81]. In the peripapillary region in patients on antimalarial drugs, measurements of nerve fiber layers (NFLs) by scanning polarimetry show significant thinning of the NFL, which is dose- and

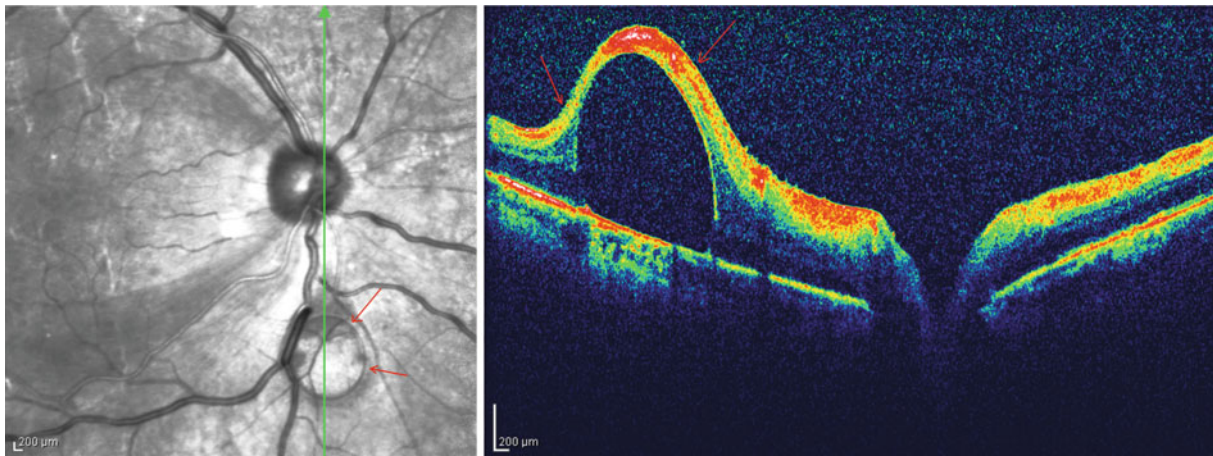


Fig. 12.73 The OCT scan from a patient who underwent vitreoretinal surgery with perfluorodecalin application. A large drop of perfluorodecalin is trapped in the peripapillary area. *OCT* optical coherence tomography

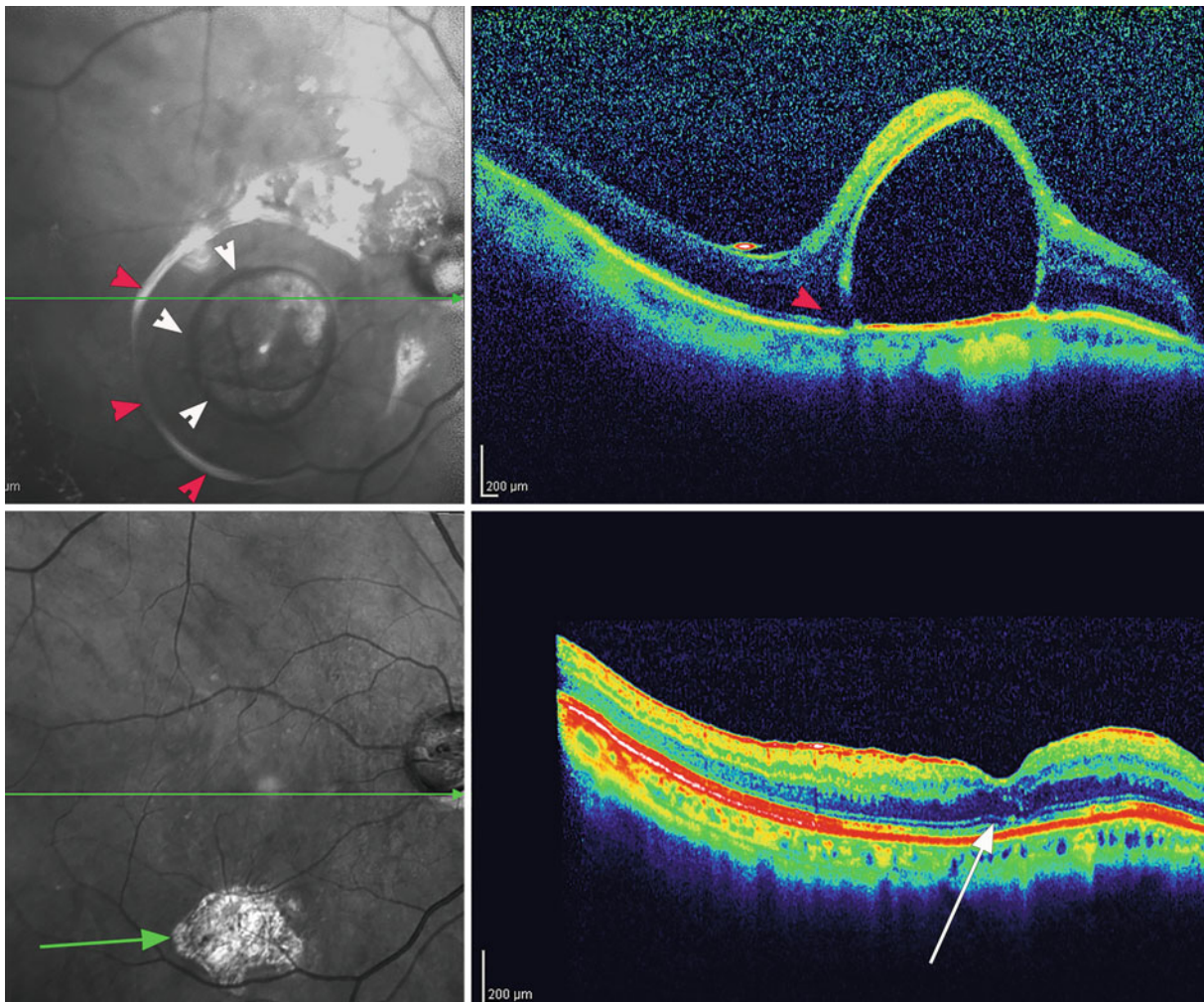


Fig. 12.74 The SLO-OCT scan from a patient who underwent vitreoretinal surgery with perfluorodecalin and a large drop of perfluorodecalin entrapment in the juxtafoveal area (above image). White arrowheads define the outer border of drop and red arrowheads

define the outer border of retinal elevation leave a space under retina. After Yag laser treatment and release of perfluorodecalin the scar (green arrow) in SLO image and the fovea with attenuated IS-OS junction (white arrow) in lower image are remarkable

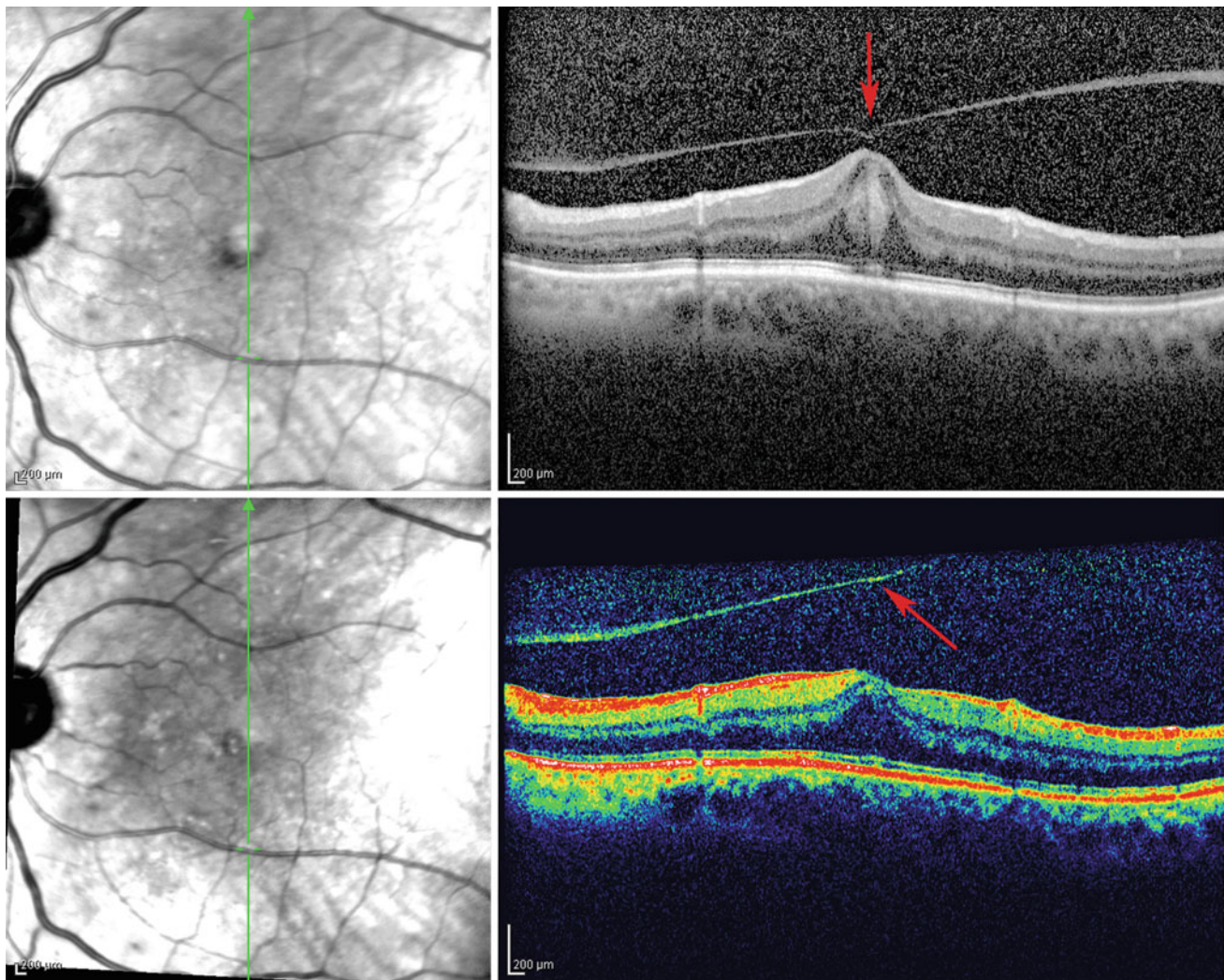


Fig. 12.75 The findings before and 6 months after intravitreal antivascular endothelial growth factor (Anti-VEGF) injection in the eye of a diabetic patient with mild diabetic macular edema and vitreomacular traction syndrome. After the injection, the release of the

posterior vitreous attachment with the resolution of edema (with subsequent visual acuity improvement) are only detected on the OCT images. *OCT* optical coherence tomography

duration-dependent [82]. Animal studies have suggested that ganglion cell damage may occur with early chloroquine consumption [82, 83].

High-speed and ultra-high-resolution OCT shows discontinuity or loss of perifoveal photoreceptor IS/OS junctions [84, 85], the thinning of the outer nuclear layer, and cyst-like hyporeflective space over the RPE layer [86] in patients receiving hydroxychloroquine [85]. Abnormalities in the perifoveal OS/IS junction may be an early OCT finding, and is seen in asymptomatic patients who have abnormalities

in the visual field and multifocal ERG examinations [85]. Some authors even believe that the OCT is useful for evaluating the regression of hydroxychloroquine retinopathy [86] (Figs. 12.77, 12.78, 12.79, 12.80, 12.81, 12.82 and 12.83).

Optical coherence tomography provides a good cross-sectional view of the macula, and may be a good tool for the detection of anatomical evidence of chloroquine macular toxicity [82]. In OCT, the anatomical evidence of the loss of ganglion cell layers and marked thinning of the macula and parafoveal region are demonstrated [87].

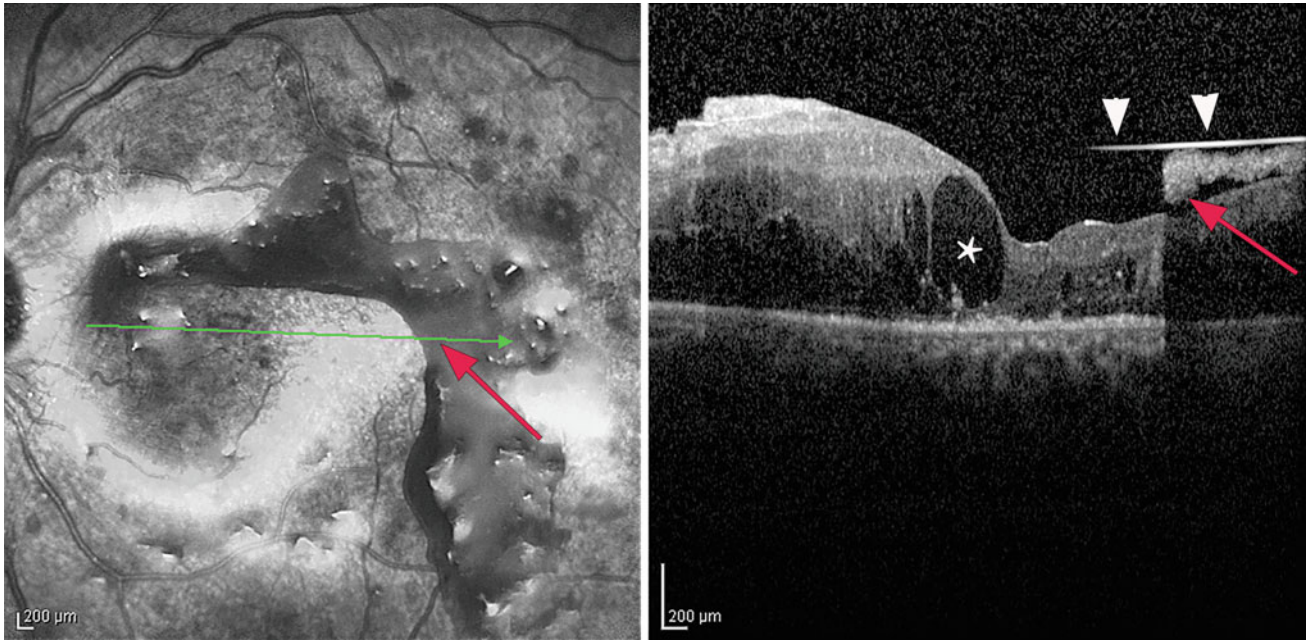


Fig. 12.76 SLO-OCT image of a advanced diabetic retinopathy case underwent pars plana vitrectomy with light silicone injection. White arrowheads define the outer boundary of silicone oil with special shine

on the SLO image. Small amount of blood entrapped between inner retina and silicone surface (red arrows)

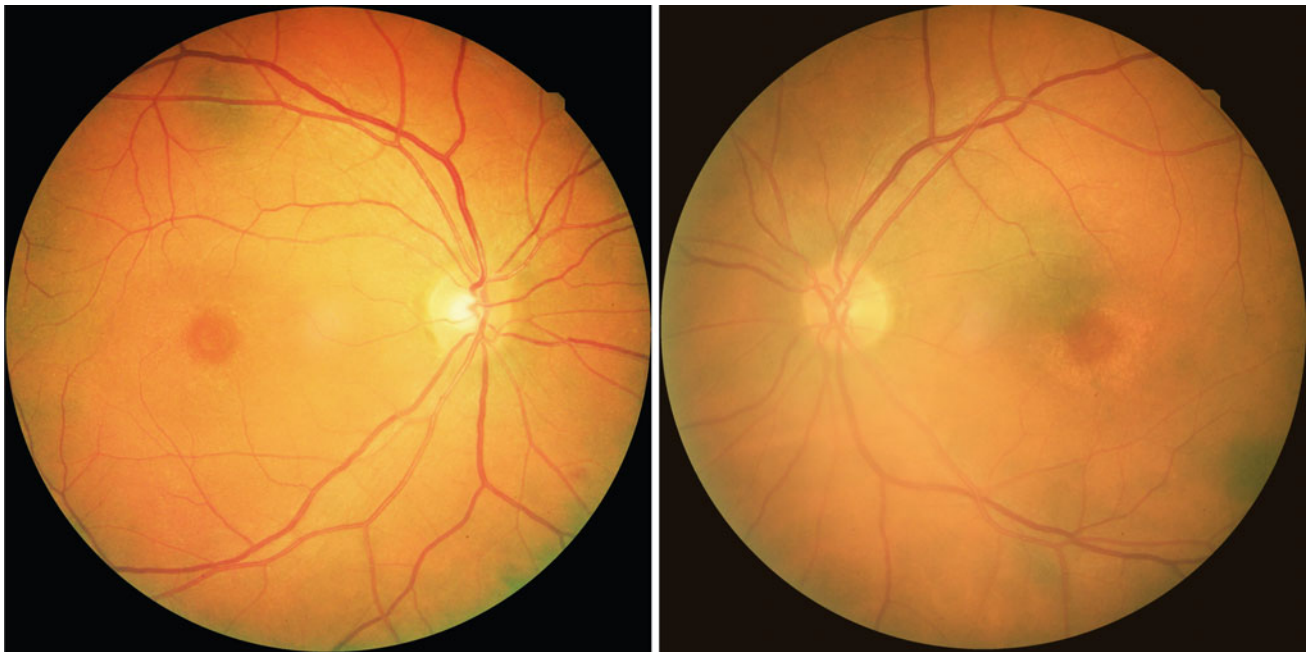


Fig. 12.77 The color fundus and autofluorescence photographs are from a 57-year-old woman with retinal atrophy and an 11-year history of chloroquine consumption, which she discontinued 1 year ago after

experiencing decreased vision. The bull's eye pattern is apparent in both images

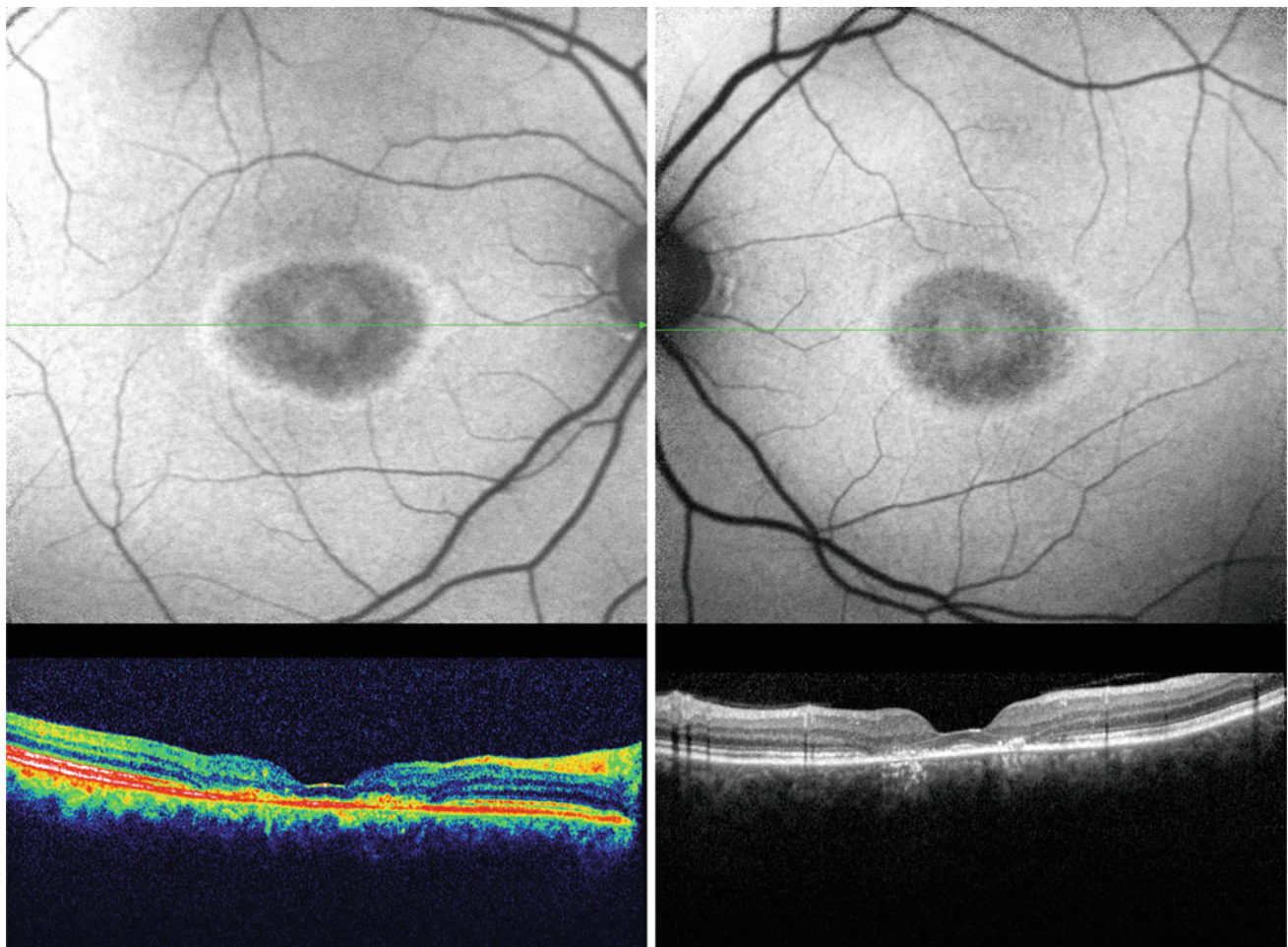


Fig. 12.78 OCT and FAF of the same patient in Fig.12.77. The OCT image also reveals the loss of RPE/photoreceptor layer with subsequent foveal atrophy. The loss of the photoreceptor inner segment/outer segment junctions and the “sink-hole” effect of the inner retinal structures in the perifoveal area are other finding. These patterns cannot

be detected from geographic atrophy in the early phase by OCT. The fundus autofluorescence images are more helpful and useful in diagnosis. The laser wave penetration is less deep than the geographic atrophy due to an age-related change; therefore, the RPE damage is less. *OCT* optical coherence tomography, *FAF* fundus autofluorescence

In areas of hydroxychloroquine toxicity, SD-OCT images demonstrate a downward “sink-hole” displacement of inner retinal structures, which corresponds to Humphrey visual field (HVF) 10–2 defects and ophthalmoscopic clinical examination findings. The IS/OS junction irregularities are also seen in areas not detected on the HVF 10–2 [84].

Adaptive optics images reveal the disruption of the cone photoreceptor mosaic in districts corresponding to the HVF 10–2. In addition, in areas with normal HVF 10–2 findings,

irregularities in cone photoreceptor density and mosaic are revealed by SD-OCT [84].

Some authors believe that bilateral visual field defects improve, and photoreceptor destruction disappears, and the cyst-like hyporeflexive space disappears in the eye after the discontinuation of chloroquine in the early stage of toxicity. Mild RPE irregularities may remain, which can be demonstrated on OCT scans [86].

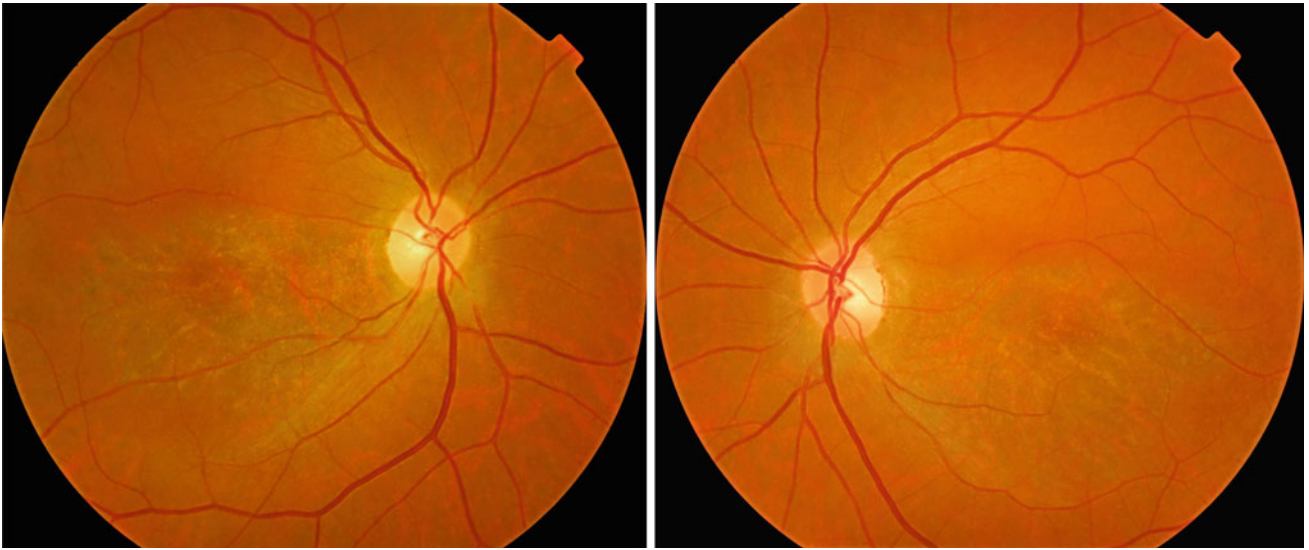


Fig. 12.79 Another example from a 61-year-old woman with retinal atrophy and a 20-year history of chloroquine consumption, which was discontinued a year ago after she experienced decreased vision. The vision in each eye is less than 20/200

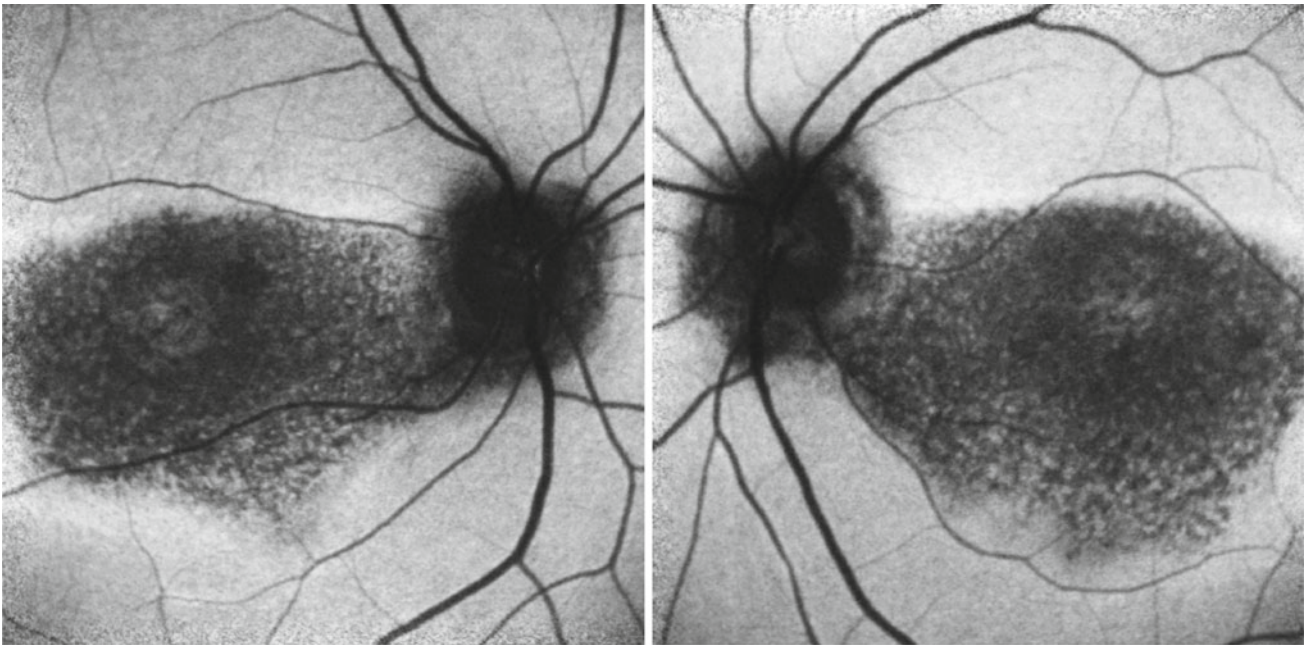


Fig. 12.80 FAF of the same patient in Fig. 12.79. The pattern of RPE loss in the FAF extends to the papillary area, which differentiates it from cone dystrophy. *FAF* fundus autofluorescence

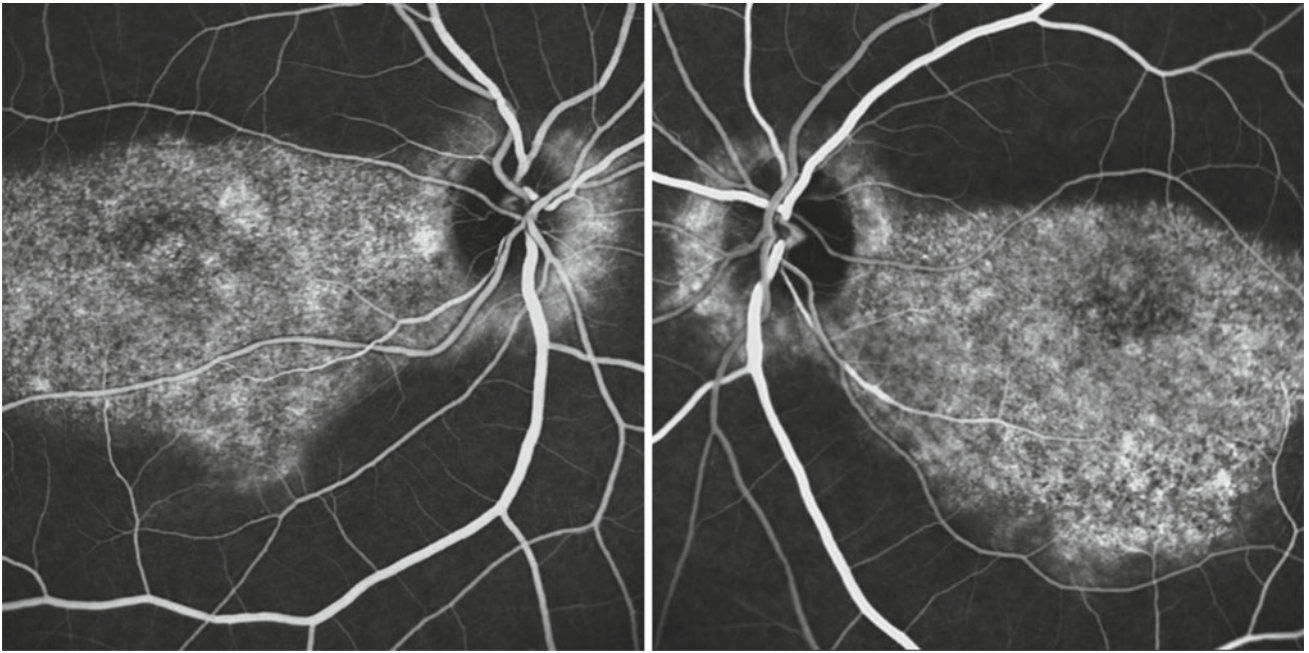


Fig. 12.81 Fluorescein angiography in late stage of the same patient in Figs. 12.79 and 12.80, clearly illustrate the hyperfluorescence pattern

around optic disk to central part of macula secondary to RPE loss and window effect

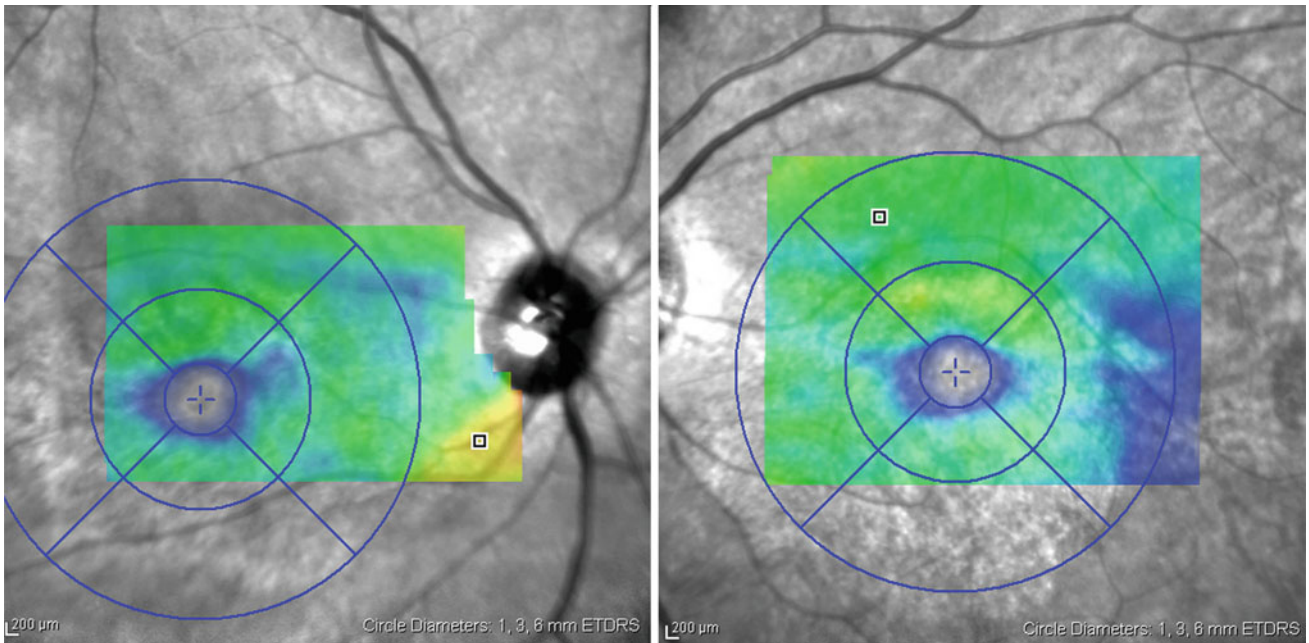


Fig. 12.82 The topographic map of the same patient in Figs. 12.79, 12.80 and 12.81, shows considerable atrophy of the central and perifoveal area

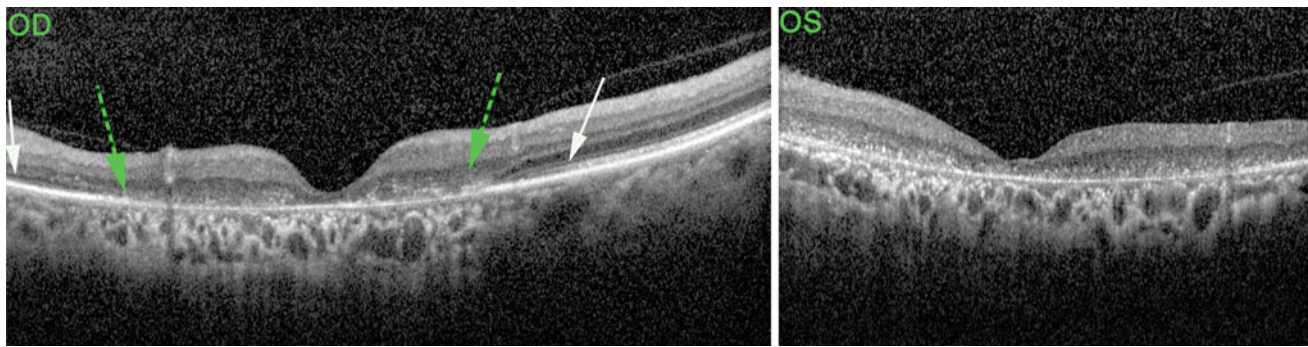


Fig. 12.83 The cross-sectional OCT images of the same patient in Figs. 12.79, 12.80, 12.81 and 12.82, show the loss or disorganization of the outer retinal layer, including the RPE and the photoreceptor layer. The dashed arrows indicate the boundary between the involved retina and the normal retina. In the left eye, complete disorganization of the

outer retina is evident. The areas between the white and dashed arrows (left panel) contain an IS/OS abnormality, which corresponds to the normal HVF 10–2 area. *HVF* Humphrey visual field, *IS/OS* inner segment/outer segment, *OCT* optical coherence tomography, *OD* oculus dexter, *OS* oculus sinister, *FAF* fundus autofluorescence

References

- Aguilar JP, Green WR. Choroidal rupture: a histopathologic study of 47 cases. *Retina*. 1984;4:269–75.
- Wyszynski RE, Grossniklaus HE, Frank KE. Indirect choroidal rupture secondary to blunt ocular trauma. A review of eight eyes. *Retina*. 1988;8:237–43.
- Fuller B, Gitter KA. Traumatic choroidal rupture with late serous detachment of macula. Report of successful argon laser treatment. *Arch Ophthalmol*. 1973;89:354–5.
- Conrath J, Forzano O, Ridings B. Photodynamic therapy for subfoveal CNV complicating traumatic choroidal rupture. *Eye (Lond)*. 2004;18:946–7.
- Chanana B, Azad RV, Kumar N. Intravitreal bevacizumab for subfoveal choroidal neovascularization secondary to traumatic choroidal rupture. *Eye (Lond)*. 2009;23:2125–6.
- Yadav NK, Bharghav M, Vasudha K, Shetty KB. Choroidal neovascular membrane complicating traumatic choroidal rupture managed by intravitreal bevacizumab. *Eye (Lond)*. 2009;23:1872–3.
- Pham TQ, Chua B, Gorbатов M, Mitchell P. Optical coherence tomography findings of acute traumatic maculopathy following motor vehicle accident. *Am J Ophthalmol*. 2007;143:348–50.
- Ismail R, Tanner V, Williamson TH. Optical coherence tomography imaging of severe commotio retinae and associated macular hole. *Br J Ophthalmol*. 2002;86:473–4.
- Knapp H. Ueber isolirte zerreissugen der aderhaut infolge von traumen auf augapfel. *Arc Augenheilkd*. 1869;1:6–29 [in German].
- Coats G. The pathology of macular hole. *Roy London Ophthalmic Hosp Rep*. 1907;17:69–96.
- Gass J. Reappraisal of biomicroscopic classification of stages of development of a macular hole. *Am J Ophthalmol*. 1995;119:752–9.
- Schepens CL. Fundus changes caused by alterations of the vitreous body. *Am J Ophthalmol*. 1955:631–3.
- Yamada H, Sakai A, Yamada E, Nishimura T, Matsumura M. Spontaneous closure of traumatic macular hole. *Am J Ophthalmol*. 2002;134:340–7.
- Parmar DN, Stanga PE, Reck AC, Vingerling JR, Sullivan P. Imaging of a traumatic macular hole with spontaneous closure. *Retina*. 1999;19:470–2.
- Yamashita T, Uemara A, Uchino E, Doi N, Ohba N. Spontaneous closure of traumatic macular hole. *Am J Ophthalmol*. 2002;133:230–5.
- Imai M, Iijima H, Gotoh T, Tsukahara S. Optical coherence tomography of successfully repaired idiopathic macular hole. *Am J Ophthalmol*. 1999;128:621–7.
- Lewis H, Cowan GM, Straatsma R. Apparent disappearance of a macular hole associated with development of an epiretinal membrane. *Am J Ophthalmol*. 1986;102:172–5.
- Takahashi R, Yuzawa M, Matsui M. Three cases of spontaneous closure of idiopathic macular hole. *Acta Ophthalmol Jpn*. 1992;39:327–8.
- Higashide T, Sugiyama K. Optical coherence tomography characteristics of a hemorrhagic detachment of the RPE after blunt trauma. *Am J Ophthalmol*. 2003;136:567–9.
- Calvetti O, Rodallec T, Blumen-Ohana E, Nordmann JP. Visual recovery of macula-off rhegmatogenous retinal detachment and six months follow-up with optical coherence tomography of the macula. *Invest Ophthalmol Vis Sci*. 2005;46:5477.
- Abouzeid H, Wolfensberger TJ. Macular recovery after retinal detachment. *Acta Ophthalmol Scand*. 2006;84:597–605.
- Wolfensberger TJ, Gonvers M. Optical coherence tomography in the evaluation of incomplete visual acuity recovery after macula-off retinal detachments. *Graefes Arch Clin Exp Ophthalmol*. 2002;40:85–9.
- Schocket LS, Witkin AJ, Fujimoto JG, Ko TH, Schuman JS, Rogers AH, et al. Ultrahigh-resolution optical coherence tomography in patients with decreased visual acuity after retinal detachment repair. *Ophthalmology*. 2006;113:666–72.
- Leclaire-Collet A, Muraine M, Menard JF, Bresseur G. Predictive visual outcome after macula-off retinal detachment surgery using optical coherence tomography. *Retina*. 2005;25:44–53.
- Panozzo G, Parolini B, Mercanti A. OCT in the monitoring of visual recovery after uneventful retinal detachment surgery. *Semin Ophthalmol*. 2003;18:82–4.
- Hagimura N, Iida T, Suto K, Kishi S. Persistent foveal retinal detachment after successful rhegmatogenous retinal detachment surgery. *Am J Ophthalmol*. 2002;133:516–20.
- Baba T, Hirose A, Moriyama M, Mochizuki M. Tomographic image and visual recovery of acute macula-off rhegmatogenous retinal detachment. *Graefes Arch Clin Exp Ophthalmol*. 2004;42:576–81.
- Benson SE, Schlottmann PG, Bunce C, Xing W, Charteris DG. Optical coherence tomography analysis of the macula after scleral buckle surgery for retinal detachment. *Ophthalmology*. 2007;114:108–12.
- Sugawara R, Nagaoka T, Kitaya N, Fujio N, Takahashi J, Takahashi A, et al. Choroidal blood flow in the foveal region in

- eyes with rhegmatogenous retinal detachment and scleral buckle procedures. *Br J Ophthalmol.* 2006;90:1363–5.
30. Diddie KR, Ernest JT. Uveal blood flow after 360 degrees constriction in the rabbit. *Arch Ophthalmol.* 1980;98:729–30.
 31. Sheth S, Dabir S, Natarajan S, Mhatre A, Labauri N. Spectral domain-optical coherence tomography study of retinas with a normal foveal contour and thickness after retinal detachment surgery. *Retina.* 2010;30:724–32.
 32. Perente I, Utine CA, Ozturker C, Cakir M, Kaya V, Eren H, et al. Evaluation of macular changes after uncomplicated phacoemulsification surgery by optical coherence tomography. *Curr Eye Res.* 2007;32:241–7.
 33. Sourdille P, Santiago PY. Optical coherence tomography of macular thickness after cataract surgery. *J Cataract Refract Surg.* 1999;25:256–61.
 34. Kim SJ, Bressler NM. Optical coherence tomography and cataract surgery. *Curr Opin Ophthalmol.* 2009;20:46–51.
 35. Ouyang Y, Keane PA, Sadda SR, Walsh AC. Detection of cystoid macular edema with three-dimensional optical coherence tomography versus fluorescein angiography. *Invest Ophthalmol Vis Sci.* 2010;51:5213–8.
 36. Ozdek SC, Erdinc MA, Gurelik G, Aydin B, Bahaceci U, Hasanreisoglu B. Optical coherence tomographic assessment of diabetic macular edema: comparison with fluorescein angiographic and clinical findings. *Ophthalmologica.* 2005;219:86–92.
 37. Greene AB, Del Priore LV, Iranmanesh R. Isolated foveolar detachment in Irvine-Gass syndrome. *Br J Ophthalmol.* 2006;90:1076–7.
 38. Dellaporta A. Ueber fältelung der netzhaut bei hypotonie [Creasing of retina in hypotonia]. *Klin Monbl Augenheilkd Augenarztl Fortbild.* 1954;125:672–8 [in German].
 39. Whiteside-Michel J, Liebmann JM, Ritch R. Initial 5-fluorouracil trabeculectomy in young patients. *Ophthalmology.* 1992;99:7–13.
 40. Costa VP, Wilson RP, Moster MR, Schmidt CM, Grandham S. Hypotony maculopathy following the use of topical mitomycin C in glaucoma filtration surgery. *Ophthalmic Surg.* 1993;24:389–94.
 41. Kitazawa Y, Suemori-Matsushita H, Yamamoto T, Kawase K. Low-dose and high-dose mitomycin trabeculectomy as an initial surgery in primary open-angle glaucoma. *Ophthalmology.* 1993;100:1624–8.
 42. Oppenheim B, Ortiz JM. Hypotonous maculopathy after trabeculectomy with subconjunctival 5-fluorouracil. *Am J Ophthalmol.* 1993;115:546–7.
 43. Shields MB, Scroggs MW, Sloop CM, Simmons RB. Clinical and histopathologic observations concerning hypotony after trabeculectomy with adjunctive mitomycin C. *Am J Ophthalmol.* 1993;116:673–83.
 44. Zacharia PT, Deppermann SR, Schuman JS. Ocular hypotony after trabeculectomy with mitomycin C. *Am J Ophthalmol.* 1993;116:314–26.
 45. Neelakantan A, Rao BS, Vijaya L, Grandham SB, Krishnan N, Priya VS, et al. Effect of the concentration and duration of application of mitomycin C in trabeculectomy. *Ophthalmic Surg.* 1994;25:612–5.
 46. Fannin LA, Schiffman JC, Budenz DL. Risk factors for hypotony maculopathy. *Ophthalmology.* 2003;110:1185–91.
 47. Jampel HD, Pasquale LR, Dibernardo C. Hypotony maculopathy following trabeculectomy with mitomycin C. *Arch Ophthalmol.* 1992;110:1049–50.
 48. Stamper RL, McMenemy MG, Lieberman MF. Hypotonous maculopathy after trabeculectomy with subconjunctival 5-fluorouracil. *Am J Ophthalmol.* 1992;114:544–53.
 49. Suñer IJ, Greenfield DS, Miller MP, Nicoleta MT, Palmberg PF. Hypotony maculopathy after filtering surgery with mitomycin C. Incidence and treatment. *Ophthalmology.* 1997;104:207–14.
 50. Palmberg P. Late complications after glaucoma filtering surgery. In: Leader BJ, Calkwood JC, editors. *Peril to the nerve—glaucoma and clinical neuro-ophthalmology.* Proceedings of the 45th Annual Symposium of the New Orleans Academy of Ophthalmology. The Hague: Kugler; 1996. p. 183–93.
 51. Kokame GT, de Leon MD, Tanji T. Serous retinal detachment and cystoid macular edema in hypotony maculopathy. *Am J Ophthalmol.* 2001;131:384–6.
 52. Stefansson E. Ocular oxygenation and the treatment of diabetic retinopathy. *Surv Ophthalmol.* 2006;51:364–80.
 53. Martinez de la Casa JM, Garcia Feijoo J, Castillo Gomez A, Macias Benitez JM, Martin Valdizan C, Garcia Sanchez J. Hypotony maculopathy diagnosed by optical coherence tomography. *Arch Soc Esp Oftalmol.* 2003;78:567–9. [in Spanish].
 54. Budenz DL, Schwartz K, Gedde SJ. Occult hypotony maculopathy diagnosed with optical coherence tomography. *Arch Ophthalmol.* 2005;123:113–4.
 55. Comer GM, Danis RP. Optical coherence tomographic identification of retinal fold resolution in chronic hypotonous maculopathy after internal limiting membrane removal. *Ann Ophthalmol.* 2005;37:123–6.
 56. Goodkin ML, Grewal DS, Greenfield DS. Three-dimensional high-speed optical coherence tomography for diagnosis of hypotony maculopathy after glaucoma filtration surgery. *J Glaucoma.* 2010;19:349–55.
 57. Gupta R, Browning AC, Amoaku WM. Multiple retinal haemorrhages (decompression retinopathy) following paracentesis for macular branch artery occlusion. *Eye (Lond).* 2005;19:592–3.
 58. Lai JS, Lee VY, Leung DY, Chung TC. Decompression retinopathy following laser peripheral iridoplasty for acute primary angle-closure. *Eye (Lond).* 2005;19:1345–7.
 59. Ben Simon GJ, Goldberg RA, McCann JD. Bilateral decompression retinopathy after decompression surgery. *Br J Ophthalmol.* 2004;88:1605–6.
 60. Nonoyama S, Tanito M, Katsube T, Matsuoka Y, Ohira A. Decompression retinopathy and serous retinal detachment after trabeculectomy in a patient with systemic amyloidosis. *Jpn J Ophthalmol.* 2009;53:73–5.
 61. Endophthalmitis Vitrectomy Study Group. Microbiologic factors and visual outcome in the Endophthalmitis Vitrectomy Study. *Am J Ophthalmol.* 1996;122:830–46.
 62. Singh R, Gupta V, Gupta A, Dogra MR. Optical coherence tomography following successful management of endophthalmitis. *Indian J Ophthalmol.* 2007;55:234–5.
 63. Goldman M, Dagan Z, Yair M, Elbaz U, Lahat E, Yair M. Severe cough and retinal hemorrhage in infants and young children. *J Pediatr.* 2006;148:835–6.
 64. Roberts DK, MacKay KA. Microhemorrhagic maculopathy associated with aerobic exercise. *J Am Optom Assoc.* 1987;58:415–8.
 65. Gatzonis S, Charakidas A, Polychronopoulou Z, Brouzas D. Unilateral visual loss following bodybuilding training. *Clin J Sport Med.* 2004;14:317–8.
 66. Ho LY, Abdelghani WM. Valsalva retinopathy associated with the choking game. *Semin Ophthalmol.* 2007;22:63–5.
 67. Peyman GA, Shulman JA, Sullivan B. Perfluorocarbon liquids in ophthalmology. *Surv Ophthalmol.* 1995;39:375–95.
 68. Bourke RD, Cooling RJ. Perfluorocarbon heavy liquids. *Aust NZJ Ophthalmol.* 1995;23:165–71.

69. Velikay M, Wedrich A, Stolba U, Datlinger P, LI Y, Binder S. Experimental longterm vitreous replacement with purified and non-purified perfluorodecalin. *Am J Ophthalmol.* 1993;116:565–70.
70. Lee GA, Finnegan SJ, Bourke RD. Subretinal perfluorodecalin toxicity. *Aust NZJ Ophthalmol.* 1998;26:57–60.
71. de Queiroz Jr JM, Blanks JC, Ozler SA, Alfaro DV, Liggett PE. Subretinal perfluorocarbon liquids: an experimental study. *Retina.* 1992;12(suppl):S33–9.
72. Elsing SH, Fekrat S, Green WR, Chang S, Wajer SD, Haller JA. Clinicopathologic findings in eyes with retained perfluoro-n-octane liquid. *Ophthalmology.* 2001;108:45–8.
73. Lai JC, Postel EA, McCuen BW 2nd. Recovery of visual function after removal of chronic subfoveal perfluorocarbon liquid. *Retina.* 2003;23:868–70.
74. Roth DB, Sears JE, Lewis H. Removal of retained subfoveal perfluoro-n-octane liquid. *Am J Ophthalmol.* 2004;138:287–9.
75. Lesnoni G, Rossi T, Gelso A. Subfoveal liquid perfluorocarbon. *Retina.* 2004;24:172–6.
76. Chang S, Lincoff H, Zimmerman NJ, Fuchs W. Giant retinal tears. Surgical techniques and results using perfluorocarbon liquids. *Arch Ophthalmol* 1989;107:761–6.
77. Chang S, Ozmert E, Zimmerman NJ. Intraoperative perfluorocarbon liquids in management of proliferative vitreoretinopathy. *Am J Ophthalmol.* 1988;106:668–74.
78. Won TY, Ho T. Retained perfluorodecalin after retinal detachment surgery. *Int Ophthalmol.* 1997;20:293–4.
79. Cambiaggi A. Unusual ocular lesions in a case of systemic lupus erythromatosis. *AMA Arch Ophthalmol.* 1957;57:451–3.
80. Hobbs HE, Sorsby A, Freedman A. Retinopathy following chloroquine therapy. *Lancet.* 1959;2:478–80.
81. Browning DJ. Hydroxychloroquine and chloroquine retinopathy: screening for drug toxicity. *Am J Ophthalmol.* 2002;133:649–56.
82. Bonanomi MT, Dantas NC, Medeiros FA. Retinal nerve fibre layer thickness measurements in patients using chloroquine. *Clin Exp Ophthalmol.* 2006;34:130–6.
83. Ramsey MS, Fine BS. Chloroquine toxicity in the human eye: histopathologic observations by electron microscopy. *Am J Ophthalmol.* 1972;73:229–35.
84. Stepien KE, Han DP, Schell J, Godara P, Rha J, Carroll J. Spectral-domain optical coherence tomography and adaptive optics may detect hydroxychloroquine retinal toxicity before symptomatic vision loss. *Trans Am Ophthalmol Soc.* 2009;107:28–33.
85. Rodriguez-Padilla JA, Hedges TR 3rd, Monson B, Srinivasan V, Wojtkowski M, Reichel E, et al. High-speed ultra-high-resolution optical coherence tomography findings in hydroxychloroquine retinopathy. *Arch Ophthalmol.* 2007;125:775–80.
86. Turgut B, Turkcuoglu P, Serdar Koca S, Aydemir O. Detection of the regression on hydroxychloroquine retinopathy in optical coherence tomography. *Clin Rheumatol.* 2009;28:607–9.
87. Korah S, Kuriakose T. Optical coherence tomography in a patient with chloroquine-induced maculopathy. *Indian J Ophthalmol.* 2008;56:511–3.